Polymer tandem solar cells

Polymer tandem solar cells

PROEFSCHRIFT

ter verkrijging van de graad van doctor aan de
Technische Universiteit Eindhoven, op gezag van de
rector magnificus, prof.dr.ir. C.J. van Duijn, voor een
commissie aangewezen door het College voor
Promoties in het openbaar te verdedigen
op donderdag 1 juli 2010 om 16.00 uur

door

Jan Gilot

geboren te Turnhout, België

Dit proefschrift is goedgekeurd door de promotor:

prof.dr.ir. R.A.J. Janssen

Copromotor:
dr.ir. M.M. Wienk

This research was financially supported by the Senter/Novem in the EOS project Zomer (EOSLT03026).

Cover design: Pieter Heyns

Printed by: Wöhrmann print service, Zutphen

A catalogue record is available from the Eindhoven University of Technology Library.
ISBN: 978-90-386-2279-8

Polymer tandem solar cells

Kerncommissie:

Prof. dr. ir. R.A.J. Janssen (Technische Universiteit Eindhoven)
Dr. ir. M.M. Wienk (Technische Universiteit Eindhoven)
Prof. dr. ir. P.W.M. Blom (Rijksuniversiteit Groningen & Holst Centre)
Prof. dr. C.J. Brabec (Friedrich-Alexander-University of Erlangen-Nürnberg)
Prof. dr. ir. M.C.M. van de Sanden (Technische Universiteit Eindhoven)

Overige commissieleden:

Prof. dr. D.J. Broer (Technische Universiteit Eindhoven)
Dr. J.M. Kroon (Energieonderzoek Centrum Nederland)

Voorzitter:

Prof. dr. P.J. Lemstra (Technische Universiteit Eindhoven)

Brief contents

Table of contents

Chapter 1

Introduction

Abstract

This chapter introduces the concept, fabrication, and characterization of polymer solar cells. Polymer solar cells possess several attractive properties, but their power conversion efficiency and stability must be further enhanced before they can become successful in large scale renewable energy production. A tandem configuration can improve the ultimate efficiency of polymer solar cells by utilizing the energy of the absorbed photons more effectively, but poses new, additional requirements to the active materials and the intermediate contact layers. Different strategies towards organic and polymer tandem solar cells presented during the past few years are described and elucidate the scope of the research described in this thesis.

1.1 Solar cells

The growing need for energy by the human society demands a renewable, sustainable, low-cost and omnipresent energy source. With 174 PW incident power of which 95.7 PW reaches the earth's surface,[1] the sun is the number one candidate to fulfill the expected 71 TW global energy power demand in 2050.[2] Solar energy is especially attractive as it can be converted in one of the most useful forms of energy—electricity—by photovoltaic devices. Solar cells convert incident photons directly into electricity, by employing the "photovoltaic effect". After the first observation of this effect by Becquerel in 1839[3] and the discovery of the spectral sensitivity of selenium by Adams and Day in 1877,[4] Fritts built the first solar cell in 1883: selenium coated with a thin layer of gold, exhibiting a power conversion efficiency of 1%.[5-6] The presently most-used solar cells are based on silicon and were first developed in 1953 by Chapin *et al.*[7] Silicon solar cells have undergone a series of developments to reach the highest confirmed power conversion efficiency of 25% nowadays.[8-9]

However, the expensive, time and energy consuming production process of mono-crystalline silicon solar cells impels the search for alternative semiconductor materials. Amorphous silicon, cadmium telluride (CdTe) and copper-indium-gallium-selenide (CIGS) solar cells require lower energy input for manufacture, but their efficiency is lower than for mono-crystalline silicon with highest reported efficiencies of 9.5%, 16.7%, and 19.4%, respectively.[8] For some materials, possible risks for environmental pollution and shortage of raw materials could become a future problem.

1.2 Polymer solar cells

In recent years, organic materials with semiconductor properties have become an active research area, aiming for electronic applications like field effect transistors, light emitting diodes, solar cells, and memories. Since the discovery of the ability to dope polyacetylene to a metallic conduction level by Shirakawa, MacDiarmid, and Heeger,[10-11] π-conjugated polymers are considered as a valid alternative for inorganic semiconductors. Especially the excellent processing and mechanical properties of polymers, obtained through the tunable chemical and synthetic diversity, attract attention. The research on organic semiconductor materials is intensified owing to the potential cost reduction on account of the high absorption

coefficients permitting the use of ultrathin films (several hundred nanometers), the compatibility with flexible substrates, and the possibility of low-temperature processing allowing deployment of well established cheap printing techniques.[12] The focus of this thesis will be on polymer solar cells. Despite the auspicious benefits of polymers, the commercialization of polymer solar cells only just started. However, recent progress up to 6-7% power conversion efficiency[13-17] on lab scale opens the way to efficiencies of 10-11% that are thought to be feasible for single layer solar cells[18-19] and represent the estimated threshold for successful commercialization of polymer solar cells.

One origin of the lower efficiency of polymer compared to inorganic solar cells is the difference in photogeneration of free charge carriers (Figure 1.1a).[20-23] Upon illumination of inorganic semiconductors with photons having energies larger than the band gap (E_g), *i.e.* the energy difference between valence and conduction bands, free charge carriers (*i.e.* electrons and holes) are generated, which can then be separated by a junction in the solar cell. A possible excess energy of the photon ($E_{photon} - E_g$) is lost via thermalization, while photons with $E_{photon} < E_g$ are not absorbed. In organic semiconductors, however, absorbed photons excite an electron from the highest occupied molecular orbital (HOMO) to the lowest unoccupied molecular orbital (LUMO) (step 1.). Whereas in inorganic solar cells free charge carriers are formed in the bulk upon photoexcitation, the relatively low dielectric constant of organic materials results in a Coulombically bound electron-hole pair, *i.e.* an exciton. To dissociate the exciton into free charges, Tang presented in 1986 a bilayer heterojunction composed of two organic materials with offset energy levels.[24] This organic/organic interface is responsible for creating charges from the photogenerated bound excitons. Owing to the energy offset between the respective frontier orbitals, the materials serve either as electron donor or acceptor. At the donor-acceptor interface charge transfer occurs, resulting in a hole in the material with the lowest ionization potential (donor) and an electron in the material with the highest electron affinity (acceptor) (step 3.). These carriers are still attracted by Coulombic interaction but can often be separated in the internal electric field (or built-in potential) in the cell that is created by the difference in work function of the two collecting electrodes sandwiching the organic heterojunction (step 4.). Holes (electrons) travel through the donor (acceptor) material phase to the high (low) work function electrode (step 5.).

The diffusion length of excitons in organic semiconductors is limited to about 10 nm due to their short lifetime and low mobility.[25-28] This implies that only excitons created close enough to the interface can effectively migrate to the interface to yield charge carriers (step

2.). The solution to increase the carrier generation efficiency was first presented in 1995 by mixing donor and acceptor materials and relying on the intrinsic tendency of polymer materials to phase separate on a nanometer dimension (*i.e.* a bulk heterojunction solar cell).[29-30] The ubiquitous interface throughout the bulk of the material (Figure 1.1b) ensures quantitative dissociation of photogenerated excitons and percolating pathways facilitate electron and hole transport to the electrodes.[31-33]

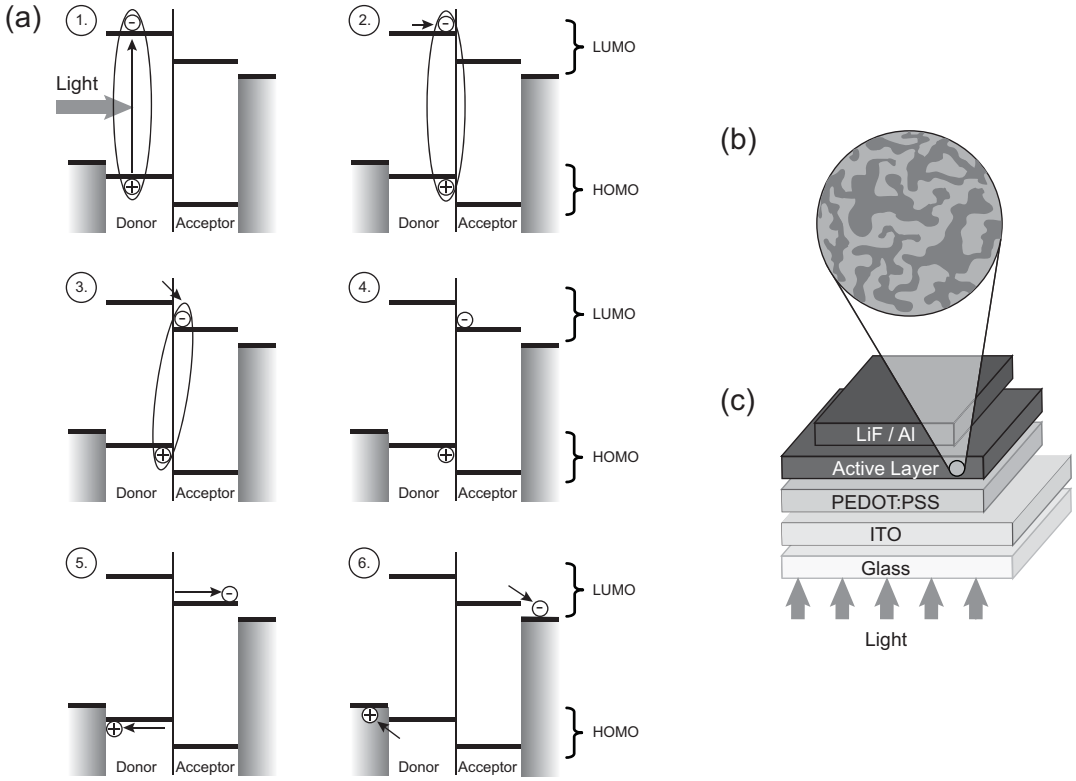

Figure 1.1 (a) The subsequent steps in photogeneration of charge carriers in a bilayer heterojunction organic solar cell: 1. absorption, 2. exciton diffusion, 3. charge transfer, 4. charge separation, 5. charge transport, and 6. charge collection. (b) Visualization of the ubiquitous interface throughout the bulk of a blended film. (c) Common device set-up of a bulk heterojunction solar cell.

The most successful acceptor materials used in polymer bulk heterojunction solar cells are soluble fullerene derivatives: (6,6)-phenyl-C_{61}-butyric acid methyl ester ([60]PCBM) and (6,6)-phenyl-C_{71}-butyric acid methyl ester ([70]PCBM) (Figure 1.2).[34-35] Combined in a blend with a π-conjugated polymer, [60]PCBM or [70]PCBM form the active layer of polymer solar cells.

To collect the charges from the active layer two electrodes (step 6.), with a high/low work function to collect the holes/electrons respectively, sandwich the active layer (Figure 1.1c). In the most commonly used device structure for polymer solar cells, indium tin oxide (ITO) deposited on glass or flexible plastic foil functions as the transparent, high work function electrode. ITO is mostly covered by a hole transporting layer, poly(3,4-ethylenedioxythiophene):poly(styrenesulfonate) (PEDOT:PSS) (Figure 1.2). This hole conducting polymer is used for smoothing of the ITO surface preventing shunts as a result of spikes, for improved wetting by the solvent in depositing the active layer, and for enhancing the hole collection by improved energy level alignment between the work function of the electrode and the HOMO of the donor polymer. On the opposite side of the active layer a reflective, low work function metal electrode is deposited. The common Al electrode is modified by inserting a thin layer (~1 nm) of LiF that improves the performance of light emitting diodes and solar cells.[36] The mechanism that leads to the improved performance by the insertion of LiF is still under debate. Suggested mechanisms include dipole formation generating a lower work function and enhancing electron transfer from the active layer to the metal electrode either by the orientation of LiF or by a chemical reaction, protection of the active layer and more specifically the π-conjugation of the polymers by preventing Al:organic complexes, and diffusion in and doping of the active layer by LiF.[36-43]

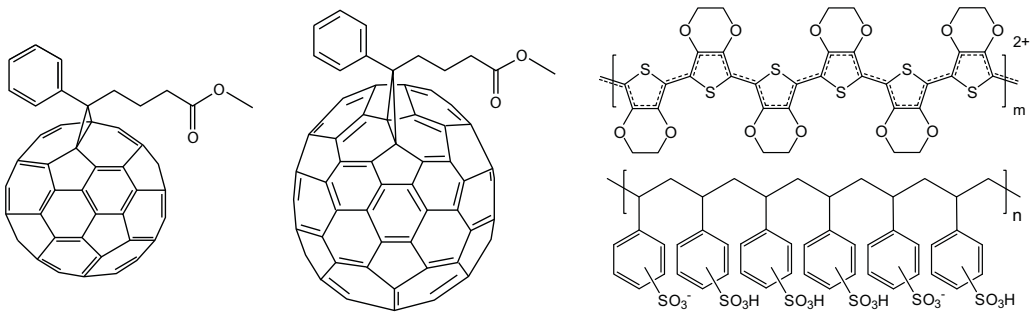

Figure 1.2 Molecular structure of commonly used acceptor molecules: [60]PCBM and [70]PCBM, and the hole transporting layer PEDOT:PSS.

1.3 Characterization of a solar cell

The performance of a solar cell is characterized by measuring the current density to voltage (*J*–*V*) characteristics under illumination with the AM1.5G solar spectrum (1000 W/m^2) at a temperature of 25 ºC (Figure 1.3a).[44] The term AM1.5G (air mass 1.5 global) refers to the mass of air that solar light has to travel through being 1.5 times larger than for light incident at zenith (*i.e.* on a surface facing the sun with a solar zenith angle of 48.2º). A typical *J*–*V* curve of a solar cell is displayed in Figure 1.3b. The power density in the maximum power point (P_{MPP}) is defined by three parameters: short-circuit current density (J_{sc}), open-circuit voltage (V_{oc}), and fill factor (*FF*):

$$P_{MPP} = J_{sc} \cdot V_{oc} \cdot FF \qquad \textbf{(1.1)}$$

The *FF* is determined by the resistances present in the cell indicating the ease of charge collection and the amount of leakage current in the device. *FF* can be calculated as the ratio between P_{MPP} and the theoretically maximum obtainable power density (P_{max}):

$$FF = \frac{P_{MPP}}{P_{max}} = \frac{J_{MPP} \cdot V_{MPP}}{J_{sc} \cdot V_{oc}} \qquad \textbf{(1.2)}$$

The power conversion efficiency of a solar cell is defined by the ratio between P_{MPP} and the power density of the incident light (P_{inc}):

$$\eta = \frac{P_{MPP}}{P_{inc}} \qquad \textbf{(1.3)}$$

The spectral response (SR) is a measure for the external quantum efficiency (*EQE*) of a solar cell, which is the fraction of incident photons at a certain wavelength λ that is converted into electrons flowing through an external circuit at short-circuit conditions. From the spectral response, the J_{sc} under AM1.5G illumination can be calculated by convolution with the power density of the solar spectrum (P_{sun}).

$$J_{sc}(\mathrm{SR}) = \int EQE(\lambda) \cdot P_{sun}(\lambda) \cdot \frac{e \cdot \lambda}{h \cdot c} \mathrm{d}\lambda \qquad \textbf{(1.4)}$$

Here, *e* represents the elementary charge, *h* the constant of Planck and *c* the speed of light. The determination of the spectral response of organic solar cells is preferably performed under continuous illumination to ensure one-sun operating conditions. The sub-linear light intensity dependence of some organic solar cells can result in an overestimation of the J_{sc} and

is attributed to an increased carrier concentration under illumination which increases recombination and hinders carrier transport due to space-charge build up in the device.[45]

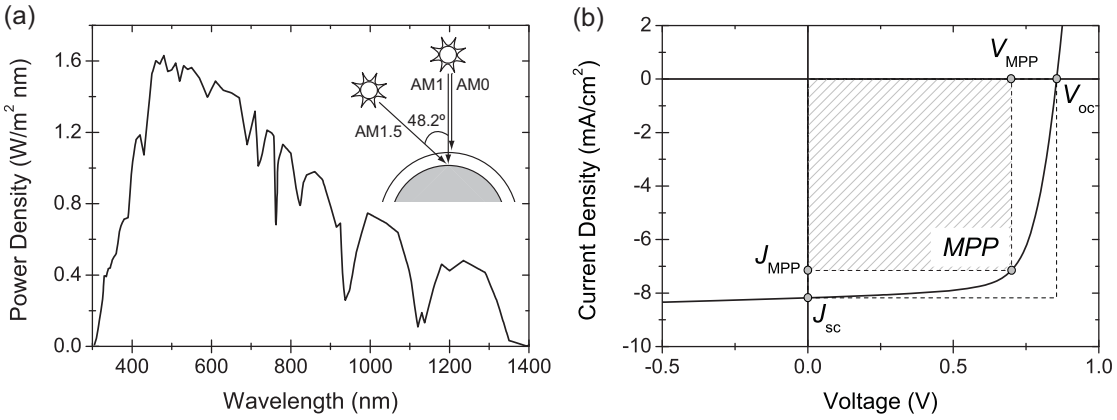

Figure 1.3 (a) The AM1.5G solar spectrum. The cartoon shows the angle of incidence of the spectrum. (b) A typical *J*–*V* characteristic of a solar cell with indication of the short-circuit current density (J_{sc}), the open-circuit voltage (V_{oc}), and the maximum power point (*MPP*) with the corresponding current density (J_{MPP}) and voltage (V_{MPP}).

Accurate determination of the efficiency is a must for the credibility of the organic solar cell community.[46-48] A first important parameter for standard test conditions is the lamp spectrum and the intensity of the solar simulator used which only approximates the AM1.5G solar spectrum. The difference in spectrum regularly results in discrepancies between the claimed J_{sc} based on the *J*–*V* characteristics measured with a solar simulator and the J_{sc} based on the spectral response after convolution with the AM1.5G solar spectrum.[49-51] The intensity of the solar simulator is set by a calibrated reference solar cell and a solar simulator spectral mismatch factor *M* corrects for the approximated match of the solar spectrum and the difference in spectral response between the tested and calibrated cell.[52-53] *M* is computed via the following formula:

$$M = \frac{\int E_R(\lambda)\cdot S_R(\lambda)\mathrm{d}\lambda}{\int E_S(\lambda)\cdot S_R(\lambda)\mathrm{d}\lambda}\cdot\frac{\int E_S(\lambda)\cdot S_T(\lambda)\mathrm{d}\lambda}{\int E_R(\lambda)\cdot S_T(\lambda)\mathrm{d}\lambda} \qquad \textbf{(1.5)}$$

with $E_S(\lambda)$ the solar simulator spectrum, $E_R(\lambda)$ the AM1.5G solar spectrum, and $S_T(\lambda)$ and $S_R(\lambda)$ the spectral response of the test cell and reference cell respectively.[54-55] A detailed description of accurate efficiency determination is presented by Kroon *et al*.[52] where precise execution of the procedure is emphasized to minimize measurement errors.

For established solar cells, a reference cell of more-or-less the same materials with comparable spectral response is used. For organic solar cells, suitable and stable reference cells are hard to fabricate. As a result, the spectral response of the applied calibrated reference cell departs from the spectral response of the test cell, which leads to mismatch factors that significantly deviate from unity.

A second important parameter for accurate determination of the current density of a device is the actual active area. Usually this is defined as the overlapping area between the high and low work function electrodes. A significant error can arise from shadow effects during the evaporation of the top electrode resulting in an ill-defined electrode area.[53] Another undesirable error is the occurrence of edge effects. The high conductivity of several PEDOT:PSS dispersions leads to parasitic current generation next to the overlapping electrodes and thereby to an overestimation of the efficiency (Figure 1.4).[56-58] Holes collected by the PEDOT:PSS in the areas bordering the active area can be transported parallel to the surface towards the active area, so that the current generated in bordering areas contributes to the current of the device leading to an overestimation of the current density. The size of these contributing, bordering areas depends on the conductivity of PEDOT:PSS.[56] To prevent this error in characterization, the illuminated area should equal the active area which is easily done by masking the bordering areas with a non-reflective material.

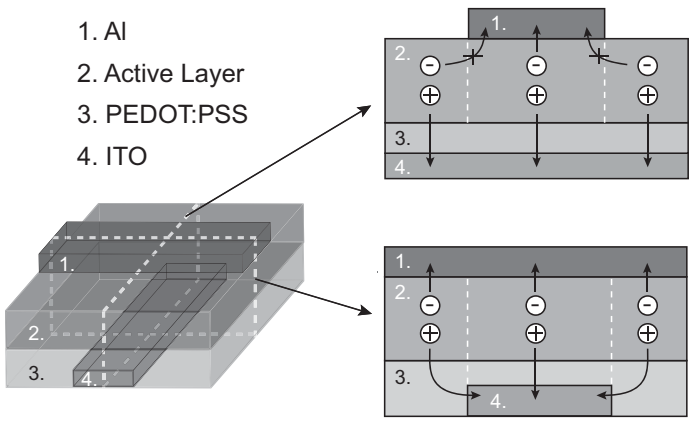

Figure 1.4 Cartoon of parasitic charge generation in the case of high conductive PEDOT:PSS for two cross-sections of a common polymer solar cell.

1.4 Tandem solar cells

Because of the high absorption coefficient of conjugated polymers compared to fullerenes, the efficiency of a polymer solar cell strongly depends on the band gap of the donor polymer ($E_{g,donor}$). Variation of $E_{g,donor}$ has an opposite effect on J_{sc} (negative relation) and V_{oc} (positive relation). A small band gap allows for more absorbed photons and hence a higher J_{sc}, while a wide band gap enables a high V_{oc}[59]:

$$eV_{oc} \leq \min\left(E_{g,donor}; E_{g,acceptor}\right) - 0.6\,eV \qquad \textbf{(1.6)}$$

This is related to the fact that photons with energies smaller than $E_{g,donor}$ cannot be absorbed and photons with larger energies will lose their excess energy via thermal equilibration (Figure 1.5a). This tradeoff between J_{sc} and V_{oc} limits the theoretical efficiency of a single band gap solar cell under non-concentrated sunlight to 30% as described by Shockley and Queisser with an optimal E_g of 1.1 eV.[60] The thermodynamic losses can be reduced by using separate subcells which convert a different part of the solar spectrum. In a tandem solar cell, thermalization losses of high-energy photons are reduced by conversion in the subcell with a wide $E_{g,donor}$ and transmission losses are lowered by absorption of the low energy photons in the subcell with a small $E_{g,donor}$. The theoretical limit under non-concentrated sunlight rises to 42% for a tandem cell with E_gs of 1.9 and 1.0 eV, and to 49% for triple junction solar cells with E_gs of 2.3, 1.4 and 0.8 eV.[61-62] Translation to polymer solar cells where an additional loss is introduced by the necessity of the donor/acceptor concept leads to a comparable increase in efficiency when going from single junction to tandem and triple cells.[19,63-65]

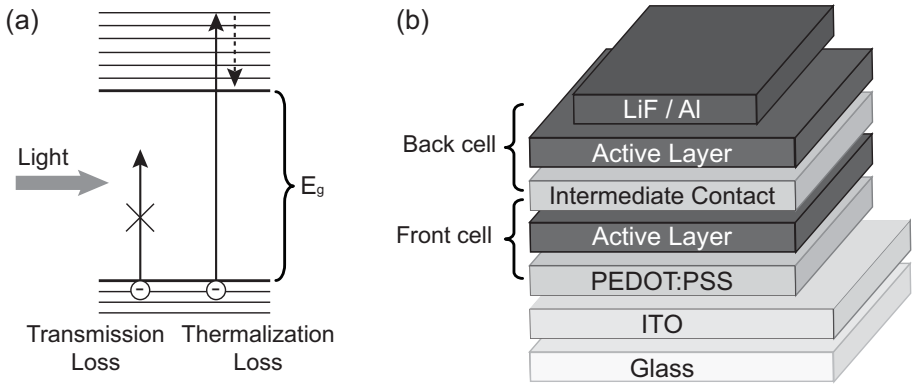

Figure 1.5 (a) Visualization of thermodynamic losses related to absorption. (b) Device layout of a polymer tandem solar cell.

Polymers are well suited for multiple junction solar cells as the strong and narrow absorption bands enable subcells with complementary absorption spectra. Wide band gap polymer solar cells (E_g>1.8 *e*V) based on thiophene (P3HT[66]), phenylene vinylene (MDMO-PPV[67]), and the combination of fluorene and dithienylbenzothiadiazole (APFO3,[68] PFTBT[69]) blended with [60]PCBM are widely investigated and reach efficiencies up to 4% (Figure 1.6). The last years, small band gap polymers (E_g<1.7 *e*V) are an attractive topic for polymer solar cells focusing on the strategy of alternating donor and acceptor units in a polymer. This strategy leads to a hybridization of the donor and acceptor energy levels and affords hence smaller band gaps. The most successful combinations of donor/acceptor units today are cyclopentadithiophene (PCPDTBT[70]) and dithienosilole (PSBTBT[71]) with benzothiadiazole, carbazole with dithienylbenzothiadiazole (PCDTBT[17]), and benzodithiophene with thienothiophene (PTB7[16]), each mixed with [70]PCBM resulting in efficiencies above 5% (Figure 1.6). A more complete review of recent progress on small band gap polymers is presented by Bundgaard *et al.* and Kroon *et al.*[72-73] The combination of a wide and a small band gap polymer in a tandem configuration enables coverage of the visible and near-infrared range of the solar spectrum and improved use of the photon energy.

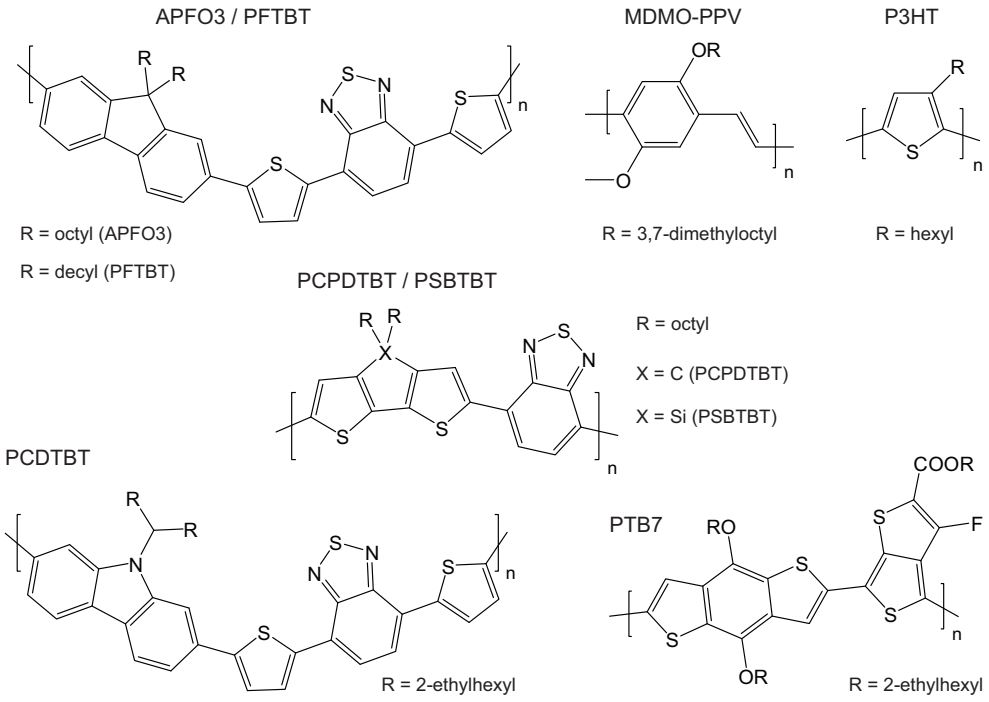

Figure 1.6 Molecular structure of widely investigated wide band gap polymers (P3HT, MDMO-PPV, APFO3, and PFTBT) and small band gap polymers (PCPDTBT, PSBTBT, PCDTBT, and PTB7) which are highly efficient in polymer solar cells.

The layered structure of a common solar cell facilitates the commercially most interesting two-terminal series configuration by stacking two active layers (Figure 1.5b). By Kirchhoff's law, equal currents flow through the subcells and the voltage is a summation of the voltages of the subcells. The active layers are separated by an intermediate contact. Generally, this contact consists of an electron transporting (ET) layer, collecting electrons from one subcell, and a hole transporting (HT) layer, collecting holes from the other subcell. To avoid voltage losses at ET/HT interface, these opposite charges have to meet at the same energy level. Further requirements for the intermediate contact are transparency and—in case of solution processing—it is important that these layers prevent impairing of the first active layer during deposition of the second active layer.

The energy band diagram of a polymer tandem solar cell under V_{oc} conditions is shown in Figure 1.7. The energy levels of ET and HT layer align with $LUMO_{acceptor}$ and $HOMO_{donor}$ respectively. At the interface of ET and HT layer the levels also align to minimize the voltage loss. Modifying the thickness of these layers redistributes the optical electric field inside the solar cell enabling an extra tool for optimizing tandem solar cells.[74-76] At the interface between ET and HT layer, the electrons extracted from the front cell can recombine with the holes collected from the back cell. Polymer (PEDOT:PSS[77-80]) and metal oxide (NiO,[81] MoO_3,[82-87] V_2O_5,[88-89] WO_3,[90-91] ITO[92-93]) based HT layers are widely used in single junction and polymer tandem solar cells, while ZnO,[78,83,94-96] TiO_2[58,80,97-98] and Cs_2CO_3[99-101] are commonly applied as ET layer.

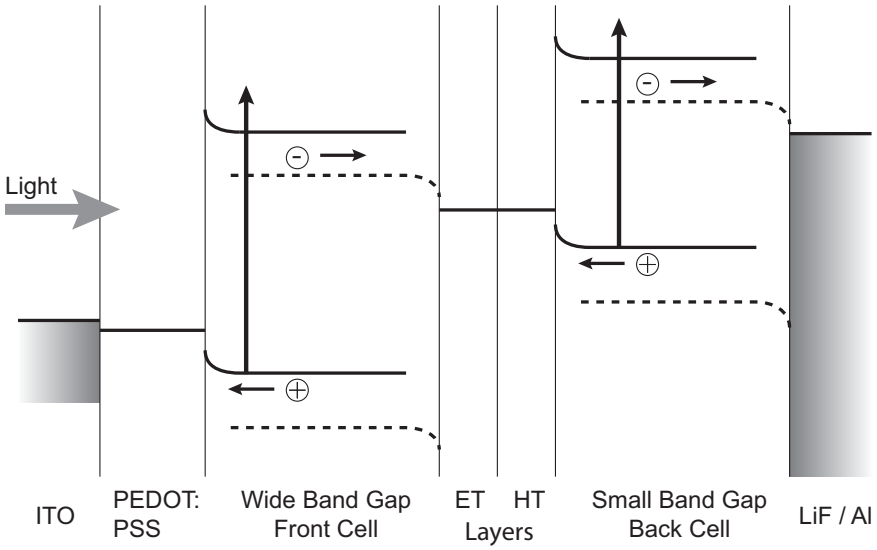

Figure 1.7 Energy band diagram of a polymer tandem solar cell under V_{oc} conditions.

1.5 Literature on organic and polymer tandem solar cells with vacuum processed recombination layers

Hadipour *et al.* and Ameri *et al.* have published comprehensive reviews on the recent progress in organic and polymer tandem solar cells.[61,102] Here, we present a brief summary of recent developments.

In 1990, Hiramoto *et al.* reported on the first organic tandem solar cell stacking two identical small molecule subcells (Me-PTC/H_2Pc).[103] To provide effective recombination, a 2 nm gold layer was evaporated between the subcells. In 2002, Yakimov and Forrest presented an identical approach with comparable small molecules (CuPc/PTCBI) stacking two, three, and five subcells resulting in a V_{oc} that was almost the summation of the V_{oc}s of the subcells.[104] Ultrathin (~0.5 nm) layers of Ag clusters were placed between each subcell to serve as recombination centers. In 2004, Xue *et al.* improved the device efficiency up to 5.7% by using a hybrid planar mixed heterojunction where a blend of donor and acceptor molecules was co-evaporated and sandwiched between homogeneous donor and acceptor layers.[105] The same year, Drechsel *et al.* and Männig *et al.* introduced the p-i-n type heterojunction architecture with doped ET and HT layers differing from the materials in the active layer.[106-107] Tuning the thickness of the ET and HT layer layers enabled the optimization of optics where these layers can act as an optical spacer.[74] Simultaneously, Triyana *et al.* attempted to optimize a triple junction solar cell by modifying the type of metal clusters together with the order of donor and acceptor and by fine-tuning the thickness of the middle subcell.[108-109] In 2007, Cheyns *et al.* studied different metals as efficient recombination centers.[110] Recently, Schueppel *et al.* have shown that a high doping level in the ET and HT layer allows for omitting the metal clusters to obtain efficient conversion contacts.[76]

The next step towards polymer tandem solar cells was reported in 2006 by Dennler *et al.* who stacked two different subcells with different absorption spectra.[111] The first subcell was a solution processed diffused bilayer P3HT:[60]PCBM and second a ZnPc:C_{60} based subcell separated by evaporated ET and HT layers based on C_{60} and ZnPc with a 1 nm Au recombination layer in between, resulting in a 2.3% efficiency. The V_{oc} of the tandem was the addition of the V_{oc}s of the subcells. Later, several authors used a similar approach with an intermediate layer based on doped small molecule layers, metal oxides, and metal carbonates.[82,87,90,99,112]

The first tandem cell composed of two polymer subcells was presented by Kawano *et al.* in 2005 by stacking two MDMO-PPV:[60]PCBM subcells with an ITO (sputtered)/PEDOT:PSS (spin cast) intermediate layer.[92] Sakai *et al.* deposited MoO_3 on a sputtered ITO layer to separate a P3HT:[60]PCBM subcell from a P3HT:[70]PCBM subcell, resulting in a 5.1% polymer tandem cell.[93] The triple cell reported by Zhoa *et al.* stacking three P3HT:[60]PCBM subcells separated by Al/MoO_3 resulted in a V_{oc} of 1.73 V.[113]

The polymer tandem solar cell shown by Hadipour *et al.* in 2006 consisted of subcells with complementary absorption spectra.[79] The intermediate contact was a combination of evaporated metals. Later, Hadipour *et al.* introduced an embedded spacer in the stack, resulting in a four-terminal device allowing for arbitrary series or parallel connection of the two subcells.[75] By varying the thickness of the spacer layer, the transmission of the front cell and spacer were tuned to maximize the absorption in the back cell.

More parallel constructions were proposed by combining a subcell with a common structure and an inverted subcell in a three-terminal solar cell. Guo *et al.* proposed a MoO_3/Al/Ag/MoO_3 middle contact resulting in a 3.1% parallel tandem cell, while Sista *et al.* constructed a 4.8% device with a PEDOT:PSS/Au/V_2O_5 intermediate contact.[89,114]

1.6 Aim and scope of the thesis

All the above examples from literature require an evaporation or sputter step in vacuum to accomplish ET and HT layers. Solution processed ET and HT layers, however, are more interesting because printing techniques are less time and energy consuming and eventually allow roll-to-roll production.[115-116] The aim of this thesis is to develop polymer tandem solar cells processed from solution. This thesis explores the fabrication, optimization, modeling, and characterization of polymer tandem solar cells.

1.7 Recent progress of solution processed polymer tandem solar cells during the realization of the thesis

In the last four years during the realization of this thesis several improvements and alternatives for polymer tandem solar cells processed from solution appeared in literature. In 2007, Kim *et al.* reported on a 6.5% efficient tandem cell with PCPDTBT:[60]PCBM as small band gap front cell and P3HT:[70]PCBM as wide band gap back cell.[80] These two materials cover the solar spectrum up to 900 nm. The two subcells were separated by TiO_x deposited via a sol-gel technique and a spin cast layer of highly conductive PEDOT:PSS. An extra TiO_x layer functioning as an optical spacer to optimize the absorption in both active layers was deposited between the back cell and the reflective electrode. The additional current generation in the back cell caused by the use of highly conductive PEDOT:PSS assisted the performance of the tandem cell as was demonstrated by Sista *et al.* in 2009.[58] A similar device was presented with a P3HT:[70]PCBM wide band gap front cell and PSBTBT:[70]PCBM small band gap back cell separated by a TiO_2/PEDOT:PSS intermediate contact. An ultrathin Al layer was evaporated on top of the front cell prior to the deposition of TiO_2 to improve the wettability and the electrical contact. To identify the beneficial effect of the highly conductive PEDOT:PSS, two dispersions of PEDOT:PSS with different conductivity were compared. The highly conductive PEDOT:PSS resulted in a higher J_{sc} and hence efficiency. However, by redefining the effective active area by scratching along the Al electrode, the efficiencies of tandem cells with different PEDOT:PSS dispersions were similar. A 5.8% polymer tandem solar cell was obtained.

Alternative constructions avoiding processing difficulties of tandem solar cells were presented using independent subcells. Shrotriya and coworkers developed a semitransparent back electrode (LiF/Al/Au) for the front cell in order to pile up two discrete single junction solar cells.[117] Tvingstedt *et al.* and Rim *et al.* proposed simultaneously a folded reflective tandem device enabling either parallel or series connection.[118-119] An enhanced path length upon tilting, light trapping upon multiple reflections and enabling complementary absorption spectra on both sides of the V-shaped geometry upon reflection of non-absorbed light, are three major benefits according to the authors.

1.8 Outline of the thesis

The objective of this thesis is to fabricate, optimize, and characterize polymer tandem solar cells processed from solution.

As a first step we developed an electron transporting layer which could be deposited from solution on top of an active layer based on ZnO nanoparticles (Chapter 2). Therefore, at first we sought for a solvent which was innocuous to the active layer, yet gave a sufficient wetting. The ET layer incorporated in solar cells between the active layer and the reflective electrode functioned as optical spacer which was studied in detail with optical modeling. Subsequently, we investigated a suitable hole transporting layer (Chapter 3). A pH neutral dispersion of PEDOT could be spin cast on the ZnO ET layer enabling the fabrication of wet processed polymer tandem solar cells. Photodoping of ZnO was required to obtain an Ohmic contact between the two layers of the intermediate contact and the accompanying mechanism is described in depth.

For achieving efficient polymer tandem solar cells, the combination of wide and small band gap polymers is inevitable. Therefore, we examined a novel small band gap polymer based on diketopyrrolopyrrole as acceptor unit where the choice of solvent and the processing conditions determine the morphology of the active layer and hence the performance of the solar cell (Chapter 4). In combination with [70]PCBM we obtained a 4.0% efficient solar cell. In the following step we combined this small band gap polymer with a wide band gap polymer, reaching a high V_{oc} when blended with [60]PCBM, in a polymer tandem solar cell and endeavored to optimize these tandem cells (Chapter 5). The multiparameter optimization process involved an optical and electrical analysis of the subcells in the tandem structure. The parameters of the experimental 4.9% efficient device, where the current density generating capacities of the subcells were unmatched, corresponded well with the predicted value.

An accurate characterization of this two-terminal solar cell requires a good approximation of the spectral response of the tandem solar cell to calculate the mismatchfactor (*M*) and the *EQE*s of the subcells. We developed an advanced technique of fine-tuning the optical and electrical bias on the tandem cell based on single junction “dummy” cells, identical to the tandem subcell, and on the absorption spectra of the active layers in the stack obtained via optical modeling (Chapter 6). This technique also enables the measurement of the *J–V* characteristics of the individual subcells in the tandem cell (Chapter 7).

1.9 References

[1] Smil V. *Energy at the crossroads : global perspectives and uncertainties* **2003**, p. 241.
[2] EUROPA **2007** *MEMO/07/02* World Energy Technology Outlook to 2050.
[3] Becquerel A.E. *Comp. Rend.* **1839**, *9*, 145.
[4] Adams W.G. and Day R.E. *Proc. R. Soc.* **1877**, *A25*, 113.
[5] Rappaport P. *RCA Rev.* **1959**, *20*, 373.
[6] Wolf M. *Proc. Power Sources Symp.* **1972**, *25*, 120.
[7] Chapin D.M., Fuller C.S. and Pearson G.L. *J. Appl. Phys.* **1954**, *25*, 676.
[8] Green M.A., Emery K., Hishikawa Y. and Warta W. *Prog. Photovoltaics* **2009**, *17*, 320.
[9] Zhao J.H., Wang A.H., Green M.A. and Ferrazza F. *Appl. Phys. Lett.* **1998**, *73*, 1991.
[10] Chiang C.K., Fincher C.R., Park Y.W., Heeger A.J., Shirakawa H., Louis E.J., Gau S.C. and MacDiarmid A.G. *Phys. Rev. Lett.* **1977**, *39*, 1098.
[11] Shirakawa H., Louis E.J., MacDiarmid A.G., Chiang C.K. and Heeger A.J. *J. Chem. Soc.-Chem. Comm.* **1977**, 578.
[12] Shaheen S.E., Ginley D.S. and Jabbour G.E. *MRS Bull.* **2005**, *30*, 10.
[13] Chen H.-Y., Hou J., Zhang S., Liang Y., Yang G., Yang Y., Yu L., Wu Y. and Li G. *Nature Photon.* **2009**, *3*, 649.
[14] Hou J., Chen H.-Y., Zhang S., Chen R.I., Yang Y., Wu Y. and Li G. *J. Am. Chem. Soc.* **2009**, *131*, 15586.
[15] Liang Y., Feng D., Wu Y., Tsai S.-T., Li G., Ray C. and Yu L. *J. Am. Chem. Soc.* **2009**, *131*, 7792.
[16] Liang Y., Xu Z., Xia J., Tsai S.-T., Wu Y., Li G., Ray C. and Yu L. *Adv. Mater.* **2010**, published online, doi: 10.1002/adma.200903528.
[17] Park S.H., Roy A., Beaupré S., Cho S., Coates N., Moon J.S., Moses D., Leclerc M., Lee K. and Heeger A.J. *Nature Photon.* **2009**, *3*, 297.
[18] Koster L.J.A., Mihailetchi V.D. and Blom P.W.M. *Appl. Phys. Lett.* **2006**, *88*, 093511.
[19] Scharber M.C., Mühlbacher D., Koppe M., Denk P., Waldauf C., Heeger A.J. and Brabec C.J. *Adv. Mater.* **2006**, *18*, 789.
[20] Benanti T.L. and Venkataraman D. *Photosynth. Res.* **2006**, *87*, 73.
[21] Dennler G., Lungenschmied C., Neugebauer H., Sariciftci N.S. and Labouret A. *J. Mater. Chem.* **2005**, *20*, 3224.
[22] Forrest S.R. *MRS Bull.* **2005**, *30*, 28.
[23] Hoppe H. and Sariciftci N.S. *J. Mater. Res.* **2004**, *19*, 1924.
[24] Tang C.W. *Appl. Phys. Lett.* **1986**, *48*, 183.
[25] Haugeneder A., Neges M., Kallinger C., Spirkl W., Lemmer U., Feldmann J., Scherf U., Harth E., Gügel A. and Müllen K. *Phys. Rev. B* **1999**, *59*, 15346.
[26] Janssen R.A.J., Hummelen J.C. and Sariciftci N.S. *MRS Bull.* **2005**, *30*, 33.
[27] Markov D.E., Hummelen J.C., Blom P.W.M. and Sieval A.B. *Phys. Rev. B* **2005**, *72*, 045216.
[28] Shaw P.E., Ruseckas A. and Samuel I.D.W. *Adv. Mater.* **2008**, *20*, 3516.
[29] Halls J.J.M., Walsh C.A., Greenham N.C., Marseglia E.A., Friend R.H., Moratti S.C. and Holmes A.B. *Nature* **1995**, *376*, 498.
[30] Yu G., Gao J., Hummelen J.C., Wudl F. and Heeger A.J. *Science* **1995**, *270*, 1789.
[31] Brabec C.J., Sariciftci N.S. and Hummelen J.C. *Adv. Funct. Mater.* **2001**, *11*, 15.
[32] Dennler G., Scharber M.C. and Brabec C.J. *Adv. Mater.* **2009**, *21*, 1323.
[33] Thompson B.C. and Fréchet J.M.J. *Angew. Chem.-Int. Edit.* **2008**, *47*, 58.
[34] Hummelen J.C., Knight B.W., LePeq F., Wudl F., Yao J. and Wilkins C.L. *J. Org. Chem.* **1995**, *60*, 532.
[35] Wienk M.M., Kroon J.M., Verhees W.J.H., Knol J., Hummelen J.C., van Hal P.A. and Janssen R.A.J. *Angew. Chem.-Int. Edit.* **2003**, *42*, 3371.
[36] Brabec C.J., Shaheen S.E., Winder C., Sariciftci N.S. and Denk P. *Appl. Phys. Lett.* **2002**, *80*, 1288.

[37] Ahlswede E., Hanisch J. and Powalla M. *Appl. Phys. Lett.* **2007**, *90*, 163504.
[38] Jönsson S.K.M., Carlegrim E., Zhang F., Salaneck W.R. and Fahlman M. *Jpn. J. Appl. Phys.* **2005**, *44*, 3695.
[39] Jönsson S.K.M., Salaneck W.R. and Fahlman M. *J. Appl. Phys.* **2005**, *98*, 014901.
[40] Lee D., Park J., Noh S., Kim J., Lee S. and Lee C. *Thin Solid Films* **2009**, *518*, 541.
[41] Singh V., Thakur A.K., Pandey S.S., Takashima W. and Kaneto K. *Org. Electron.* **2008**, *9*, 790.
[42] Singh V., Thakur A.K., Pandey S.S., Takashima W. and Kaneto K. *Jpn. J. Appl. Phys.* **2008**, *47*, 1251.
[43] van Gennip W.J.H., van Duren J.K.J., Thune P.C., Janssen R.A.J. and Niemantsverdriet J.W. *J. Chem. Phys.* **2002**, *117*, 5031.
[44] American Society for Testing and Materials (ASTM) Standard G173-03. Source: http://rredc.nrel.gov/solar/spectra/am1.5/.
[45] Peumans P., Uchida S. and Forrest S.R. *Nature* **2003**, *425*, 158.
[46] Emery K.A. *Appl. Phys. Lett.* **2007**, *91*, 266101.
[47] Gilot J., Wienk M.M. and Janssen R.A.J. *Nature Mater.* **2007**, *6*, 704.
[48] Riede M.K., Mueller T., Männig B., Leo K., Sylvester-Hvid K.O., Zimmermann B., Niggemann M. and Gombert A. *Appl. Phys. Lett.* **2008**, *92*, 076101.
[49] Chen M.-H., Hou J., Hong Z., Yang G., Sista S., Chen L.-M. and Yang Y. *Adv. Mater.* **2009**, *21*, 4238.
[50] Hau S.K., Yip H.-L., Ma H. and Jen A.K.Y. *Appl. Phys. Lett.* **2008**, *93*, 233304.
[51] Li G., Shrotriya V., Huang J., Yao Y., Moriarty T., Emery K. and Yang Y. *Nature Mater.* **2005**, *4*, 864.
[52] Kroon J.M., Wienk M.M., Verhees W.J.H. and Hummelen J.C. *Thin Solid Films* **2002**, *403-404*, 223.
[53] Shrotriya V., Li G., Yao Y., Moriarty T., Emery K. and Yang Y. *Adv. Funct. Mater.* **2006**, *16*, 2016.
[54] Emery K.A. and Osterwald C.R. *Sol .Cells* **1986**, *17*, 253.
[55] Osterwald C.R. *Sol. Cells* **1986**, *18*, 269.
[56] Cravino A., Schilinsky P. and Brabec C.J. *Adv. Funct. Mater.* **2007**, *17*, 3906.
[57] Kim M.-S., Kang M.-G., Guo L.J. and Kim J. *Appl. Phys. Lett.* **2008**, *92*, 133301.
[58] Sista S., Park M.-H., Hong Z., Wu Y., Hou J., Kwan W.L., Li G. and Yang Y. *Adv. Mater.* **2009**, *22*, 380.
[59] Veldman D., Meskers S.C.J. and Janssen R.A.J. *Adv. Funct. Mater.* **2009**, *19*, 1939.
[60] Shockley W. and Queisser H.J. *J. Appl. Phys.* **1961**, *32*, 510.
[61] Ameri T., Dennler G., Lungenschmied C. and Brabec C.J. *Energy Environ. Sci.* **2009**, *2*, 347.
[62] De Vos A. *J. Phys. D: Appl. Phys.* **1980**, *13*, 839.
[63] Bijleveld J.C., Shahid M., Gilot J., Wienk M.M. and Janssen R.A.J. *Adv. Funct. Mater.* **2009**, *19*, 3262.
[64] Dennler G., Scharber M., Ameri T., Denk P., Forberich K., Waldauf C. and Brabec C.J. *Adv. Mater.* **2008**, *20*, 579.
[65] Van Eersel H., Gilot J., Wienk M.M. and Janssen R.A.J. **2010**, unpublished results.
[66] Ma W., Yang C., Gong X., Lee K. and Heeger A.J. *Adv. Funct. Mater.* **2005**, *15*, 1617.
[67] Shaheen S.E., Brabec C.J., Sariciftci N.S., Padinger F., Fromherz T. and Hummelen J.C. *Appl. Phys. Lett.* **2001**, *78*, 841.
[68] Svensson M., Zhang F., Veenstra S.C., Verhees W.J.H., Hummelen J.C., Kroon J.M., Inganäs O. and Andersson M.R. *Adv. Mater.* **2003**, *15*, 988.
[69] Moet D.J.D., Slooff L.H., Kroon J.M., Chevtchenko S.S., Loos J., Koetse M.M., Sweelssen J. and Veenstra S.C. *Mater. Res. Soc. Symp. Proc.* **2006**, *974E*, CC03.
[70] Peet J., Kim J.Y., Coates N.E., Ma W.L., Moses D., Heeger A.J. and Bazan G.C. *Nature Mater.* **2007**, *6*, 497.
[71] Hou J., Chen H.-Y., Zhang S., Li G. and Yang Y. *J. Am. Chem. Soc.* **2008**, *130*, 16144.
[72] Bundgaard E. and Krebs F.C. *Sol. Energy Mater. Sol. Cells* **2007**, *91*, 954.
[73] Kroon R., Lenes M., Hummelen J.C., Blom P.W.M. and De Boer B. *Polym. Rev.* **2008**, *48*, 531.
[74] Drechsel J., Männig B., Kozlowski F., Pfeiffer M., Leo K. and Hoppe H. *Appl. Phys. Lett.* **2005**, *86*, 244102.
[75] Hadipour A., de Boer B. and Blom P.W.M. *J. Appl. Phys.* **2007**, *102*, 074506.

[76] Schueppel R., Timmreck R., Allinger N., Mueller T., Furno M., Uhrich C., Leo K. and Riede M. *J. Appl. Phys.* **2010**, *107*, 044503.
[77] Arias A.C., Granstrom M., Petritsch K. and Friend R.H. *Synth. Met.* **1999**, *102*, 953.
[78] Gilot J., Wienk M.M. and Janssen R.A.J. *Appl. Phys. Lett.* **2007**, *90*, 143512.
[79] Hadipour A., de Boer B., Wildeman J., Kooistra F.B., Hummelen J.C., Turbiez M.G.R., Wienk M.M., Janssen R.A.J. and Blom P.W.M. *Adv. Funct. Mater.* **2006**, *16*, 1897.
[80] Kim J.Y., Lee K., Coates N.E., Moses D., Nguyen T.-Q., Dante M. and Heeger A.J. *Science* **2007**, *317*, 222.
[81] Irwin M.D., Buchholz D.B., Hains A.W., Chang R.P.H. and Marks T.J. *Proc. Natl. Acad. Sci.* **2008**, *105*, 2783.
[82] Chen F.-C. and Lin C.-H. *J. Phys. D: Appl. Phys.* **2010**, *43*, 025104.
[83] Kyaw A.K.K., Sun X.W., Jiang C.Y., Lo G.Q., Zhao D.W. and Kwong D.L. *Appl. Phys. Lett.* **2008**, *93*, 221107.
[84] Tao C., Ruan S., Zhang X., Xie G., Shen L., Kong X., Dong W., Liu C. and Chen W. *Appl. Phys. Lett.* **2008**, *93*, 193307.
[85] Tetsuro H., Takeshi S., Varutt K., Hiroki M., Jun S., Hitoshi K., Akihiko F. and Masanori O. *Thin Solid Films* **2009**, *518*, 522.
[86] Zhao D.W., Liu P., Sun X.W., Tan S.T., Ke L. and Kyaw A.K.K. *Appl. Phys. Lett.* **2009**, *95*, 153304.
[87] Zhao D.W., Sun X.W., Jiang C.Y., Kyaw A.K.K., Lo G.Q. and Kwong D.L. *Appl. Phys. Lett.* **2008**, *93*, 083305.
[88] Li G., Chu C.W., Shrotriya V., Huang J. and Yang Y. *Appl. Phys. Lett.* **2006**, *88*, 253503.
[89] Sista S., Hong Z., Park M.-H., Xu Z. and Yang Y. *Adv. Mater.* **2010**, *22*, E77.
[90] Janssen A.G.F., Riedl T., Hamwi S., Johannes H.H. and Kowalsky W. *Appl. Phys. Lett.* **2007**, *91*, 073519.
[91] Tao C., Ruan S., Xie G., Kong X., Shen L., Meng F., Liu C., Zhang X., Dong W. and Chen W. *Appl. Phys. Lett.* **2009**, *94*, 043311.
[92] Kawano K., Ito N., Nishimori T. and Sakai J. *Appl. Phys. Lett.* **2006**, *88*, 073514.
[93] Sakai J., Kawano K., Yamanari T., Taima T., Yoshida Y., Fujii A. and Ozaki M. *Sol. Energy Mater. Sol. Cells* **2010**, *94*, 376.
[94] Gilot J., Barbu I., Wienk M.M. and Janssen R.A.J. *Appl. Phys. Lett.* **2007**, *91*, 113520.
[95] White M.S., Olson D.C., Shaheen S.E., Kopidakis N. and Ginley D.S. *Appl. Phys. Lett.* **2006**, *89*, 143517.
[96] Yip H.-L., Hau S.K., Baek N.S. and Jen A.K.Y. *Appl. Phys. Lett.* **2008**, *92*, 193313.
[97] Kim J.Y., Kim S.H., Lee H.-H., Lee K., Ma W., Gong X. and Heeger A.J. *Adv. Mater.* **2006**, *18*, 572.
[98] Kuwabara T., Sugiyama H., Yamaguchi T. and Takahashi K. *Thin Solid Films* **2009**, *517*, 3766.
[99] Bong J.L., Hyo J.K., Won-ik J. and Jang-Joo K. *Sol. Energy Mater. Sol. Cells* **2010**, *94*, 542.
[100] Chen F.-C., Wu J.-L., Yang S.S., Hsieh K.-H. and Chen W.-C. *J. Appl. Phys.* **2008**, *103*, 103721.
[101] Liao H.-H., Chen L.-M., Xu Z., Li G. and Yang Y. *Appl. Phys. Lett.* **2008**, *92*, 173303.
[102] Hadipour A., de Boer B. and Blom P.W.M. *Adv. Funct. Mater.* **2008**, *18*, 169.
[103] Hiramoto M., Suezaki M. and Yokoyama M. *Chem. Lett.* **1990**, 327.
[104] Yakimov A. and Forrest S.R. *Appl. Phys. Lett.* **2002**, *80*, 1667.
[105] Xue J., Uchida S., Rand B.P. and Forrest S.R. *Appl. Phys. Lett.* **2004**, *85*, 5757.
[106] Drechsel J., Männig B., Kozlowski F., Gebeyehu D., Werner A., Koch M., Leo K. and Pfeiffer M. *Thin Solid Films* **2004**, *451-452*, 515.
[107] Männig B., Drechsel J., Gebeyehu D., Simon P., Kozlowski F., Werner A., Li F., Grundmann S., Sonntag S., Koch M., Leo K., Pfeiffer M., Hoppe H., Meissner D., Sariciftci N.S., Riedel I., Dyakonov V. and Parisi J. *Appl. Phys. A-Mater. Sci. Process.* **2004**, *79*, 1.
[108] Triyana K., Yasuda T., Fujita K. and Tsutsui T. *Jpn. J. Appl. Phys.* **2004**, *43*, 2352.
[109] Triyana K., Yasuda T., Fujita K. and Tsutsui T. *Thin Solid Films* **2005**, *477*, 198.

[110] Cheyns D., Gommans H., Odijk M., Poortmans J. and Heremans P. *Sol. Energy Mater. Sol. Cells* **2007**, *91*, 399.
[111] Dennler G., Prall H.-J., Koeppe R., Egginger M., Autengruber R. and Sariciftci N.S. *Appl. Phys. Lett.* **2006**, *89*, 073502.
[112] Colsmann A., Junge J., Kayser C. and Lemmer U. *Appl. Phys. Lett.* **2006**, *89*, 203506.
[113] Zhao D.W., Sun X.W., Jiang C.Y., Kyaw A.K.K., Lo G.Q. and Kwong D.L. *IEEE Electron Device Lett.* **2009**, *30*, 490.
[114] Guo X., Liu F., Yue W., Xie Z., Geng Y. and Wang L. *Org. Electron.* **2009**, *10*, 1174.
[115] Shaheen S.E., Radspinner R., Peyghambarian N. and Jabbour G.E. *Appl. Phys. Lett.* **2001**, *79*, 2996.
[116] Tuomikoski M., Suhonen R., Vaelimaeki M., Maaninen T., Maaninen A., Sauer M., Rogin P., Mennig M., Heusing S., Puetz J. and Aegerter M.A. *SPIE-Int. Soc. Opt. Phot. Proc.* **2006**, *6192*, 619204.
[117] Shrotriya V., Wu E.H.-E., Li G., Yao Y. and Yang Y. *Appl. Phys. Lett.* **2006**, *88*, 064104.
[118] Rim S.-B., Zhao S., Scully S.R., McGehee M.D. and Peumans P. *Appl. Phys. Lett.* **2007**, *91*, 243501.
[119] Tvingstedt K., Andersson V., Zhang F. and Inganäs O. *Appl. Phys. Lett.* **2007**, *91*, 123514.

Chapter 2

Zinc oxide as electron transporting layer and optical spacer in polymer solar cells*

Abstract

As a first step towards polymer tandem solar cells, a solution processed electron transporting layer is developed. Spin casting zinc oxide nanoparticles from acetone solution on photoactive layers, composed of conjugated polymers mixed with [6,6]-phenyl-C_{61}-butyric acid methyl ester ([60]PCBM), results in a closed ZnO electron transporting layer, without affecting the integrity of the photoactive layer. For poly(3-hexylthiophene) (P3HT):[60]PCBM bulk heterojunction solar cells, the additional ZnO layer between the photoactive layer and the reflective electrode results in an improved current density and performance as a result of a redistribution of the optical electric field. Theoretical calculations using optical modeling are in excellent agreement with experimental results and support the conclusion that the increased performance is an optical effect.

* Part of this work has been published:
Gilot J., Barbu I., Wienk M.M. and Janssen R.A.J. *Appl. Phys. Lett.* **2007**, *91*, 113520.
Gilot J., Wienk M.M. and Janssen R.A.J. *Appl. Phys. Lett.* **2007**, *90*, 143512.

2.1 Introduction

In two-terminal series connected tandem cells the two active layers are separated by an intermediate contact consisting of an electron and a hole transporting layer to extract the corresponding charges from an active layer. Starting from the common cell configuration (substrate/high work function electrode/active layer/low work function electrode) the electrode on top of the first active layer must be replaced by an electron transporting (ET) layer. This layer has to exhibit several properties to be applicable in tandem solar cells. The purpose of the ET layer is to collect electrons from the photoactive layer and to block holes and excitons. The preferred ET layer shows a high electron affinity and mobility and its conduction band aligns closely with the lowest unoccupied molecular orbital (LUMO) of the acceptor material in the active layer to facilitate an Ohmic contact. Preferably, this layer is transparent in the region of absorption of the active layer.

Established ET layers are metal oxides and carbonates. Zinc oxide (ZnO), titanium dioxide (TiO_2) and cesium carbonate (Cs_2CO_3) are used in organic light emitting diodes as hole blocking layers to enhance brightness and efficiency.[1-3] Furthermore, ZnO and TiO_2 have successfully been applied as acceptor material in bilayer and bulk heterojunction polymer solar cells demonstrating their good electron accepting and transporting properties.[4-6] ZnO, annealed at elevated temperatures, and electron-beam deposited TiO_2 have also served as low work function electrode in inverted devices.[7-8] Moreover, solution deposited amorphous TiO_x and Cs_2CO_3 layers have been incorporated in solar cells as electron transporting layer.[9-12] This not only leads to an improvement in device performance[10-11]; it also improves the air stability of the devices.[10,13]

Here, we describe the integration of a ZnO ET layer in organic bulk heterojunction solar cells, composed of a π-conjugated polymer mixed with a fullerene derivative ([6,6]-phenyl-C_{61}-butyric acid methyl ester ([60]PCBM or PCBM in short)). We first check the applicability of several solvents to deposit a layer from solution on top of an active layer. Subsequently, the processing of ZnO layers is described followed by polymer solar cells with inserted ZnO layer. The effect of the ZnO layer on the current density of the device was examined by optical modeling.

2.2 Choice of solvent

The choice of the solvent to deposit the ET layer from is very important. The solvent should be innocuous to the active layer and should also wet the surface sufficiently so that the dissolved material can stick to the active layer during spin casting. Several solvents were tested and their effect on the integrity of the photoactive layer was checked by UV/vis absorption spectroscopy.

Common solvents for active layer blends as chloroform, chlorobenzene, toluene, 1,2-dichlorobenzene, 1,2,4-trichlorobenzene, and *o*-xylene are unsuitable for this purpose as the underlying active layer will be dissolved upon deposition of the ET layer. The solubility, especially of the PCBM, turned out to be the largest obstacle. Even solvents that are considered as bad solvents for PCBM could effectively extract all PCBM out of the active layer despite the very low solubility of PCBM in these solvents (cyclohexane, cyclohexanone, and THF). For example, spin casting diisopropylether or heptane on an active layer partly dissolves PCBM and repeating this process eventually completely extracts all PCBM. The removal of PCBM and exposure to a poor solvent for the polymer also invokes crystallization of poly(3-hexylthiophene) (P3HT), as demonstrated by a significant increased and red-shifted absorption (Figure 2.1a).[14] No PCBM extraction was observed for nitrile group containing solvents (acetonitrile, proprionitrile, and butyronitrile), but for these the wetting was insufficient. Of all solvents tested that wet the active layers properly, only acetone and isopropanol left the active layer untouched. Others demonstrated that also methanol, ethanol and 2-ethoxyethanol are suitable media.[2,10,15]

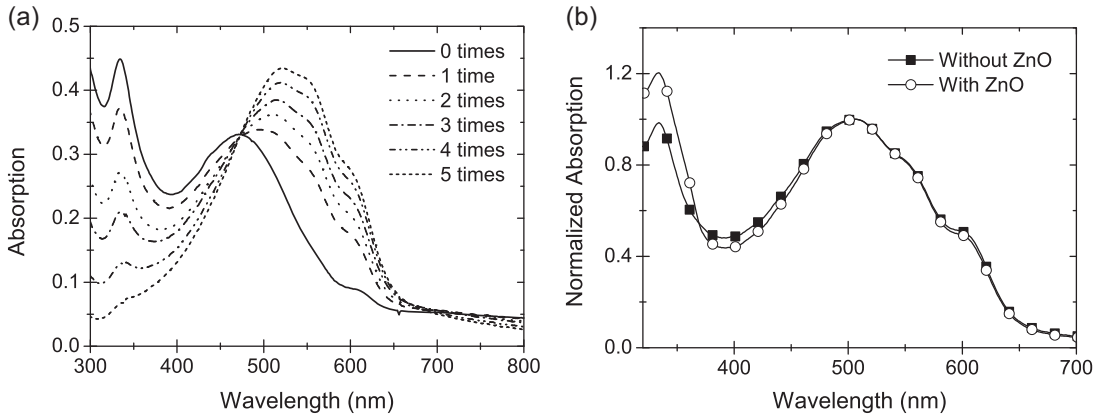

Figure 2.1 UV/vis absorption spectra of a P3HT:PCBM active layer (a) after subsequent spin casting of diisopropylether and (b) without and with a ZnO layer spin cast from acetone (normalized).

2.3 ZnO as electron transporting layer

ZnO closely meets the prerequisite properties of an ideal ET layer. With a band gap of 3.3 *e*V and an accompanying absorption onset at 375 nm it is transparent to most of the solar spectrum.[16-17] The good positioning of the conduction band of ZnO (–4.4 *e*V) makes it well suited as ET layer in combination with PCBM as electron acceptor.[17] ZnO films can be processed from solution in the form of nanoparticles. These ZnO nanoparticles have previously been used successfully as electron acceptor in bulk heterojunction solar cells.[4,18-21]

The synthesis of the crystalline ZnO nanoparticles has been described before[20,22] and results in monodisperse 5 nm diameter nanoparticles (Figure 2.2a) which are soluble in acetone or isopropanol, suitable for ET layer deposition.[23-24] Spin casting ZnO nanoparticles dissolved in acetone (10 mg/ml) on top of an active layer composed of P3HT and PCBM results in a 30 nm smooth closed layer with a peak-to-peak roughness of 10 nm (Figure 2.2b,c). Comparing the absorption spectra before and after deposition of ZnO (Figure 2.1b) shows that the active layer remains intact; as the only difference is the increased absorption below 450 nm.

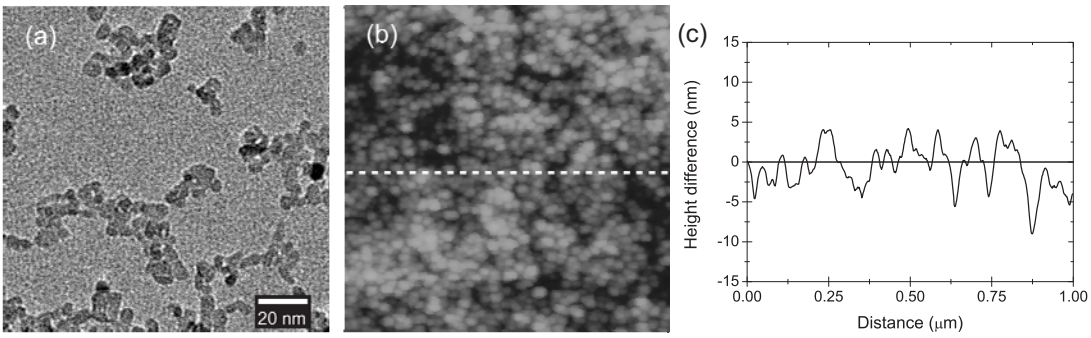

Figure 2.2 (a) Transmission electron microscopy (TEM) image of ZnO nanoparticles. (b) Height image of ZnO nanoparticles on a P3HT:PCBM active layer measured by atomic force microscopy (1 × 1 μm^2, *z*-range is 25 nm). (c) The height difference of a section in the middle of (b).

To determine the effectiveness of ZnO as ET layer, complete solar cells with an extra ZnO layer sandwiched between the active layer and a LiF/Al back electrode were made (Figure 2.3a). Devices with active layers composed of P3HT, poly[2-methoxy-5-(3',7'-dimethyloctyloxy)-*p*-phenylene vinylene] (MDMO-PPV), and poly(5,7-di-2-thienyl-2,3-

bis(3,5-di(2-ethylhexyloxy)phenyl)-thieno[3,4-b]pyrazine)) (PTBEHT) mixed with PCBM resulted in well working devices for different ZnO layer thicknesses (Table 2.1). The open-circuit voltage (V_{oc}) and fill factor (*FF*) remained constant regardless the ZnO layer thickness for devices with identical active layers, demonstrating that these ZnO nanoparticles can be effectively used as ET layer. On the other hand, the short-circuit current density (J_{sc}) for a given active layer fluctuates substantially with varying ZnO layer thicknesses. P3HT:PCBM solar cells with a thin ZnO layer even show an increased J_{sc} and maximum power point (*MPP*), compared to identical cells without the ZnO (Figure 2.3b, Table 2.1).

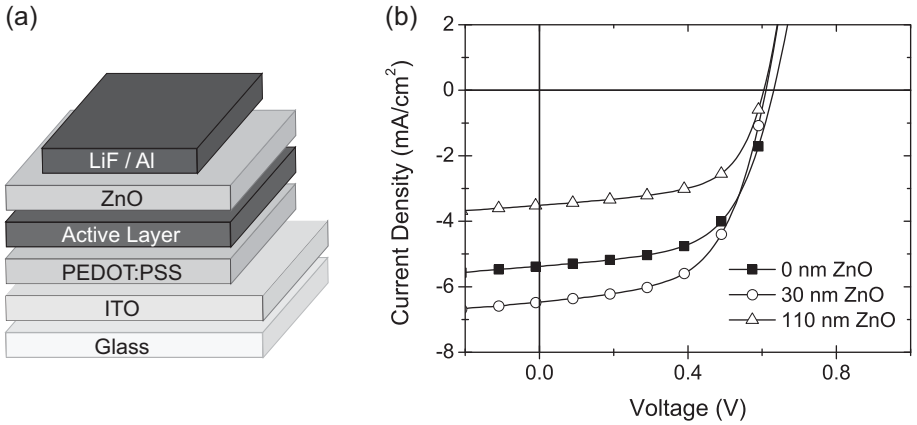

Figure 2.3 (a) Device layout of a polymer solar cell with a ZnO ET layer. (b) Current density to voltage characteristics of P3HT:PCBM bulk heterojunction solar cells with a ZnO ET layer of various thicknesses.

Table 2.1 Solar cell characteristics of polymer:PCBM solar cells without or with a ZnO ET layer.

Polymer	ZnO	Thickness ZnO (nm)	J_{sc} (mA/cm^2)	V_{oc} (V)	*FF*	*MPP* (mW/cm^2)
P3HT (45 nm)	No	—	5.4	0.63	0.59	2.0
	Yes	30	6.5	0.61	0.58	2.3
	Yes	110	3.5	0.60	0.60	1.3
MDMO-PPV (70 nm)	No	—	4.7	0.82	0.57	2.2
	Yes	30	4.0	0.82	0.56	1.8
PTBEHT (85 nm)	No	—	3.6	0.57	0.51	1.1
	Yes	110	2.0	0.55	0.50	0.5

2.4 ZnO as optical spacer

These improvements in J_{sc} can be attributed to an optical spacer effect of the ET layer.[11,25-28] Light absorption within thin active layers can be increased by changing the spatial distribution of the optical electric field inside the device. The optical electric field is the oscillating electric field originating from the incident light. Inserting an extra transparent layer between the active layer and the metal top electrode can place the active layer in a more favorable region of the internal optical electric field. It has been suggested that, besides the optical incoupling effects, the addition of a metal oxide layer could also enhance the performance by creating an extra donor-acceptor interface,[29] or by acting as a hole[10] and exciton blocking layer.[30] The validity of these hypotheses is elucidated here by comparing theoretical and experimental results.

Theoretical analysis by optical modeling is a powerful method, increasingly often used to understand and predict optical effects in polymer solar cells. It is based on the transfer matrix formalism.[31-34] Absorption, transmission, reflection, and phase shift can all be described by the real and imaginary part of the complex refractive index ($\tilde{n} = n + i \cdot k$, with n the refractive index and k the extinction coefficient) of each layer. The optical electric field at each position can be calculated with the resulting system transfer matrix.

Figure 2.4a,b show the calculated optical electric fields for a 40 nm thick P3HT:PCBM layer using wavelength dependent n and k values from literature as described in the experimental section. Without optical spacer, the thin photoactive layer is situated well outside the maximum of the optical electrical field of the relevant wavelengths of light and insertion of a 39 nm layer of ZnO shifts the position of the absorption maximum into the absorbing layer. From these calculations, one would predict a significantly higher photocurrent for such a thin photoactive layer as a result of improved light incoupling.

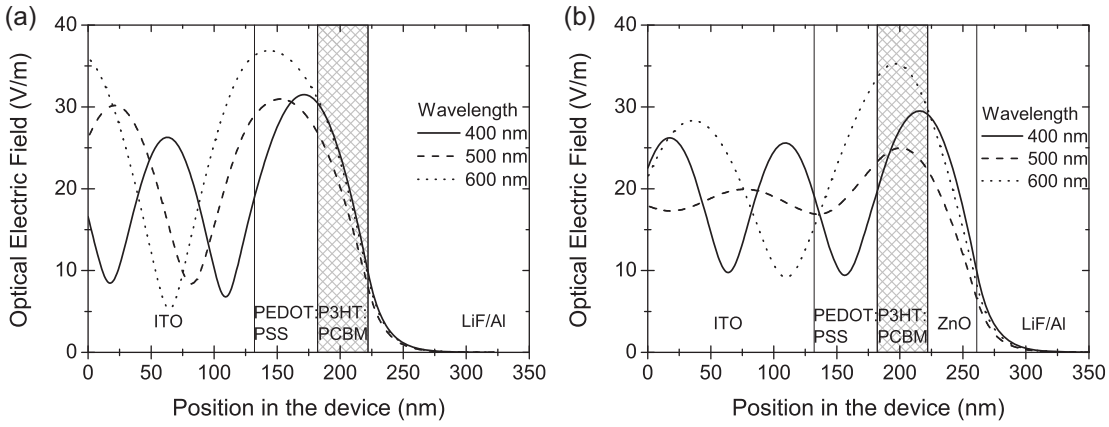

Figure 2.4 The calculated optical electric field for light of different wavelengths in devices with a 40 nm thick active layer, without (a) and with (b) 39 nm ZnO.

To quantify this effect, the maximum obtainable J_{sc} ($J_{sc,max}$) in the active layer was calculated, assuming an internal quantum efficiency (conversion efficiency of absorbed photons to collected charges) of unity and illumination with the AM1.5G solar spectrum at 1000 W/m^2 over a whole range of active layer and optical spacer thicknesses (Figure 2.5a). For bulk heterojunction solar cells based on P3HT:PCBM, the calculated $J_{sc,max}$ oscillates with active layer thickness due to interference effects (Figure 2.5b, solid line). Maxima are observed at 80 nm and 210 nm. By inserting a ZnO layer, these maxima are shifted towards lower layer thicknesses. The extent of this shift corresponds to the thickness of the ZnO layer. Because $J_{sc,max}$ is necessarily zero at zero thickness, the initial increase of the current with layer thickness becomes much steeper upon insertion of a ZnO layer, resulting in a large increase of the maximum obtainable $J_{sc,max}$ for thin active layers. For a 40 nm thick active layer, there is an almost three fold increase by adding a 40 nm ZnO layer (Figure 2.5b). However, for thicker films, ranging from 70 to 130 nm, insertion of an extra layer is expected to be detrimental for the device performance. In this case, the active layer is already in the most effective position without ZnO, and adding the spacer layer shifts it away from the maximum of the optical electric field. Clearly, one would expect the magnitude of the perturbation caused by the ZnO to decrease for thicker layers.

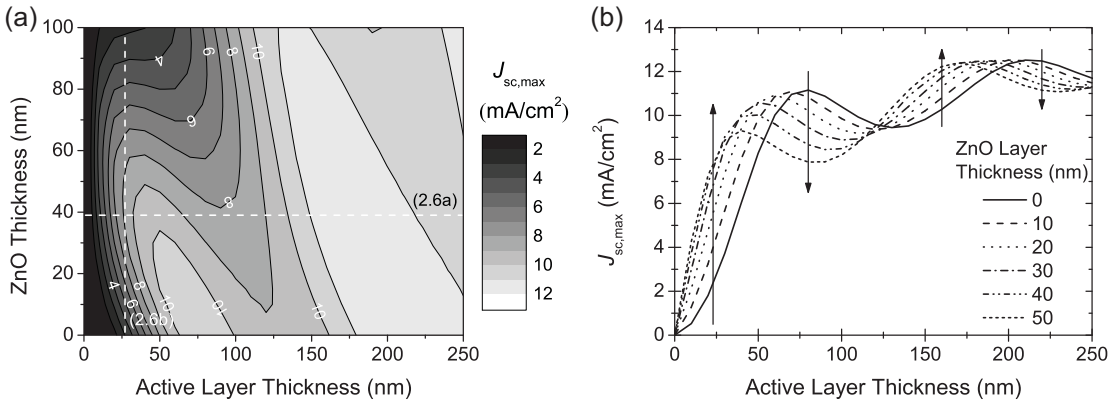

Figure 2.5 (a) Contour plot of $J_{sc,max}$ vs. the active layer and optical spacer thickness, assuming 100% *IQE* and illumination with the AM1.5G solar spectrum (1000 W/m^2). The dotted lines indicate the cross-sections for experimental comparison as shown in Figure 2.6. (b) Calculated active layer thickness dependent $J_{sc,max}$ for different thicknesses of the ZnO layer.

To verify these calculations experimentally, solar cells representing cross-sections of Figure 2.5a with either varying active layer or optical spacer thickness were made. Short-circuit current densities of these cells were determined by convoluting the spectral response with the AM1.5G solar spectrum (1000 W/m^2). On one hand, devices with photoactive layer thicknesses ranging from 27 to 220 nm, without and with a 39 nm thick ZnO spacer layer were made. For active layers less than 60 nm, cells with ZnO give higher J_{sc}s, whereas between 60 nm and 130 nm the devices without spacer generate higher current densities (Figure 2.6a). These crossover points originate from out-of-phase progression of the modulation of the current densities for cells with and without the ZnO layer. On the other hand, devices with a fixed 27 nm thick active layer and optical spacer thicknesses varying from 0 to 77 nm were constructed. The current densities increase to a maximum for 40 to 50 nm of ZnO where J_{sc} is more than doubled compared to a device without optical spacer. For ZnO layers thicker than 50 nm, the J_{sc} reduces again to the level without optical spacer (Figure 2.6b). The periodicity of both experimental curves corresponds excellently to the calculated data.

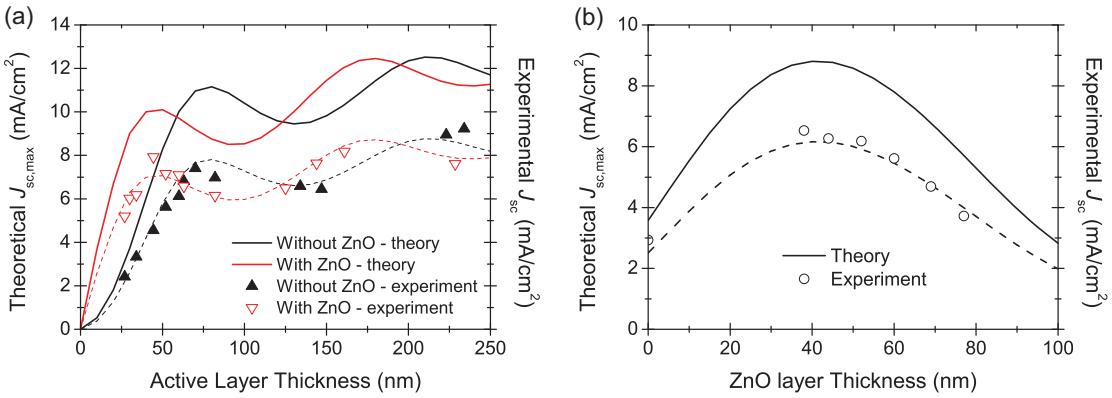

Figure 2.6 Theoretical vs. experimental cross-sections of Figure 2.5a. (a) Active layer thickness dependence of J_{sc} without and with 39 nm ZnO optical spacer. (b) ZnO layer thickness dependence of J_{sc} for a 27 nm thick active layer. The dashed lines are theoretical J_{sc}s with an *IQE* of 0.7 as a guide to the eye.

The good correlation between predicted and measured current densities indicates that the observed effect of the extra ZnO layer can, at least in a qualitative way, be attributed to an optical effect. To further corroborate this, the internal quantum efficiency (*IQE*) was calculated for the devices shown in Figure 2.6a by dividing the measured current densities by the corresponding $J_{sc,max}$ (Figure 2.7).[35-36] This affords invariant *IQE* values of 0.7 ± 0.1 for all cells, irrespective whether it contains a ZnO spacer layer or not. If the ZnO layer would affect more than just the absorption profiles, for example by providing an additional donor-acceptor interface,[29] or by acting as an exciton blocking layer,[30] this would afford higher *IQE* values for cells with ZnO, especially for thin photoactive layers, where the relative contribution of an interface effect should be largest. This experiment indicates, however, that a ZnO layer in P3HT:PCBM cells only significantly affects the incoupling of light and no additional electronic effects need to be considered to explain the moderation of the current densities.

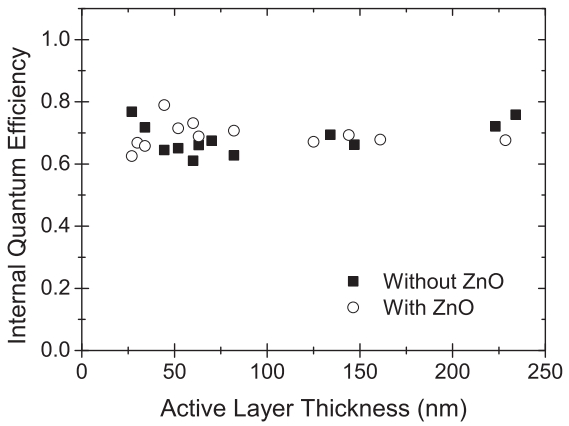

Figure 2.7 Internal quantum efficiencies vs. active layer thickness for solar cells with and without a ZnO spacer layer.

Based on these results, it is clear that the usage of an optical spacer to enhance the *MPP* is only interesting in cases where the active layer thickness is restricted due to limited and/or unbalanced charge transport. For cases where the *IQE* is not decreasing with increasing layer thickness, an optical spacer only complicates the fabrication process for a marginal gain in efficiency.[26]

The same effect is applicable to MDMO-PPV:PCBM and PTBEHT:PCBM solar cells. However, it is not observed in the experiments shown in Table 2.1 because the active layer thickness corresponds to a region where the current density is reduced upon insertion of a ZnO layer which was verified by optical modeling.

2.5 Conclusions

A thin, smooth, and closed film of ZnO nanoparticles can be deposited from acetone solution onto the photoactive layer of bulk heterojunction organic solar cells without affecting the photoactive layer. This ZnO layer fulfills all requirements for an ET layer in tandem cells. Solar cells incorporating such a ZnO layer sandwiched between the active layer and the reflective electrode were working properly for active layers consisting of various polymers with PCBM. Devices based on P3HT:PCBM as active layer even show an increase in $J_{sc,max}$ and *MPP* upon insertion of a thin ZnO layer. This improvement is mainly attributed to a redistribution of the optical electric field inside the device. The ZnO layer functions as an optical spacer by shifting the position of the maximum optical field into the active layer. This hypothesis was verified by comparing the J_{sc} of experimental results with the $J_{sc,max}$ calculated

with optical modeling using the transfer matrix formalism. The periodicity of experimental and theoretical results matches closely both for variation of the active layer and ZnO layer thickness. By inserting a thin ZnO layer, the absorption is significantly enhanced for thin films (<60 nm). For thicker absorbing layers, the effect of the optical spacer is less pronounced. Especially polymer solar cells where the film thickness is limited by a low charge carrier mobility can benefit from an optical spacer.

2.6 Experimental

ZnO synthesis

ZnO nanoparticles were synthesized as follows. $Zn(Ac)_2.2H_2O$ (98+%, Acros) (2.95 g) was dissolved in methanol (125 ml) at 60 ºC under magnetic stirring. Over a period of exactly 10 min., KOH (pellets extra pure, Merck) (1.48 g) dissolved in methanol (65 ml) was added at a constant speed to the zinc acetate solution. After 2 h of reaction at 60 ºC, the solution was cooled down for 2 h to precipitate the solute. After removing the mother liquor, the precipitate was washed with methanol (50 ml). After subsequent stirring for 10 min. and another hour of precipitation, the mother liquor was removed a second time. Fresh methanol (50 ml) was added and the solution was centrifuged. The liquid was decanted and the remaining solid was dissolved completely in acetone after sufficient sonication. The stock solution had a concentration of 70 mg/ml and was transparent with a milky glow.[20]

Devices

For preparing polymer solar cells, precleaned ITO coated substrates (Philips Research) were covered with a 50 nm thick PEDOT:PSS film (Clevios® P VP AI 4083, H.C. Starck, passed a 5.0 µm Whatman Puradisc FP30 syringe filter). The active layer was then deposited on top in air, followed by the possible ZnO layer. After completion of the solution processing, the samples were moved into a glovebox with a nitrogen atmosphere to evaporate 1 nm LiF and 100 nm Al film as top electrode at 6×10^{-6} mbar.

P3HT:PCBM: Poly(3-hexylthiophene) (P3HT) (Rieke Metals) was mixed with PCBM (Solenne BV) in chlorobenzene in a 1:1 ratio at 10 or 15 mg/ml polymer concentration. For the series with varying active layer thickness, the thin films (<100 nm) were obtained from a 10 mg/ml solution at 750-4000 RPM and the thick layers (>100 nm) from a 15 mg/ml solution at 500-800 RPM. The spin speed was 4500 RPM for the series with varying ZnO layer thickness resulting in a 27 nm thick layer. The completed samples were annealed at 140 ºC for 5 min. inside the glovebox before characterization.

MDMO-PPV:PCBM: Poly[2-methoxy-5-(3',7'-dimethyloctyloxy)-*p*-phenylene vinylene] (MDMO-PPV) (TNO) was mixed with PCBM in chlorobenzene in a 1:4 ratio at 3 mg/ml polymer concentration. The spin speed for the active layer was 1500 RPM.

PTBEHT:PCBM: Poly(5,7-di-2-thienyl-2,3-bis(3,5-di(2-ethylhexyloxy)phenyl)-thieno[3,4-b]pyrazine)) (PTBEHT) (synthesized by M.G.R. Turbiez) was mixed with PCBM in chloroform in a 1:4 ratio at 5 mg/ml polymer concentration.[37] The active layer was deposited at a fixed spin speed (3000 RPM).

ZnO: The 39 nm thick ZnO layer on P3HT:PCBM was spin cast from a 10 mg/ml solution at 2000 RPM for the series with varying active layer thickness. For the variation in ZnO layer thickness on P3HT:PCBM a 15 mg/ml solution was used and the spin speed changed between 500-3000 RPM. The ZnO layer on MDMO-PPV:PCBM was deposited at 5000 RPM from a 15 mg/ml solution and on PTBEHT:PCBM at 1500 RPM from a 30 mg/ml solution.

Device characterization

Current density to voltage characteristics were measured with a Keithley 2400 source measurement unit. Illumination was carried out with UV (GG 385) and infrared (KG1) filtered light from an uncalibrated tungsten halogen lamp (750 W/m^2). Because of the arbitrary light source, maximum power points are compared instead of power conversion efficiencies.

Layer thicknesses were measured with a Tencor® P-10 Surface Profiler.

Current densities were determined by convoluting the spectral response with the AM1.5G solar spectrum (1000 W/m^2). During the spectral response measurement, the sample is illuminated by monochromatic (Oriel Cornerstone 130 1/8 m, Newport) light (Halotone halogen lamp, Philips) and the current (measured with a Keithley 2400 source meter) is compared to a calibrated reference silicon solar cell. Devices were kept behind a quartz window in a nitrogen filled box.

Optical modeling

Calculations of the optical electrical field were performed with the Essential Macleod software package (Thin Film Center Inc., Tucson, USA). The optical constants of PEDOT:PSS, P3HT:PCBM and Al were obtained from literature.[38-40] The optical constants of glass and ITO were provided by Thin Film Center and those of ZnO were obtained with ellipsometry measurements.[16]

Apparatus

UV/vis absorption spectra were measured with a Perkin-Elmer Lambda 900 spectrometer. Tapping mode AFM was performed with a Nanoscope Dimension 3100 microscope (Veeco, Digital instruments) using PPP-NCHR probes. TEM images were recorded using a TENCAI G^2 20 transmission electron microscope (FEI Co., The Netherlands) operated at 200 kV.

2.7 References

[1] Bai F., Deng Z., Gao X., Chen X. and Cai Q. *Synth. Met.* **2003**, *137*, 1139.
[2] Huang J., Li G., Wu E., Xu Q. and Yang Y. *Adv. Mater.* **2006**, *18*, 114.
[3] Tan H., Jiang Y., Zhang B., Zhang H., Yao J. and Sun G. *Proc. SPIE-Int. Soc. Opt. Eng.* **2005**, *5632*, 72.
[4] Beek W.J.E., Wienk M.M. and Janssen R.A.J. *Adv. Mater.* **2004**, *16*, 1009.
[5] Breeze A.J., Schlesinger Z., Carter S.A. and Brock P.J. *Phys. Rev. B* **2001**, *64*, 125205.
[6] van Hal P.A., Wienk M.M., Kroon J.M., Verhees W.J.H., Slooff L.H., van Gennip W.J.H., Jonkheijm P. and Janssen R.A.J. *Adv. Mater.* **2003**, *15*, 118.
[7] Glatthaar M., Niggemann M., Zimmermann B., Lewer P., Riede M., Hinsch A. and Luther J. *Thin Solid Films* **2005**, *491*, 298.
[8] White M.S., Olson D.C., Shaheen S.E., Kopidakis N. and Ginley D.S. *Appl. Phys. Lett.* **2006**, *89*, 143517.
[9] Chen F.-C., Wu J.-L., Yang S.S., Hsieh K.-H. and Chen W.-C. *J. Appl. Phys.* **2008**, *103*, 103721.
[10] Hayakawa A., Yoshikawa O., Fujieda T., Uehara K. and Yoshikawa S. *Appl. Phys. Lett.* **2007**, *90*, 163517.
[11] Kim J.Y., Kim S.H., Lee H.-H., Lee K., Ma W., Gong X. and Heeger A.J. *Adv. Mater.* **2006**, *18*, 572.
[12] Li G., Chu C.W., Shrotriya V., Huang J. and Yang Y. *Appl. Phys. Lett.* **2006**, *88*, 253503.
[13] Lee K., Kim J.Y., Park S.H., Kim S.H., Cho S. and Heeger A.J. *Adv. Mater.* **2007**, *19*, 2445.
[14] Mihailetchi V.D., Xie H.X., de Boer B., Koster L.J.A. and Blom P.W.M. *Adv. Funct. Mater.* **2006**, *16*, 699.
[15] Wu H., Huang F., Mo Y., Yang W., Wang D., Peng J. and Cao Y. *Adv. Mater.* **2004**, *16*, 1826.
[16] Lakhwani G., Roijmans R., Kronemeijer A.J., Gilot J., Janssen R.A.J. and Meskers S.C.J. submitted for publication.
[17] Linsebigler A.L., Lu G. and Yates J.T., Jr. *Chem. Rev.* **1995**, *95*, 735.
[18] Beek W.J.E., Wienk M.M. and Janssen R.A.J. *J. Mater. Chem.* **2005**, *15*, 2985.
[19] Beek W.J.E., Wienk M.M. and Janssen R.A.J. *Adv. Funct. Mater.* **2006**, *16*, 1112.
[20] Beek W.J.E., Wienk M.M., Kemerink M., Yang X. and Janssen R.A.J. *J. Phys. Chem. B* **2005**, *109*, 9505.
[21] Wong H.M.P., Wang P., Abrusci A., Svensson M., Andersson M.R. and Greenham N.C. *J. Phys. Chem. C* **2007**, *111*, 5244.
[22] Pacholski C., Kornowski A. and Weller H. *Angew. Chem.-Int. Edit.* **2002**, *41*, 1188.
[23] Gilot J., Wienk M.M. and Janssen R.A.J. *Appl. Phys. Lett.* **2007**, *90*, 143512.
[24] Stouwdam J.W. and Janssen R.A.J. *J. Mater. Chem.* **2008**, *18*, 1889.
[25] Ameri T., Dennler G., Waldauf C., Denk P., Forberich K., Scharber M.C., Brabec C.J. and Hingerl K. *J. Appl. Phys.* **2008**, *103*, 084506.
[26] Andersson B.V., Huang D.M., Moulé A.J. and Inganäs O. *Appl. Phys. Lett.* **2009**, *94*, 043302.
[27] Lee J.K., Coates N.E., Cho S., Cho N.S., Moses D., Bazan G.C., Lee K. and Heeger A.J. *Appl. Phys. Lett.* **2008**, *92*, 243308.
[28] Roy A., Park S.H., Cowan S., Tong M.H., Cho S., Lee K. and Heeger A.J. *Appl. Phys. Lett.* **2009**, *95*, 013302.
[29] Hänsel H., Zettl H., Krausch G., Kisselev R., Thelakkat M. and Schmidt H.-W. *Adv. Mater.* **2003**, *15*, 2056.
[30] Chan M.Y., Lai S.L., Lau K.M., Lee C.S. and Lee S.T. *Appl. Phys. Lett.* **2006**, *89*, 163515.
[31] Hoppe H., Arnold N., Meissner D. and Sariciftci N.S. *Thin Solid Films* **2004**, *451-452*, 589.
[32] Moulé A.J. and Meerholz K. *Appl. Phys. B-Lasers Opt.* **2007**, *86*, 721.
[33] Pettersson L.A.A., Roman L.S. and Inganäs O. *J. Appl. Phys.* **1999**, *86*, 487.
[34] Sievers D.W., Shrotriya V. and Yang Y. *J. Appl. Phys.* **2006**, *100*, 114509.
[35] Dennler G., Forberich K., Scharber M.C., Brabec C.J., Tomis I., Hingerl K. and Fromherz T. *J. Appl. Phys.* **2007**, *102*, 054516.

[36] Slooff L.H., Veenstra S.C., Kroon J.M., Moet D.J.D., Sweelssen J. and Koetse M.M. *Appl. Phys. Lett.* **2007**, *90*, 143506.
[37] Wienk M.M., Turbiez M.G.R., Struijk M.P., Fonrodona M. and Janssen R.A.J. *Appl. Phys. Lett.* **2006**, *88*, 153511.
[38] Monestier F., Simon J.-J., Torchio P., Escoubas L., Flory F., Bailly S., de Bettignies R., Guillerez S. and Defranoux C. *Sol. Energy Mater. Sol. Cells* **2007**, *91*, 405.
[39] Palik E.D. and Ghosh G. *Handbook of optical constants of solids* **1998**, p. 394.
[40] Pettersson L.A.A., Ghosh S. and Inganäs O. *Org. Electron.* **2002**, *3*, 143.

Chapter 3

Multiple junction polymer solar cells processed from solution*

Abstract

Multiple junction solar cells incorporating solution processed electron and hole transporting layers are presented for polymer:fullerene bulk heterojunction solar cells. The intermediate contact, separating the active layers, is fabricated by spin casting ZnO nanoparticles from acetone, followed by spin casting pH neutral poly(3,4-ethylenedioxythiophene) (PEDOT) from water and short UV illumination of the completed device. The exposure to UV light photodopes the ZnO layer to obtain an Ohmic contact between the hole and electron transporting layers. The key necessity of this simple procedure is that each new step does not affect the integrity of previously deposited layers. The open-circuit voltage (V_{oc}) for double and triple junction solar cells processed in this way is close to the sum of the V_{oc} of the individual cells.

* Part of this work has been published:
Gilot J., Wienk M.M. and Janssen R.A.J. *Appl. Phys. Lett.* **2007**, *90*, 143512.
Lakhwani G., Roijmans R., Kronemeijer A.J., Gilot J., Janssen R.A.J. and Meskers S.C.J. submitted for publication.

3.1 Introduction

One possible way to improve the efficiency of polymer solar cells is by using a multiple junction configuration in which two or more cells with different absorption spectra, *i.e.* different band gaps, are stacked. Splitting the absorption of the solar spectrum in distinct parts allows for utilizing the photon energy more effectively by minimizing the transmission and thermalization losses. In a two-terminal tandem cell, with the active layers connected in series, the open-circuit voltage (V_{oc}) is the sum of the V_{oc}s of the subcells.

In order to construct an organic or polymer tandem solar cell, a transparent intermediate contact, positioned between the two active layers is required that provides electrical contact between the two cells via efficient recombination of the holes and electrons generated in the different subcells, without voltage loss. Preferably, the intermediate contact consists of a transparent electron transporting (ET) layer in contact with the front cell and a hole transporting (HT) layer in contact with the back cell (Figure 3.1).

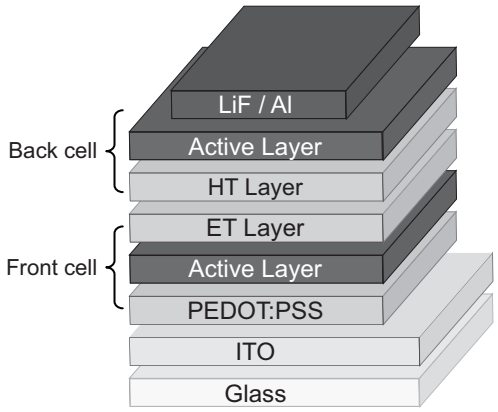

Figure 3.1 Device layout for a solution processed tandem solar cell.

Organic tandem solar cells based on small molecules have been described and indeed show increased V_{oc} and efficiencies.[1-3] Also solution processed polymer tandem solar cells with evaporated or sputtered intermediate layers have been reported.[4-5] Solution processed ET and HT layers, however, are more interesting because solution based coating and printing techniques are less time and energy consuming and eventually allow to roll-to-roll production.[6-7] While an example of an intermediate contact processed from solution has been reported recently containing a hydrolysis and annealing step,[8-9] an efficient, straightforward

and versatile solution-based method to process ET and HT layers is required to make efficient multiple junction solar cells.

We have established an orthogonal solvent combination for ET and HT layers that allows subsequent layers to be processed without affecting previously deposited layers. To demonstrate the technique, we use well-established material combinations for the active layers, employing blends of poly(3-hexylthiophene) (P3HT) or poly[2-methoxy-5-(3',7'-dimethyloctyloxy)-*p*-phenylene vinylene] (MDMO-PPV) as electron donors mixed with a soluble fullerene derivative [6,6]-phenyl-C_{61}-butyric acid methyl ester ([60]PCBM or PCBM in short) as electron acceptor.[10-11] We show that the method is fast, easy, and extendible to multiple junction solar cells.

3.2 Polymer tandem solar cells with ZnO as electron transporting and PEDOT:PSS as hole transporting layer

The intended layout for polymer tandem solar cells is shown in Figure 3.1. We have described the application of ZnO as ET layer in single junction polymer solar cells processed from ZnO nanoparticles dissolved in acetone before.[12] Here we combine this ZnO layer with the most commonly used HT layer in polymer solar cells: poly-(3,4-ethylenedioxylenethiophene):poly(styrenesulfonate) (PEDOT:PSS).[13] However, the standard dispersion of PEDOT:PPS in water from H.C. Starck (Clevios P) dissolved the ZnO layer because it is acidic in nature (pH ≈ 2) and, consequently, could not be used to deposit the HT layer onto the ZnO ET layer. This is clearly visible in UV/vis absorption spectra by the disappearance of the ZnO signals below 375 nm, after deposition of Clevios P (Figure 3.2). Therefore, we applied a PEDOT dispersion at neutral pH (pH ≈ 7) from Agfa N.V. which is innocuous towards the ZnO layer. The work function and the conductivity of the two PEDOT dispersions differ significantly engendering additional considerations like energy level offset and parasitic current generation.

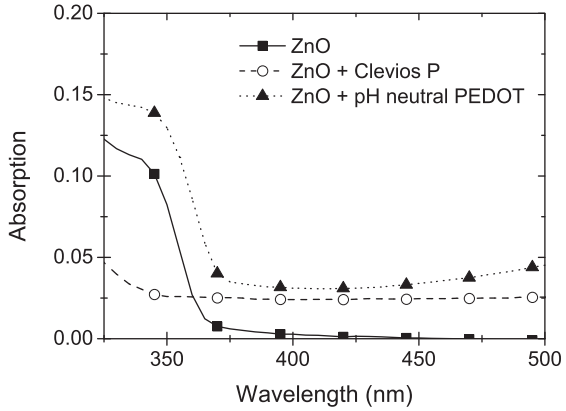

Figure 3.2 UV/vis absorption spectra of a ZnO layer without and with a Clevios P or pH neutral PEDOT layer spin cast on top.

3.3 pH neutral PEDOT as hole transporting layer

To test the applicability of the pH neutral PEDOT, we compared the performance of single junction solar cells with ITO/pH neutral PEDOT as high work function electrode to cells with an ITO/Clevios P electrode for polymers with different oxidation potentials[14-16] blended with PCBM as active layer. With Clevios P, poly[3,6-bis(4'-dodecyl-[2,2']bithiophenyl-5-yl)-2,5-bis(2-ethylhexyl)-2,5-dihydro-pyrrolo[3,4-]pyrrole-1,4-dione] (pBBTDPP2),[17] P3HT, MDMO-PPV and poly[2,7-(9,9-didecylfluorene)-*alt*-5,5-(4′,7′-di-2-thienyl-2′,1′,3′-benzothiadiazole)] (PFTBT)[18] give rise to a V_{oc} of 0.62 V, 0.75 V, 0.82 V and 0.98 V respectively. Note that the P3HT:PCBM device has not been annealed which explains the higher V_{oc}. Replacing Clevios P by the pH neutral PEDOT has no influence on the performance of a pBBTDPP2:PCBM cell, but for the other three blends the V_{oc} is significantly reduced (Figure 3.3a).

This change in V_{oc} is caused by the reduction in work function of pH neutral PEDOT. Scanning Kelvin probe microscopy (SKPM) reveals a drop in work function of 0.40 *e*V from –5.05 *e*V (Clevios P) to –4.65 *e*V (pH neutral PEDOT). Frohne *et al.* have already demonstrated that the V_{oc} changes proportionally to the electrochemically altered work function of PEDOT:PSS.[19] Moreover, this effect is also proportional to the oxidation potential of the polymer. Where the V_{oc} increases proportionally with the oxidation potential of the polymers for solar cells with Clevios P, the V_{oc} of devices with pH neutral PEDOT remains constant around 0.71 V for oxidation potentials larger than +0.05 V vs. ferrocene/ferrocenium (Fc/Fc^+) (Figure 3.3a).[20] This indicates that the difference in energy

between the oxidation potential of the polymer and the work function of the pH neutral PEDOT is too large for energy level alignment and an Ohmic contact. As a result, the V_{oc} is no longer determined by the offset between the highest occupied molecular orbital of the donor ($HOMO_{donor}$) and the lowest unoccupied molecular orbital of the acceptor ($LUMO_{acceptor}$),[21] but by the pH neutral PEDOT work function/$LUMO_{acceptor}$ offset.[22]

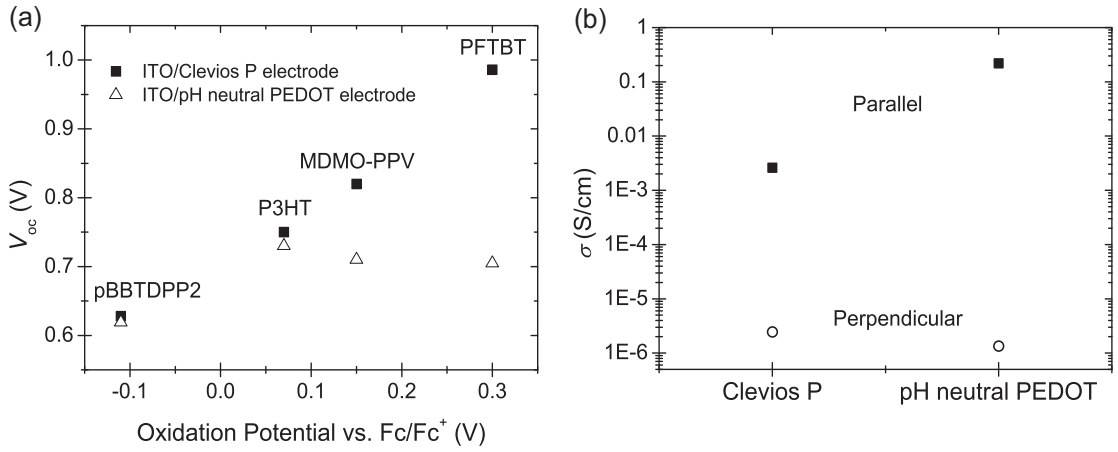

Figure 3.3 (a) The V_{oc} of single junction solar cells with ITO/Clevios P or ITO/pH neutral PEDOT as high work function electrode as a function of the oxidation potential of the polymers. (b) The parallel and perpendicular conductivity (σ) of Clevios P and pH neutral PEDOT.

Another substantial difference between the two PEDOT dispersions is the conductivity. The measured values of Clevios P correspond to those reported in literature.[23] Although the conductivity perpendicular to the surface is similar, the parallel conductivity is much higher for the pH neutral PEDOT (Figure 3.3b). As a consequence, care should be taken to illuminate only the active area (*i.e.* the overlap between the two electrodes) by masking other parts of the device. The performance of the tandem cell can only be characterized correctly by preventing parasitic charge collection in adjacent illuminated areas.[24-25] In this chapter, this issue does not yet play a roll because the goal is not to improve the efficiency but rather to provide a proof of principle for solution processed multiple junction polymer solar cells. It is, however, crucial in subsequent chapters.

3.4 Polymer tandem solar cells

For multiple junction solar cells, the intermediate contact is built up by ZnO as ET and pH neutral PEDOT as HT layer. After deposition of the pH neutral PEDOT on the ZnO layer, the second active layer was deposited via the same procedure as used for the first layer. All layers were processed on top of each other without disrupting the underlying layers (Figure 3.4a).

The transparent ZnO/pH neutral PEDOT intermediate contact was tested in tandem solar cells with MDMO-PPV:PCBM and P3HT:PCBM blends as active layers. For a tandem cell with MDMO-PPV:PCBM as front cell and P3HT:PCBM as back cell, an increase in V_{oc} from 0.75-0.82 V to 1.38 V was obtained (Figure 3.4b and Table 3.1).

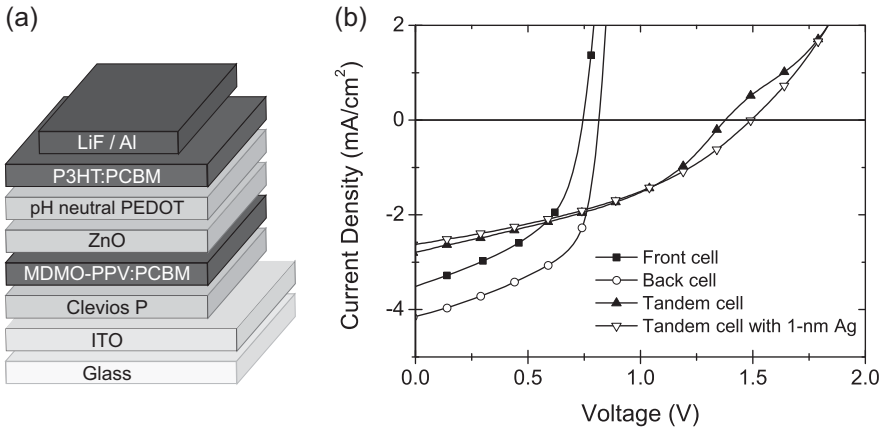

Figure 3.4 (a) Device layout for a MDMO-PPV:PCBM / P3HT:PCBM tandem solar cell. (b) *J–V* characteristics of the front (MDMO-PPV:PCBM), back (P3HT:PCBM), and tandem cells (MDMO-PPV:PCBM / P3HT:PCBM) under an arbitrary halogen lamp. The *J–V* characteristics of the front and back cell were measured from a single junction cell with the same active layer thickness.

This voltage, however, is not the sum of the voltages of the two single junction cells. We attribute this to a non-Ohmic contact between the ZnO and the pH neutral PEDOT layers. This *p-n* junction acts as a counter diode, which causes a small voltage drop and results in an s-shaped current density to voltage (*J–V*) curve attributable to a low carrier density in ZnO (Figure 3.4b). One way to align the energy levels of ET and HT layer is by evaporating a thin metal recombination layer between ET and HT layer.[3] When 1 nm of silver is evaporated onto the ZnO before depositing the pH neutral PEDOT, the inflection point in the *J–V* curve

disappears and V_{oc} increases to 1.49 V (Figure 3.4b). However, this is not in line with our aim of fully solution processed polymer tandem solar cells. Alternatively, an Ohmic contact between ZnO and pH neutral PEDOT can be obtained by sufficient doping of the two materials. The pH neutral PEDOT is already heavily doped and ZnO can very easily be doped by exposure to UV irradiation.[26-27] The effect of UV illumination on ZnO nanoparticles and on the ZnO/pH neutral PEDOT contact will be shown in the next section for multiple junction cells and described in more detail in section 3.6.

Table 3.1 Solar cell characteristics of single junction and tandem solar cells with ITO/Clevios P as transparent electrode, and LiF/Al as reflective electrode. All cells are polymer:PCBM cells. The single junction front cell has a ZnO layer incorporated between the active layer and the reflective electrode. The tandem cell has a ZnO/pH neutral PEDOT intermediate contact.

Front cell (45 nm)	Back cell (55 nm)	V_{oc} (V)	J_{sc} (mA/cm^2)	*FF*	*MPP* (mW/cm^2)
MDMO-PPV	—	0.82	4.1	0.55	1.9
—	P3HT	0.75	3.5	0.48	1.3
MDMO-PPV	P3HT	1.38	2.8	0.40	1.6
1 nm Ag		1.49	2.7	0.39	1.6

3.5 Double, triple and multiple junction polymer solar cells

UV illumination of a MDMO-PPV:PCBM / P3HT:PCBM tandem cell leads to photodoping of the ZnO nanoparticles and the formation of an Ohmic contact at the ZnO/pH neutral PEDOT interface (Figure 3.5a). Because of the absorption of UV light by the active layers, longer UV illumination is required in tandem cell devices, compared to stand-alone ZnO films. Figure 3.5a clearly shows that due to the increased conductivity of the doped ZnO, the shape of the *J–V* curve improved, the V_{oc} rose to 1.53 V, and also the short-circuit current density (J_{sc}) increased, resulting in an overall 25% improvement of the maximum power point (*MPP*).

In a similar fashion, multiple junction solar cells with three and six active layers were processed within 20 minutes (excluding metal evaporation) (Figure 3.5a). A P3HT:PCBM active layer was preceded by respectively 2 and 5 MDMO-PPV:PCBM active layers (Figure

3.5c). The layer thicknesses are increased from front to back cell to permit sufficient light transmission to the back cell in order to maintain a decent current. V_{oc}s of 1.71 and 1.84 V were obtained for the completed device before UV illumination, but these increased significantly to 2.19 and 3.58 V respectively upon applying UV light. Results are shown in Figure 3.5b and Table 3.2.

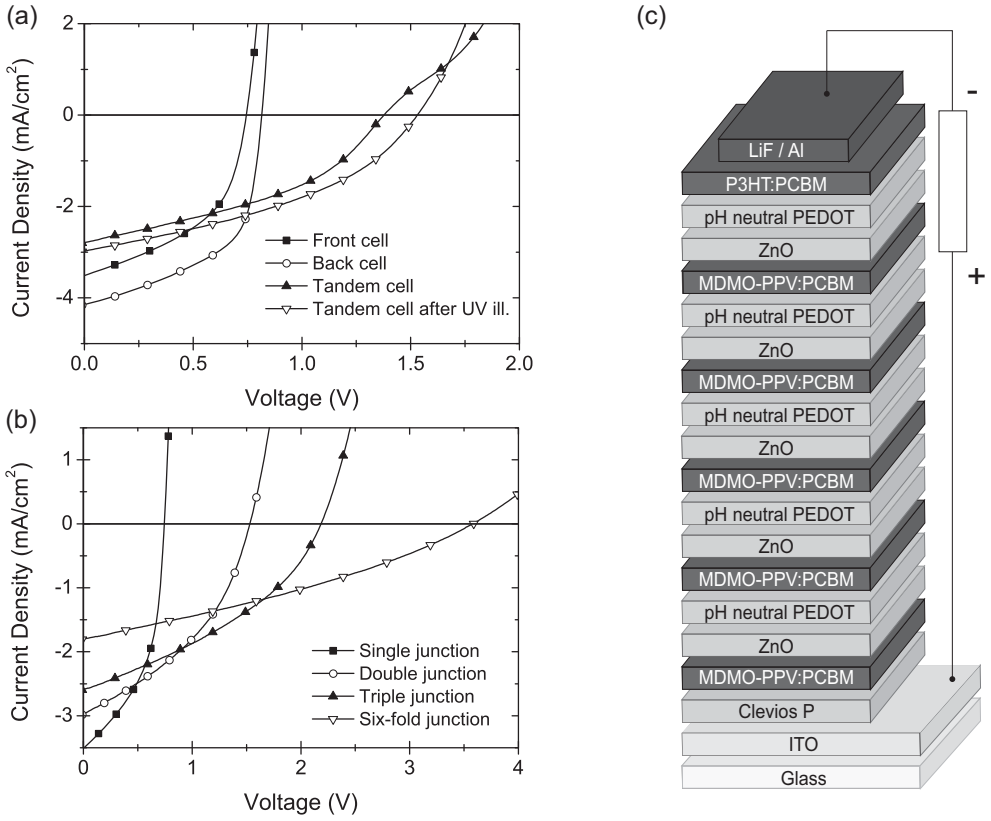

Figure 3.5 (a) *J–V* characteristics of the front (MDMO-PPV:PCBM), back (P3HT:PCBM), and tandem cells (MDMO-PPV:PCBM / P3HT:PCBM) under an arbitrary halogen lamp. Notice the improved performance after UV illumination. (b) *J–V* characteristics after UV illumination of a single junction P3HT:PCBM cell with additional MDMO-PPV:PCBM layers forming a double, triple and six-fold junction device. (c) Device layout of a six-fold junction based on MDMO-PPV:PCBM and P3HT:PCBM active layers.

The V_{oc} of the multiple junction cells deviates significantly from the estimated V_{oc} (V_{est}) obtained via addition of the voltages of the single junction cells. This is a consequence of the lower work function of pH neutral PEDOT and the related loss in V_{oc} for all layers except the first one deposited on Clevios P. Also the reduced light intensity reaching the active layers closest to the reflective electrode results in a decrease of the actual V_{oc}.[28]

Table 3.2 Solar cell characteristics of multiple junction polymer solar cells with ITO/Clevios P as transparent electrode, ZnO/pH neutral PEDOT as intermediate contact, and LiF/Al as reflective electrode. All cells are polymer:PCBM cells. The front and middle cells have a ZnO layer incorporated between the active layer and the reflective electrode. V_{est} is the estimated value for the voltage of a multiple junction solar cell obtained via addition of the V_{oc}s of the single junction cells.

Front cell (45 nm)	Middle cell (65 nm)	Back cell (55 nm)	UV	V_{est} (V)	V_{oc} (V)	J_{sc} (mA/cm^2)	*FF*	*MPP* (mW/cm^2)
MDMO-PPV	—	—			0.82	4.1	0.55	1.9
—	MDMO-PPV	—			0.82	4.4	0.55	2.0
—	—	P3HT			0.75	3.5	0.48	1.3
MDMO-PPV	—	P3HT	No	1.57	1.38	2.7	0.40	1.6
			Yes		1.53	3.0	0.42	1.9
MDMO-PPV	MDMO-PPV	P3HT	No	2.39	1.71	2.2	0.36	1.4
			Yes		2.19	2.6	0.37	2.1
Six-fold junction (Figure 3.5b)			No	4.85	1.84	1.1	0.30	0.6
			Yes		3.58	1.8	0.32	2.1

3.6 The effect of UV illumination on ZnO nanoparticles and on the ZnO/pH neutral PEDOT contact

To explain the beneficial effect of UV light on the ZnO/pH neutral PEDOT contact, it is important to consider that the electrical properties of ZnO are strongly dependent on the precise stoichiometry of the ZnO. In the ZnO particles that we use, trapped positively charged defects are compensated by electrons in the conduction band that have reacted with molecular oxygen from the ambient to form bound O_2^- at the surface.[29-30] Generation of an electron/hole pair by exposure to UV light in the absence of O_2 results in recombination of the generated hole with the electron trapped by O_2^- at the surface of ZnO, inducing desorption of neutral O_2 (Figure 3.6a) and leaving the mobile electron in the conduction band.[26,31] As a consequence, the concentration of mobile electrons in the nanoparticle is enhanced resulting in a high conductivity of a layer of ZnO nanoparticles.[32-33] This process is reversed upon exposure to air.

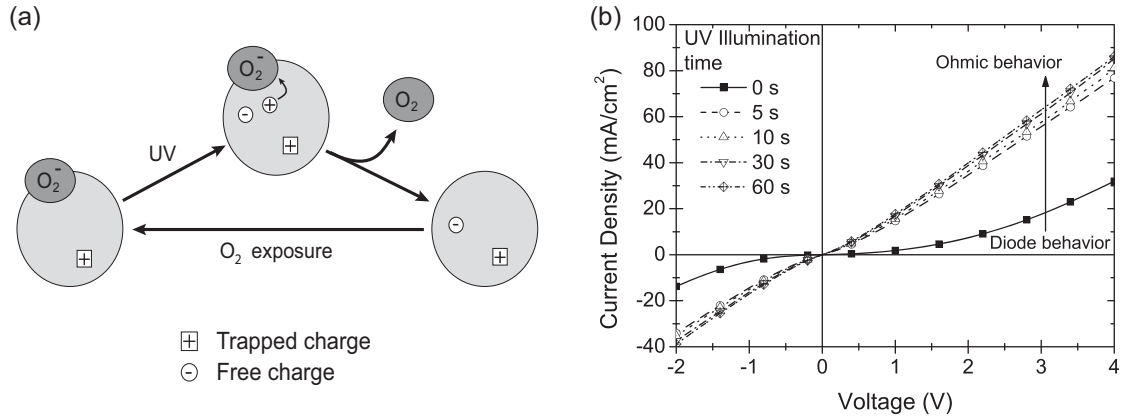

Figure 3.6 (a) Schematic representation of the changes induced by UV illumination of ZnO nanoparticles. A photogenerated hole induces desorption of O_2 resulting in a mobile electron. This process is reversed upon exposure to O_2. (b) *J–V* characteristics of an ITO/ZnO/pH neutral PEDOT/LiF/Al device before and after UV illumination.

To clarify the influence of UV illumination on the ZnO/pH neutral PEDOT contact, we studied the electrical characteristics of an ITO/ZnO/pH neutral PEDOT/LiF/Al device. The *J-V* characteristic in dark of the pristine diode shows some rectification (Schottky contact). As a check for Ohmic contact at the ITO/ZnO and pH neutral PEDOT/LiF/Al interface, also the reverse structure (ITO/pH neutral PEDOT/ZnO/LiF/Al) was measured and led to identical results.[34] This rectification can be explained by the presence of an injection barrier for electrons from ZnO into pH neutral PEDOT. Upon exposure to UV light, the junction becomes Ohmic (Figure 3.6b). The increase in current density (for $V \neq 0$) saturates after 30 seconds of UV illumination.

The formation of an Ohmic contact between n-type ZnO and p-type pH neutral PEDOT upon photodoping implies a considerable amount of charge transfer between the n-type ZnO and the p-type pH neutral PEDOT. Using ellipsometry, Lakhwani *et al.* observed significant changes in Ψ and Δ values and thus in the optical constants of ZnO and pH neutral PEDOT upon UV illumination measured on a glass substrate covered with ZnO/pH neutral PEDOT.[35] A reversible decrease of the extinction coefficient was noticed in the band of the pH neutral PEDOT centered around ~900 nm. This band is assigned to the oxidized form of PEDOT and its decrease provides an indication that some reduction of oxidized PEDOT segments occurred by transfer of electrons from the photodoped ZnO.

The carrier density in ZnO after photodoping was estimated to be 10^{19}/cm^3 determined from ellipsometry measurements of the Moss-Burstein shift and Kelvin probe

measurements.[35] This doping level is comparable to the results of other experimental studies independent of the type of dopant used (In,[36] Al[37] or native (non-stoichiometric ZnO)[38]) or the deposition method of the ZnO. This number density corresponds to about one positively charged defect per nanoparticle.[35]

A more comprehensive view on the formation of the Ohmic contact with ZnO upon UV illumination can now be sketched. From the carrier density of photodoped ZnO, we calculated the Fermi energy level of the n-doped ZnO layer after UV illumination in respect to the Fermi energy level of intrinsic ZnO (–6.1 *e*V vs. vacuum) to be +1.61 *e*V.[39] This indicates that the Fermi energy level of photodoped ZnO is positioned close to the conduction band energy level of ZnO (–4.4 *e*V) and more importantly close to the work function of pH neutral PEDOT (–4.65 *e*V) creating an Ohmic contact. This gives rise to a V_{oc} of the tandem cell which is close to the sum of the V_{oc}s of the subcells (Figure 3.7b).

Before UV illumination, the non-aligned Fermi energy levels of ZnO and pH neutral PEDOT cause a voltage drop at the ZnO/pH neutral PEDOT interface, which reduces the V_{oc} of the tandem cell (Figure 3.7a). The MDMO-PPV:PCBM / P3HT:PCBM tandem cell depicted in Figure 3.5a shows a voltage loss of 0.19 V before UV illumination compared to the estimated value. This voltage loss indicates a lower carrier density of at least a factor 2×10^3. Thus the exposure to UV irradiation increases the mobile carrier concentration and affords an Ohmic contact at the ZnO/pH neutral PEDOT interface.

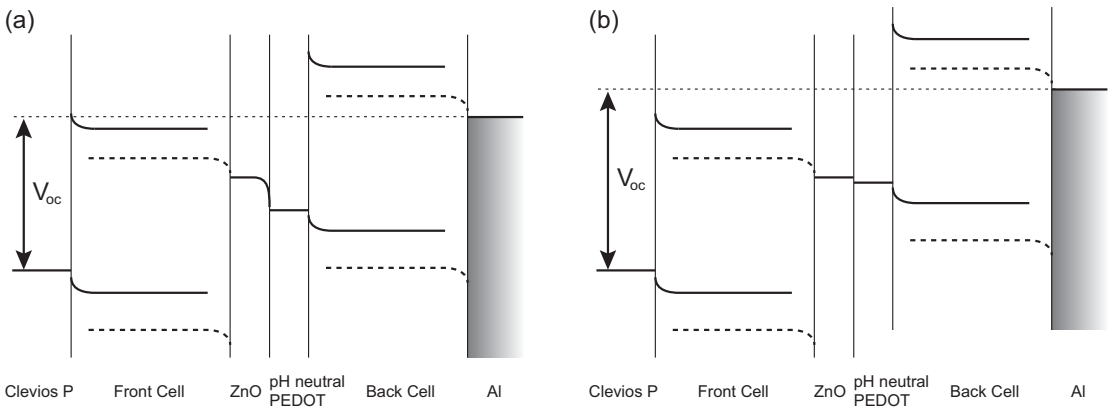

Figure 3.7 The energy band diagram of a tandem cell with ZnO/pH neutral PEDOT as intermediate contact (a) before and (b) after UV illumination. The band bending of ZnO is modified upon exposure to UV light.

3.7 Conclusions

We deposited pH neutral PEDOT as hole transporting layer on a layer of ZnO nanoparticles for the fabrication of solution processed multiple junction polymer solar cells. This pH neutral PEDOT dispersion has a lower work function than Clevios P giving rise to a loss in V_{oc} for polymers with an oxidation potential larger than +0.05 V vs. Fc/Fc^{+}. Also the parallel conductivity differs significantly requiring masking of the active area for correct characterization of efficient devices. For the multiple junction solar cells, no other techniques than spin casting were required besides evaporation of the final metal back electrode. The non-optimal V_{oc} and the s-shaped *J–V* curve of an as-processed tandem cell can be resolved by photodoping of the ZnO by exposure to UV light. This photodoping involves desorption of O_2 and creation of mobile electrons in the ZnO nanoparticles. The high doping level in ZnO creates an Ohmic contact between ZnO and pH neutral PEDOT. The maximum power point of a tandem cell improved by 25% upon UV illumination. A V_{oc} of 2.19 V was achieved for a triple junction solar cell close to the sum of single junction cell V_{oc}s. The newly developed procedure for solution processing of multiple junction polymer solar cells could even be extended to a six-fold junction solar cell reaching a V_{oc} of 3.58 V. It is interesting to note that this value is almost twice the energy of the lowest energy photon absorbed by the cell, considering that the optical gap of PCBM is 1.76 V. This simple procedure to create multiple junction devices will enable to increase the overall efficiency when active materials with different optical band gaps are used.

3.8 Experimental

Devices

For preparing polymer solar cells, precleaned ITO coated substrates (Philips Research) were covered with a 50 nm thick PEDOT:PSS film (Clevios® P VP AI 4083, H.C. Starck, passed a 5.0 µm Whatman Puradisc FP30 syringe filter). The active layer of the front cell was then spin cast on top in air. For the multiple junction cells the sequence of deposition by spin casting of ZnO (30 nm; 10 mg/ml in acetone), pH neutral PEDOT (15 nm; ORGACON, batch 5541073, pH = 7, 1.2 w%, Agfa NV; 1:1 dilution with water) and the next active layer was repeated until the aimed number of active layers was reached. After completion of the solution processing, the samples were moved into a glovebox with a nitrogen atmosphere to evaporate 1 nm LiF and 100 nm Al film as top electrode at 6×10^{-6} mbar.

P3HT:PCBM: Poly(3-hexylthiophene) (Rieke Metals) was mixed with [60]PCBM (Solenne BV) in chlorobenzene in a 1:1 ratio at 10 mg/ml polymer concentration. A spin speed of 1500 RPM resulted in a 55 nm thick layer. This layer was not annealed. The performance of a P3HT:PCBM cell with ITO/pH neutral PEDOT as high work function electrode reduced significantly after annealing, especially the V_{oc}.

MDMO-PPV:PCBM: Poly[2-methoxy-5-(3',7'-dimethyloctyloxy)-*p*-phenylene vinylene] (MDMO-PPV) (TNO) was mixed with PCBM in chlorobenzene in a 1:4 ratio at 3 mg/ml polymer concentration. Spin speeds of 1500 and 4500 RPM resulted in 65 and 45 nm thick layers. The spin speeds for the six-fold junction varied from 1000 to 5000 RPM.

PFTBT:PCBM: Poly[2,7-(9,9-didecylfluorene)-*alt*-5,5-(4′,7′-di-2-thienyl-2′,1′,3′-benzothiadia-zole)] (PFTBT)[18] (TNO) was mixed with PCBM in chlorobenzene in a 1:4 ratio at 5 mg/ml polymer concentration. A spin speed of 4000 RPM resulted in an 80 nm thick layer.

pBBTDPP2:PCBM: poly[3,6-bis(4'-dodecyl-[2,2']bithiophenyl-5-yl)-2,5-bis(2-ethylhexyl)-2,5-dihydro-pyrrolo[3,4-]pyrrole-1,4-dione] (pBBTDPP2)[17] (CIBA SC) was mixed with PCBM in a 80/20 chloroform/*o*-dichlorobenzene mixture in a 1:2 ratio at 7.5 mg/ml polymer concentration. A spin speed of 3000 RPM resulted in a 105 nm thick layer.

The ZnO and pH neutral PEDOT of Figure 3.6b are respectively 40 and 30 nm thick. The ZnO synthesis is described elsewhere.[12]

Device characterization

J–V characteristics were measured with a Keithley 2400 source measurement unit. Illumination was carried out with UV (GG 385) and infrared (KG1) filtered light from an uncalibrated tungsten halogen lamp (750 W/m^2). Because of the arbitrary light source, maximum power points are compared instead of power conversion efficiencies. UV illumination was performed with the same halogen lamp, however without the GG 385 filter. Layer thicknesses were determined with a Tencor® P-10 Surface Profiler.

For the parallel conductivity measurements, two electrodes (1 × 6 mm, 1 mm apart from each other) of 5 nm chromium followed by 95 nm of gold were evaporated on top of cleaned bare-glass substrates. For the perpendicular conductivity measurements 80 nm gold was evaporated on top of an ITO substrate (0.16 cm^2) covered with Clevios P (60 nm thick) or pH neutral PEDOT (40 nm thick). The resistance between two electrodes was measured with a Keithley 6512 programmable electrometer.

Apparatus

The work function of Clevios P and pH neutral PEDOT was determined at the Eindhoven University of Technology with a commercial AFM system (Veeco instruments MultiMode AFM with Nanoscope IIIa controller and extender module) in a glovebox under nitrogen atmosphere employing a sharp silicon tip with Pt coating (Olympus OMCL-AC240TM-B2, apex radius < 15 nm, k ≈ 2 N/m, cone angle 25º, resonant frequency ~70 kHz) and calibrated with freshly cleaved highly oriented pyrolitic graphite (HOPG), which has a stable work function of 4.48 *e*V.[40] Ellipsometry experiments were performed with a WVASE32 ellipsometer (J.A. Woollam

Co.,Inc). Further details are available in chapter 8 of reference [34]. The Kelvin probe set up (Besocke Delta Phi, Kelvin Probe S and Kelvin Control 07) for the determination of the charge density (performed at the Zernike Institute for Advanced Materials, Rijksuniversiteit Groningen) was enclosed in a home-built Faraday cage and calibrated with freshly cleaved HOPG.

3.9 References

[1] Männig B., Drechsel J., Gebeyehu D., Simon P., Kozlowski F., Werner A., Li F., Grundmann S., Sonntag S., Koch M., Leo K., Pfeiffer M., Hoppe H., Meissner D., Sariciftci N.S., Riedel I., Dyakonov V. and Parisi J. *Appl. Phys. A-Mater. Sci. Process.* **2004**, *79*, 1.

[2] Xue J., Uchida S., Rand B.P. and Forrest S.R. *Appl. Phys. Lett.* **2004**, *85*, 5757.

[3] Yakimov A. and Forrest S.R. *Appl. Phys. Lett.* **2002**, *80*, 1667.

[4] Hadipour A., de Boer B., Wildeman J., Kooistra F.B., Hummelen J.C., Turbiez M.G.R., Wienk M.M., Janssen R.A.J. and Blom P.W.M. *Adv. Funct. Mater.* **2006**, *16*, 1897.

[5] Kawano K., Ito N., Nishimori T. and Sakai J. *Appl. Phys. Lett.* **2006**, *88*, 073514.

[6] Shaheen S.E., Radspinner R., Peyghambarian N. and Jabbour G.E. *Appl. Phys. Lett.* **2001**, *79*, 2996.

[7] Tuomikoski M., Suhonen R., Vaelimaeki M., Maaninen T., Maaninen A., Sauer M., Rogin P., Mennig M., Heusing S., Puetz J. and Aegerter M.A. *SPIE-Int. Soc. Opt. Phot. Proc.* **2006**, *6192*, 619204.

[8] Dennler G., Prall H.-J., Koeppe R., Egginger M., Autengruber R. and Sariciftci N.S. *Appl. Phys. Lett.* **2006**, *89*, 073502.

[9] Kim J.Y., Lee K., Coates N.E., Moses D., Nguyen T.-Q., Dante M. and Heeger A.J. *Science* **2007**, *317*, 222.

[10] Ma W., Yang C., Gong X., Lee K. and Heeger A.J. *Adv. Funct. Mater.* **2005**, *15*, 1617.

[11] Shaheen S.E., Brabec C.J., Sariciftci N.S., Padinger F., Fromherz T. and Hummelen J.C. *Appl. Phys. Lett.* **2001**, *78*, 841.

[12] See Chapter 2.

[13] Arias A.C., Granstrom M., Petritsch K. and Friend R.H. *Synth. Met.* **1999**, *102*, 953.

[14] The oxidation potential of pBBTDPP2 is discussed in Chapter 4.

[15] Veldman D., Meskers S.C.J. and Janssen R.A.J. *Adv. Funct. Mater.* **2009**, *19*, 1939.

[16] Veldman D., Offermans T., Sweelssen J., Koetse M.M., Meskers S.C.J. and Janssen R.A.J. *Thin Solid Films* **2006**, *511-512*, 333.

[17] Wienk M.M., Turbiez M., Gilot J. and Janssen R.A.J. *Adv. Mater.* **2008**, *20*, 2556.

[18] Moet D.J.D., Slooff L.H., Kroon J.M., Chevtchenko S.S., Loos J., Koetse M.M., Sweelssen J. and Veenstra S.C. *Mater. Res. Soc. Symp. Proc.* **2006**, *974E*, CC03.

[19] Frohne H., Shaheen S.E., Brabec C.J., Müller D.C., Sariciftci N.S. and Meerholz K. *ChemPhysChem* **2002**, *3*, 795.

[20] Slooff L.H., Böhme S., Eerenstein W., Veenstra S.C., Verhees W., Kroon J.M. and Söderström T. *SPIE-Int. Soc. Opt. Phot. Proc.* **2008**, *7052*, 705217.

[21] Scharber M.C., Mühlbacher D., Koppe M., Denk P., Waldauf C., Heeger A.J. and Brabec C.J. *Adv. Mater.* **2006**, *18*, 789.

[22] Mihailetchi V.D., Blom P.W.M., Hummelen J.C. and Rispens M.T. *J. Appl. Phys.* **2003**, *94*, 6849.

[23] Nardes A.M., Kemerink M. and Janssen R.A.J. *Phys. Rev. B* **2007**, *76*, 085208.

[24] Cravino A., Schilinsky P. and Brabec C.J. *Adv. Funct. Mater.* **2007**, *17*, 3906.

[25] Kim M.-S., Kang M.-G., Guo L.J. and Kim J. *Appl. Phys. Lett.* **2008**, *92*, 133301.

[26] Beek W.J.E., Wienk M.M., Kemerink M., Yang X. and Janssen R.A.J. *J. Phys. Chem. B* **2005**, *109*, 9505.

[27] Verbakel F., Meskers C.J. and Janssen R.A.J. *Appl. Phys. Lett.* **2006**, *89*, 102103.

[28] Koster L.J.A., Mihailetchi V.D., Ramaker R. and Blom P.W.M. *Appl. Phys. Lett.* **2005**, *86*, 123509.

[29] Sharma P., Sreenivas K. and Rao K.V. *J. Appl. Phys.* **2003**, *93*, 3963.

[30] van Dijken A., Meulenkamp E.A., Vanmaekelbergh D. and Meijerink A. *J. Lumin.* **2000**, *90*, 123.

[31] Arnold M.S., Avouris P., Pan Z.W. and Wang Z.L. *J. Phys. Chem. B* **2003**, *107*, 659.

[32] Studenikin S.A., Golego N. and Cocivera M. *J. Appl. Phys.* **2000**, *87*, 2413.

[33] Verbakel F., Meskers S.C.J. and Janssen R.A.J. *J. Appl. Phys.* **2007**, *102*, 083701.

[34] Lakhwani G. *PhD Thesis* Eindhoven University of Technology **2009**.

[35] Lakhwani G., Roijmans R., Kronemeijer A.J., Gilot J., Janssen R.A.J. and Meskers S.C.J. submitted for publication.
[36] Kim K.J. and Park Y.R. *Appl. Phys. Lett.* **2001**, *78*, 475.
[37] Lu J.G., Fujita S., Kawaharamura T., Nishinaka H., Kamada Y., Ohshima T., Ye Z.Z., Zeng Y.J., Zhang Y.Z., Zhu L.P., He H.P. and Zhao B.H. *J. Appl. Phys.* **2007**, *101*, 083705.
[38] Roth A.P., Webb J.B. and Williams D.F. *Solid State Commun.* **1981**, *39*, 1269.
[39] Sze S.M. *Physics of Semiconductor Devices* **1981**, p. 17.
[40] Hansen W.N. and Hansen G.J. *Surf. Sci.* **2001**, *481*, 172.

Chapter 4

The effect of processing on the performance of small band gap polymer solar cells*

Abstract

Solar cells based on a new conjugated donor polymer with alternating quarterthiophene and diketopyrrolopyrrole units in combination with [60]PCBM and [70]PCBM acceptors afford high external quantum efficiencies over a broad spectral range into the near-infrared. The choice of solvent and the accompanied morphology have a large influence on the device performance. The cells provide power conversion efficiencies of up to 4.0% under simulated AM1.5G solar light conditions.

* This work has been published:
Wienk M.M., Turbiez M., Gilot J. and Janssen R.A.J. *Adv. Mater.* **2008**, *20*, 2556.

4.1 Introduction

So far, the most successful polymer solar cells are bulk heterojunction type devices, which use a mixture of electron-rich polymer and electron-poor fullerene as the photoactive layer.[1-2] Cells combining regioregular poly(3-hexylthiophene) (P3HT) as electron donor with a fullerene derivative, [6,6]-phenyl-C_{61}-butyric acid methyl ester ([60]PCBM) as electron acceptor, achieve power conversion efficiencies of over 4%.[3] It has been demonstrated that the morphology of the mixed film, and particularly the crystallinity of the materials, are key parameters for optimization of bulk heterojunction solar cells.[4-5] Solvent additives and solvent mixtures assist in the formation of the optimal morphology for high solar cell efficiencies.[6-9]

One other important parameter for optimization of polymer photovoltaic cells is the band gap of the materials. For single junction cells, using [60]PCBM as acceptor, a band gap of ca. 1.4 *e*V is expected to be optimal, provided that the highest occupied (HOMO) and lowest unoccupied (LUMO) molecular orbital levels are correctly positioned with respect to the levels of the electron acceptor.[10-11] Recently, considerable progress has been achieved with the use of such small band gap polymers in polymer photovoltaics. Cells with an efficiency of over 5% have been reported.[7,12-14]

Here, we report on the application of a new small band gap polymer: poly[3,6-bis-(4'-dodecyl-[2,2']bithiophenyl-5-yl)-2,5-bis-(2-ethylhexyl)-2,5-dihydropyrrolo[3,4-]pyrrole-1,4-dione] (pBBTDPP2) in photovoltaic cells (Figure 4.1). The new polymer combines electron-rich quarterthiophene (BBT) with segments of electron-poor diketopyrrolopyrrole (DPP)[15-18] units to lower the optical band gap to 1.4 *e*V in thin films. After judicious and rational optimization of the processing parameters and morphology, power conversion efficiencies of 4% have been achieved under air mass 1.5 global (AM1.5G) illumination conditions.

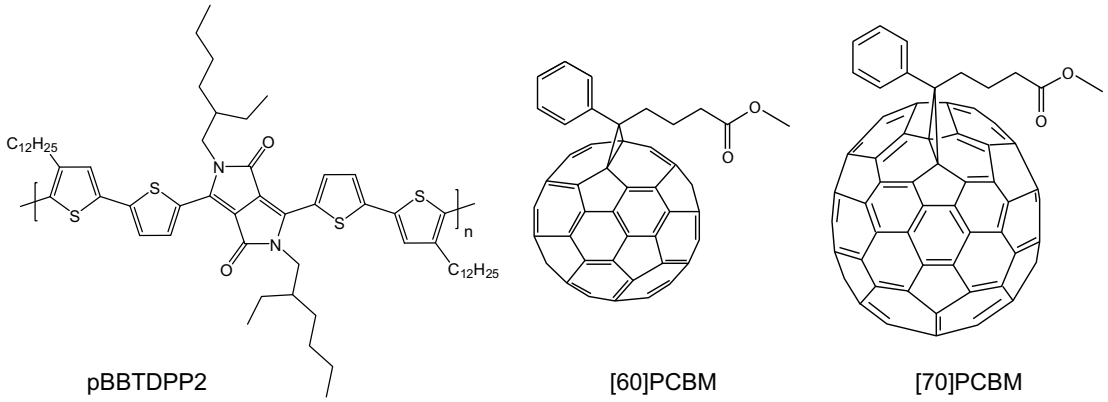

Figure 4.1 Molecular structure of the pBBTDPP2 polymer and fullerene derivatives used in this chapter.

4.2 Absorption of pBBTDPP2 in solution

The absorption spectrum of pBBTDPP2 in chloroform (Figure 4.2a) is dominated by an absorption band at 650 nm. In *o*-dichlorobenzene (ODCB) the polymer has a strong tendency to aggregate, even at low concentrations. This is exemplified by a significant shift of the onset of absorption from 720 nm (1.72 *e*V) to 860 nm (1.44 *e*V) and the appearance of a vibronic fine structure. The presence of the absorption at 660 nm suggests that part of the polymer is molecularly dissolved in ODCB. The strong red-shift of the absorption for pBBTDPP2 upon aggregation is reminiscent of the shift observed for other conjugated polymers (*e.g.* P3HT[19-20]) and is, likewise, associated with the formation of ordered, possibly semi-crystalline, domains.

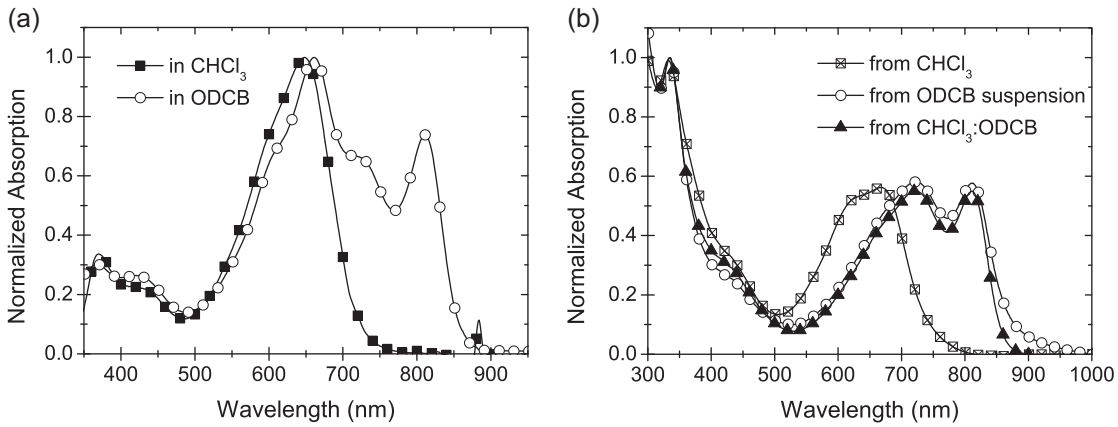

Figure 4.2 Normalized UV/visible absorption spectra of (a) pBBTDPP2 in solution and of (b) pBBTDPP2:[60]PCBM (1:2 w/w) films on glass; the films were spin cast from different media.

Cyclic voltammetry, carried out on pBBTDPP2 in ODCB reveals reversible oxidation and reduction, with the main onsets at +0.26 V and –1.42 V vs. ferrocene/ferrocenium, respectively. The potential difference between oxidation and reduction of 1.68 V is in good agreement with the optical gap of the molecularly dissolved material. A small extra onset of the oxidation potential is observable at –0.06 V vs. ferrocene/ferrocenium. This potential difference of 1.36 V corresponds closely the optical gap of the aggregated polymer in ODCB.[21]

4.3 Absorption of pBBTDPP2:[60]PCBM blends in film

When mixed solutions of pBBTDPP2 and [60]PCBM in chloroform are spin cast, the absorption peak of the polymer remains well below 700 nm (Figure 4.2b), indicating that electronic interactions between polymer chains are minimal in the mixed film and that, hence, the polymer essentially is amorphous. The fast evaporation of chloroform does not allow the pBBTDPP2 to aggregate or crystallize during spin casting and an amorphous chain arrangement is maintained. A certain degree of crystallization can be achieved by heating the film to 130 ºC, as inferred from a red-shifted absorption onset.

The limited solubility of pBBTDPP2 in ODCB causes the formation of gels that cannot be processed when the polymer is dissolved in hot ODCB and then cooled to room temperature. To prepare this suspension, the polymer is first fully dissolved in hot ODCB (170 ºC). Then, the solution is cooled while being agitated in an ultrasonic bath.[22] Upon cooling the color changes, which points to aggregation, but the formation of a gel is avoided by sonication. Dispersions prepared this way are stable for several weeks and can effectively be spin cast. This allows the preparation of films with a larger degree of crystallinity than chloroform cast films after annealing, as inferred from the height of the absorption peak at 810 nm (Figure 4.2b). We expect that the aggregates are in the nanometer range as cast films appeared smooth in atomic force microscopy (AFM) measurements. The less steep onset of the absorption may be caused by scattering due to a more grainy film as a result of the particulate nature of the suspension.

An alternative method to deposit mixed films with a large degree of semi-crystalline polymer is by using a chloroform:ODCB mixture (4:1).[9] In this solvent mixture the polymer and fullerene completely dissolve at room temperature, which allows easy and reproducible processing. Nevertheless, immediately after deposition the absorption spectrum of the film

shows the red-shifted peaks characteristic of crystalline pBBTDPP2. Because of the large difference in vapor pressure, the final film morphology is essentially determined by the slow evaporation of ODCB, leaving the polymer sufficient time to partly crystallize before precipitation.

4.4 Influence of solvent on device performance

Photovoltaic devices of the appropriate pBBTDPP2:fullerene films were made. Best results were achieved using a 1:2 pBBTDPP2:[60]PCBM ratio and photoactive layer thickness in the range of 100 to 120 nm. Analogous to the optical properties of the films, the photovoltaic performance was also greatly affected by the processing conditions. For cells in which the photoactive layer was processed from chloroform, the shape of the spectral response (Figure 4.3a) is very similar to the absorption spectrum (*i.e.* lacking the peak >800 nm). The maximum external quantum efficiency (*EQE*) is 0.13 at 680 nm.

For devices processed from an ODCB suspension the *EQE* is significantly higher, with a maximum value of 0.42. Moreover, the spectral response extends much further to lower energy. Consequently, the current density generated in the cells processed from the ODCB suspension is much higher than that from the chloroform processed cells. Convolution of the spectral response with the AM1.5G solar spectrum (1000 W/m^2) and correcting for the sub-linear light intensity dependence of the current provides an indication of the short-circuit current density (J_{sc}) of these devices under solar illumination. For the best cells processed from chloroform this amounts to 2.4 mA/cm^2, whereas 9.4 mA/cm^2 is obtained for the cells from the ODCB suspension. By using the mixed chloroform:ODCB solution, comparable quantum efficiencies were obtained, leading to an AM1.5G J_{sc} of 10.1 mA/cm^2. The small differences in spectral response between the two films (Figure 4.3a) in the 450 nm range is attributed to a dissimilar incoupling of light caused by small (~10 nm) differences in layer thickness, as inferred from specular reflection measurements.

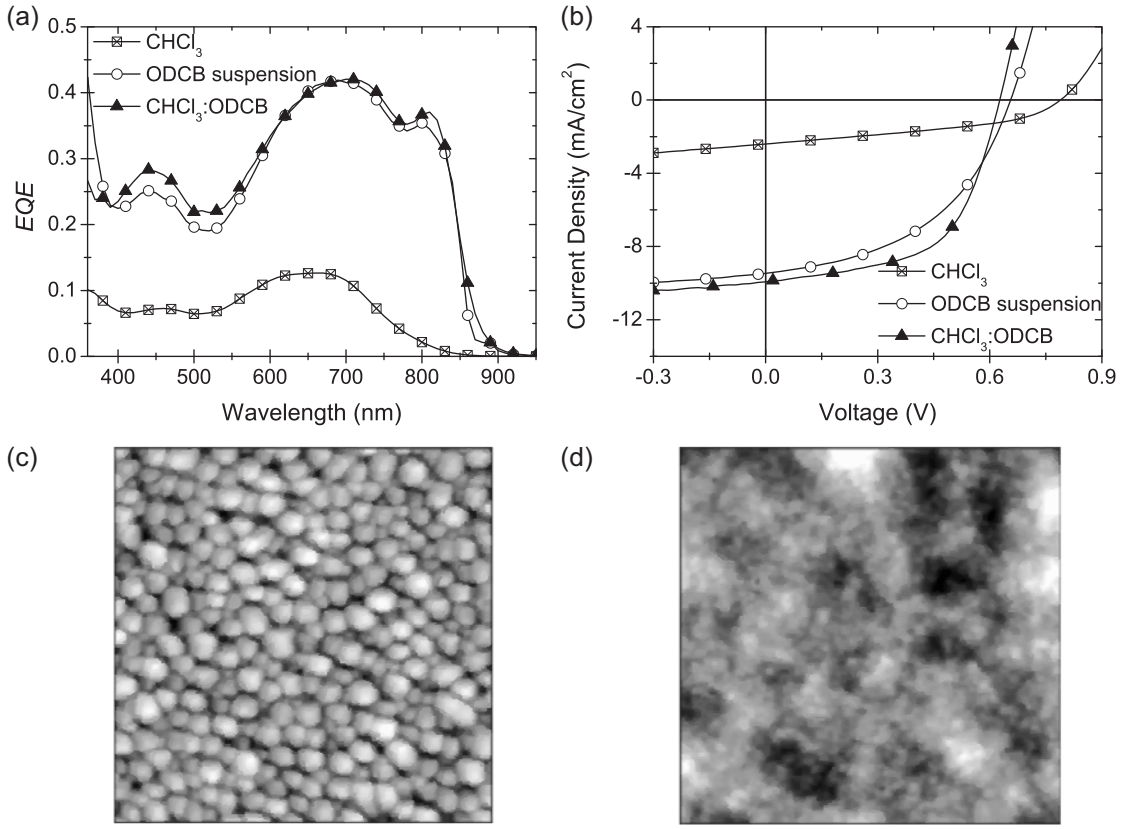

Figure 4.3 (a) Spectral response of pBBTDPP2:[60]PCBM solar cells processed from different media. (b) *J–V* characteristics under AM1.5G illumination (1000 W/m^2) of pBBTDPP2:[60]PCBM devices cast from different media. Surface topography of a pBBTDPP2:[60]PCBM film processed (c) from chloroform (5 × 5 μm^2, *z*-range is 42 nm) and (d) from chloroform:ODCB (4:1) (5 × 5 μm^2, *z*-range is 35 nm) measured by AFM.

Current density to voltage (*J–V*) measurements (Figure 4.3b) were performed under AM1.5G (1000 W/cm^2) illumination with spectral mismatch taken into account.[23-24] Note that the AM1.5G short-circuit current density, estimated from the spectral response, accurately corresponds to the actual measured J_{sc} (Table 4.1). Cells from chloroform:ODCB not only deliver a high current density, but also the highest fill factor (*FF*) of 0.58, compared to 0.47 and 0.41 for the dispersion and chloroform processed cells, respectively. Adversely, the open-circuit voltage (V_{oc}) is highest (0.79 V) for cells from chloroform. This is attributed to the lack of electronic interaction among the polymer chains, leaving the HOMO level at a more negative value, thus increasing the voltage compared to the more aggregated polymer. The overall best devices were processed from chloroform:ODCB solvent mixtures and gave an efficiency of 3.6%.

Table 4.1 Performance parameters of pBBTDPP2:[60]PCBM solar cells.

	J_{sc} (SR) [a] (mA/cm^2)	J_{sc} [b] (mA/cm^2)	*FF*	V_{oc} (V)	Efficiency (%)
pBBTDPP2:[60]PCBM from chloroform	2.4	2.4	0.41	0.78	1.1
pBBTDPP2:[60]PCBM from ODCB suspension	9.2	9.4	0.47	0.66	2.9
pBBTDPP2:[60]PCBM from chloroform:ODCB	10.1	10.2	0.58	0.62	3.6
pBBTDPP2:[70]PCBM from chloroform:ODCB	11.5	11.3	0.58	0.61	4.0

[a] Determined from convolution of the spectral response with the AM1.5G solar spectrum (1000 W/m^2). [b] Determined from *J–V* measurements under simulated AM1.5G illumination (1000 W/m^2).

The distinct lower performance of cells processed from chloroform is related to the amorphous nature of the as deposited layer. Even though a large degree of crystallinity can be introduced by thermal annealing, the efficiency of chloroform processed cells remains significantly lower than that of ODCB processed cells. AFM measurements (Figure 4.3c,d) provide some clues to why that is. Whereas the surface topography of layers from chloroform:ODCB (Figure 4.3d) and from ODCB dispersions (not shown) displays only small features (<100 nm), films from chloroform contain domains with lateral dimensions of several hundreds of nm (Figure 4.3c). While annealing may cause crystallization, it does not lead to a reduction of the dimension of the phase separated domains and the unfavorable morphology reduces the generation of charges and thereby the effectiveness of these layers.[4]

After extensive optimization of the processing parameters for pBBTDPP2:[60]PCBM solar cells, the optimal conditions were also applied to cells with [6,6]-phenyl-C_{71}-butyric acid methyl ester ([70]PCBM) instead of [60]PCBM. This higher fullerene has similar electronic properties compared to [60]PCBM, but a considerably higher absorption coefficient in the visible region.[25] In devices, this leads to a significantly higher quantum efficiency below 600 nm (Figure 4.4a). Consequently, a higher short-circuit current density of 11.3 mA/cm^2 is obtained under AM1.5G conditions (Figure 4.4b). Combined with a *FF* of 0.58 and a V_{oc} of 0.61 V, this yields a power conversion efficiency of 4.0%.

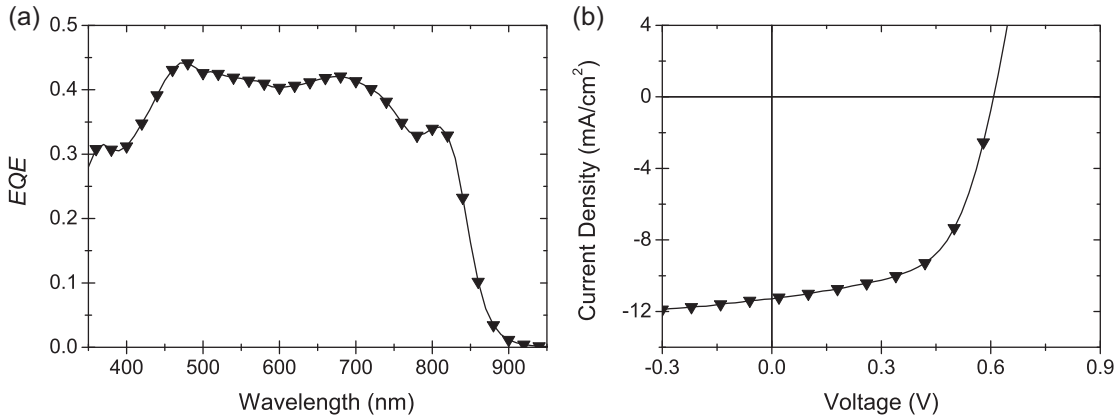

Figure 4.4 (a) Spectral response of a pBBTDPP2:[70]PCBM solar cell. (b) *J–V* characteristics under AM1.5G illumination (1000 W/m^2) of a pBBTDPP2:[70]PCBM device.

4.5 Conclusions

We have presented a new conjugated polymer based on alternating quarterthiophene and diketopyrrolopyrrole units with a band gap of 1.4 *e*V, which is close to the optimum for single junction polymer solar cells. After careful optimization of the processing conditions, the new donor polymer in combination with [60]PCBM and [70]PCBM affords external quantum efficiencies of ~0.4 over a broad spectral range and power conversion efficiencies of 3.6 and 4.0%, respectively, under simulated AM1.5G solar light conditions.

4.6 Experimental

Polymer synthesis and characterization

The synthesis and isolation of pBBTDPP2 have been described elsewhere.[26] Significant molecular weights of M_n = 20 000 and M_w = 67 000 g/mol (*PDI* = 3.35) were obtained, as determined by gel permeation chromatography (GPC) using 1,2,4-trichlorobenzene as eluent.

Devices

For preparing organic solar cells, precleaned ITO coated substrates (Philips Research) were covered with a 50 nm thick PEDOT:PSS film (Clevios® P VP AI 4083, H.C. Starck, passed a 5.0 µm Whatman Puradisc FP30 syringe filter). The active layer was then deposited on top. Finally, the samples were moved into a glovebox with a nitrogen atmosphere to evaporate 1 nm LiF and 100 nm Al film as top electrode at 2×10^{-7} mbar. The size of the devices (0.09 cm^2) was determined by the overlap of the ITO and LiF/Al electrode and was verified by optical microscopy after completion of the devices.

pBBTDPP2 (CIBA SC) was mixed with PCBM (Solenne BV) in the appropriate solvent in a 1:2 ratio at 7.5 mg/ml polymer concentration. The ODCB dispersion was made by dissolving pBBTDPP2 and PCBM in ODCB at 170 ºC for 15 min. The solution was cooled in an ultrasonic bath (Bransson) filled with ice/water mixture for 10 min.

Device characterization

Spectral response data were determined with a Keithley 2400 source measurement unit, using monochromatic light from a tungsten halogen lamp in combination with a monochromator (Oriel, Cornerstone 130). A calibrated Si cell was used as reference. The device was kept behind a quartz window in a nitrogen filled container. *J–V* measurements were carried out at the Energy Research Center of the Netherlands (ECN) with AM1.5G, 1000 W/m^2 illumination from a WXS-300S-50 solar simulator (WACOM ELECTRIC Co.) using a Keithley 2400 source measurement unit. The light intensity was adjusted to compensate for the spectral mismatch factor (1.01-1.06 for the various devices),[23-24] which were calculated using a recent spectrum of the simulator lamp, the spectral responses of the Si reference cell (calibrated at PTB, Braunschweig) and the polymer:fullerene cell.

Apparatus

Absorption measurements were performed on a Lambda 900 spectrometer (Perkin Elmer). Cyclic voltammetry was carried out with an Autolab PGSTAT30 potentiostat, using a platinum disc working electrode, a silver rod counter electrode and a silver chloride coated silver rod as pseudo reference electrode. The electrolyte was 0.1 M tetrabutylammonium hexafluorophosphate in ODCB, the scan speed 100 mV/s. Ferrocene/ferrocenium was used as internal reference. Tapping mode AFM was performed with a Nanoscope Dimension 3100 microscope (Veeco, Digital instruments) using PPP-NCHR probes.

4.7 References

[1] Dennler G., Scharber M.C. and Brabec C.J. *Adv. Mater.* **2009**, *21*, 1323.

[2] Thompson B.C. and Fréchet J.M.J. *Angew. Chem.-Int. Edit.* **2008**, *47*, 58.

[3] Ma W., Yang C., Gong X., Lee K. and Heeger A.J. *Adv. Funct. Mater.* **2005**, *15*, 1617.

[4] Hoppe H. and Sariciftci N.S. *J. Mater. Chem.* **2006**, *16*, 45.

[5] Li G., Shrotriya V., Yao Y., Huang J. and Yang Y. *J. Mater. Chem.* **2007**, *17*, 3126.

[6] Lee J.K., Ma W.L., Brabec C.J., Yuen J., Moon J.S., Kim J.Y., Lee K., Bazan G.C. and Heeger A.J. *J. Am. Chem. Soc.* **2008**, *130*, 3619.

[7] Peet J., Kim J.Y., Coates N.E., Ma W.L., Moses D., Heeger A.J. and Bazan G.C. *Nature Mater.* **2007**, *6*, 497.

[8] Yao Y., Hou J., Xu Z., Li G. and Yang Y. *Adv. Funct. Mater.* **2008**, *18*, 1783.

[9] Zhang F., Jespersen K.G., Björström C., Svensson M., Andersson M.R., Sundström V., Magnusson K., Moons E., Yartsev A. and Inganäs O. *Adv. Funct. Mater.* **2006**, *16*, 667.

[10] Bijleveld J.C., Shahid M., Gilot J., Wienk M.M. and Janssen R.A.J. *Adv. Funct. Mater.* **2009**, *19*, 3262.

[11] Scharber M.C., Mühlbacher D., Koppe M., Denk P., Waldauf C., Heeger A.J. and Brabec C.J. *Adv. Mater.* **2006**, *18*, 789.

[12] Hou J., Chen H.-Y., Zhang S., Li G. and Yang Y. *J. Am. Chem. Soc.* **2008**, *130*, 16144.

[13] Liang Y., Xu Z., Xia J., Tsai S.-T., Wu Y., Li G., Ray C. and Yu L. *Adv. Mater.* **2010**, published online, doi: 10.1002/adma.200903528.

[14] Park S.H., Roy A., Beaupré S., Cho S., Coates N., Moon J.S., Moses D., Leclerc M., Lee K. and Heeger A.J. *Nature Photon.* **2009**, *3*, 297.

[15] Bijleveld J.C., Zoombelt A.P., Mathijssen S.G.J., Wienk M.M., Turbiez M., de Leeuw D.M. and Janssen R.A.J. *J. Am. Chem. Soc.* **2009**, *131*, 16616.

[16] Huo L., Hou J., Chen H.-Y., Zhang S., Jiang Y., Chen T.L. and Yang Y. *Macromolecules* **2009**, *42*, 6564.

[17] Walker B., Tamayo A.B., Dang X.-D., Zalar P., Seo J.H., Garcia A., Tantiwiwat M. and Nguyen T.-Q. *Adv. Funct. Mater.* **2009**, *19*, 3063.

[18] Zou Y., Gendron D., Neagu-Plesu R. and Leclerc M. *Macromolecules* **2009**, *42*, 6361.

[19] Erb T., Zhokhavets U., Gobsch G., Raleva S., Stühn B., Schilinsky P., Waldauf C. and Brabec C.J. *Adv. Funct. Mater.* **2005**, *15*, 1193.

[20] Zhokhavets U., Erb T., Gobsch G., Al-Ibrahim M. and Ambacher O. *Chem. Phys. Lett.* **2006**, *418*, 347.

[21] Zoombelt A.P. *PhD Thesis* Eindhoven University of Technology **2009**.

[22] Ong B.S., Wu Y., Liu P. and Gardner S. *Adv. Mater.* **2005**, *17*, 1141.

[23] Kroon J.M., Wienk M.M., Verhees W.J.H. and Hummelen J.C. *Thin Solid Films* **2002**, *403-404*, 223.

[24] Shrotriya V., Li G., Yao Y., Moriarty T., Emery K. and Yang Y. *Adv. Funct. Mater.* **2006**, *16*, 2016.

[25] Wienk M.M., Kroon J.M., Verhees W.J.H., Knol J., Hummelen J.C., van Hal P.A. and Janssen R.A.J. *Angew. Chem.-Int. Edit.* **2003**, *42*, 3371.

[26] Turbiez M., Janssen R.A.J., Wienk M.M., Kirner H.J., Düggli M., Tieke B. and Zhu Y. **2008** *World Patent Application WO/2008/000664*.

Chapter 5

Optimizing polymer tandem solar cells*

Abstract

Polymer tandem solar cells with wide and small band gap subcells reach efficiencies of almost 5% after optimization by mathematically constructing *J*–*V* curves of the tandem cell taking optical and electrical interactions into account. In this tandem cell the short-circuit current exceeds that of the current-limiting subcell. The intermediate contact that connects the two subcells does not impose important losses.

* This work has been published:
Gilot J., Wienk M.M. and Janssen R.A.J. *Adv. Mater.* **2010**, *22*, E67.

5.1 Introduction

In single junction solar cells, significant energy losses are unavoidable. Photons with energies smaller than the band gap cannot be absorbed and photons with larger energies will lose their excess energy via thermal equilibration. Tandem solar cells can reduce these losses by using separate subcells, which each converts a different part of the solar spectrum. Thermalization losses of high energy photons are lowered by conversion in the wide band gap subcell and transmission losses are reduced by absorption of the low energy photons in the small band gap cell. Semiconducting organic molecules and polymers are being explored for tandem solar cells, often combining the strong and narrow absorption bands of the individual layers to increase the spectral coverage.[1-8] For the most efficient 6.5% polymer tandem solar cell to date,[6] the subcells have an identical open-circuit voltage (V_{oc} = 0.6 V), suggesting that the performance may be further enhanced when the principal advantages of the tandem configuration can be exploited. Owing to the large number of different layers in such devices, optimization of their performance is challenging.

Here, we demonstrate that the combined analysis of the optical absorption and electrical characteristics of the individual single junction subcells is essential to identify the optimum device layout of the corresponding tandem cell. We show that in contrast to existing views, matching the photocurrents of the subcells is not a leading design criterion for optimum performance, because the short-circuit current of a polymer tandem cell can exceed that of the current-limiting subcell. Using the new methodology, a solution processed polymer tandem solar cell with an efficiency of 4.9% under AM1.5G conditions has been obtained. In this tandem cell the intermediate contact that connects the two subcells does not impose important losses.

5.2 Materials and device structure

Tandem cells presented in this study (Figure 5.1) consist of bulk heterojunction subcells comprising wide and small band gap polymers as electron donors mixed with [6,6]-phenyl-C_{61}-butyric acid methyl ester ([60]PCBM or PCBM in short) as electron acceptor. Poly[2,7-(9,9-didecylfluorene)-*alt*-5,5-(4′,7′-di-2-thienyl-2′,1′,3′-benzothia-diazole)] (PFTBT)[9] is used as the wide band gap (1.95 *e*V) material and poly[3,6-bis(4'-dodecyl-[2,2']bithiophenyl-5-yl)-2,5-bis(2-ethylhexyl)-2,5-dihydro-pyrrolo-[3,4-]pyrrole-1,4-dione] (pBBTDPP2)[10] for the

small band gap (1.44 *e*V) cell (Figure 5.1c,d). Mixed with PCBM these polymers provide rather efficient single junction cells,[9-10] exhibiting high V_{oc}s of about 1.0 and 0.6 V, making this combination of interest to tandem cells. A stack of solution processed ZnO nanoparticles and pH neutral poly(3,4-ethylenedioxythiophene) (pH neutral PEDOT) is used as intermediate contact.[11]

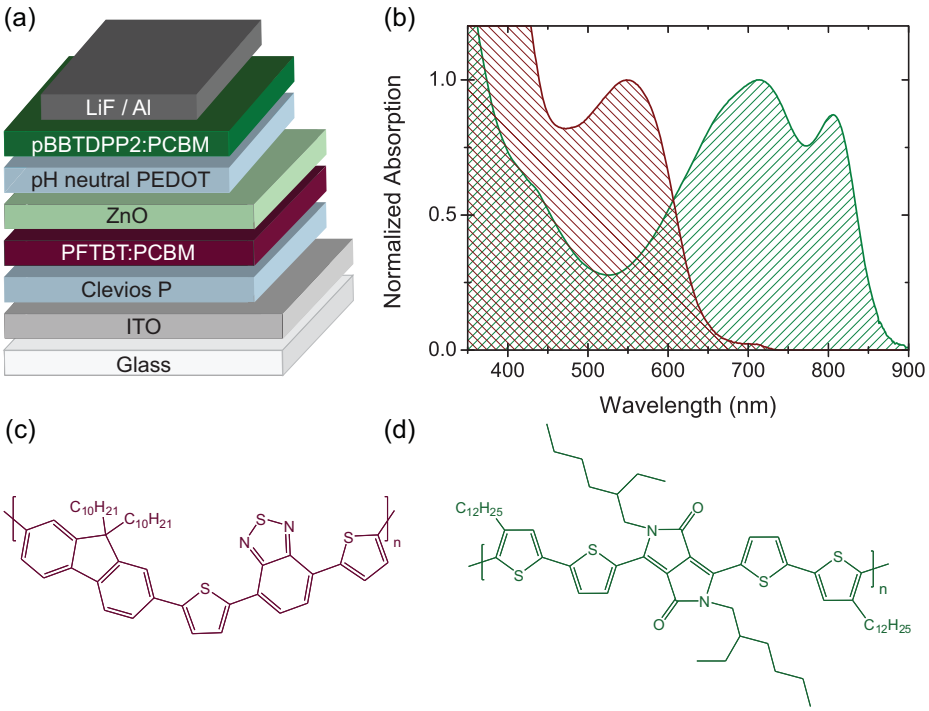

Figure 5.1 (a) Device layout of the polymer tandem solar cell. (b) Normalized absorption spectra of both individual active layers (PFTBT:PCBM in wine and pBBTDPP2:PCBM in green). Molecular structure of (c) PFTBT and (d) pBBTDPP2.

5.3 Optical modeling of polymer tandem solar cells

Rationally optimizing a tandem cell from any set of subcells is a multiparameter challenge that requires optical and electrical matching. Optical studies of organic tandem solar cells allow assessing light absorption in the individual subcells for various thicknesses[12-17] and determining the maximum obtainable short-circuit current density ($J_{sc,max}$) presuming 100% internal quantum efficiency (*IQE*).[18-20] However, the electrical performance, interaction and mutual influence of individual subcells within a tandem configuration are often unknown and more difficult to access. Only in three- or four-terminal tandem devices with semitransparent intermediate electrodes,[21-22] the current density to voltage (*J*–*V*)

characteristics of the tandem cell can be constructed from measured *J*–*V* curves of the subcells.[21] We now demonstrate, however, that a similar construction can be applied to adequately predict the performance of two-terminal devices that lack the partly absorbing intermediate contact by exploiting the optical absorption and electrical characteristics of the individual single junction subcells.

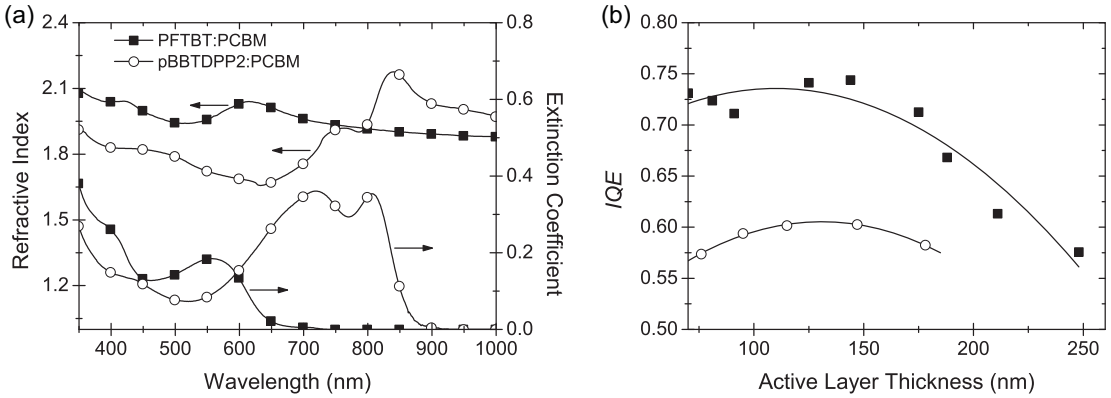

Figure 5.2 (a) The optical constants of films and (b) *IQE*s of single junction cells of PFTBT:PCBM (1:4 w/w) (■) and pBBTDPP2:PCBM (1:2 w/w) (○) active layers.

The refractive index and extinction coefficient of both mixed polymer:PCBM films were first measured by ellipsometry (Figure 5.2a) and used to determine the *IQE* as the ratio between the experimental short-circuit current density (J_{sc}) and the calculated $J_{sc,max}$ (Figure 5.2b) for a series of single junction cells with varying layer thickness.[23] The *IQE*s can be combined with optical modeling of the complete stack of layers in the tandem cell to predict the J_{sc} that would be generated by each individual subcell for a given combination of active layer thicknesses (Figure 5.3a,b).[15] In this procedure we assume that the actual spatial light absorption profile inside the layer itself does not influence the *IQE* significantly, supported by results from combined optical and electrical modeling of polymer:fullerene bulk heterojunction solar cells by Kotlarski *et al*.[24] We find that the J_{sc} generating capacity of the front cell hardly alters with varying back cell thickness and reaches a plateau at ~150 nm for the front cell thickness due to the decrease in *IQE* for thicker layers (Figure 5.2b). The bold line in Figure 5.3a,b indicates the intersection between both surfaces and defines the conditions for current matching between front and back cell.

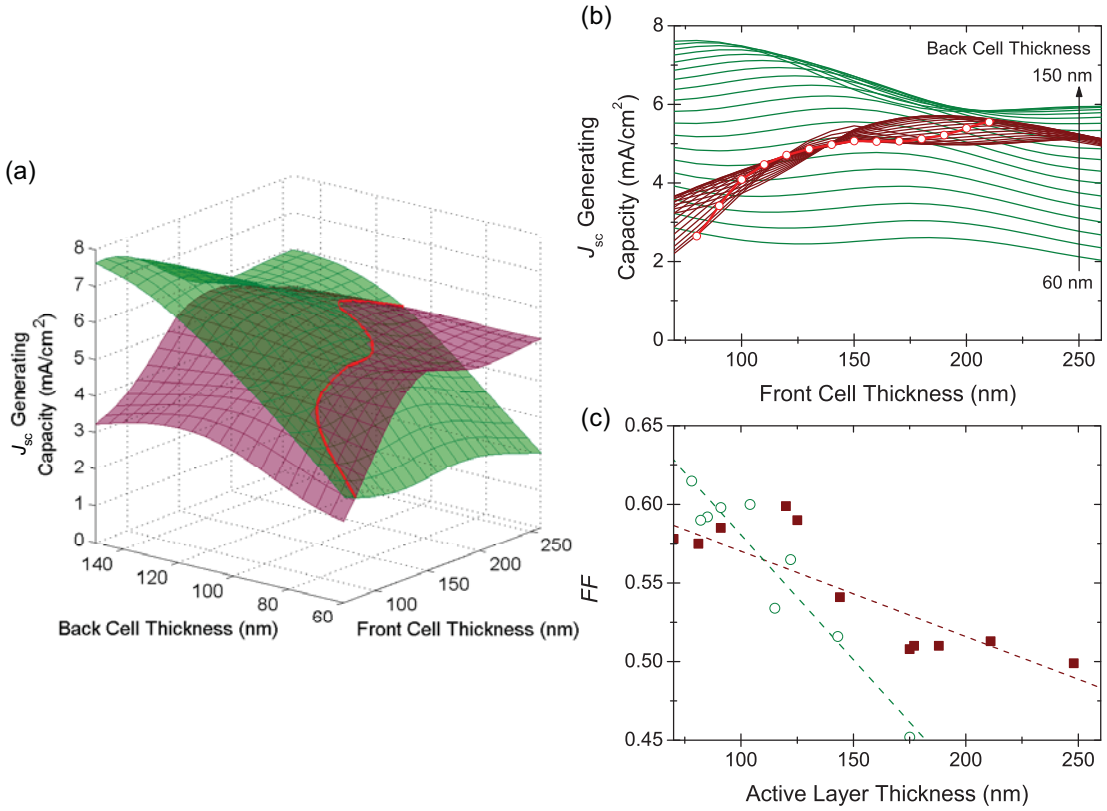

Figure 5.3 (a) 3D and (b) 2D plot of J_{sc} generating capacities of the front (wine) and back cell (green) vs. the front and back cell layer thicknesses. The red line indicates the intersection of both surfaces indicating matching current densities. (c) The *FF* of the PFTBT:PCBM (■) and pBBTDPP2:PCBM (○) single junction solar cells. The dashed lines are a guide to the eye.

5.4 J_{sc} generating capacity and fill factor matching

It is often assumed that current matching in the subcells leads to the highest efficiencies in the corresponding tandem cell.[12,15] Provided the subcells have identical fill factors (*FF*s),[14] J_{sc} and *FF* of the tandem cell are then expected to be identical to those of the subcells and V_{oc} will be equal to the sum of sub-V_{oc}s. To verify this premise a solution processed tandem cell was made with matching J_{sc} generating capacities and *FF*s. Figure 5.3 shows that similar J_{sc}s and *FF*s are expected for a 120 nm thick front cell and a 85 nm thick back cell. Under simulated solar light J_{sc} = 4.3 mA/cm^2, V_{oc} = 1.59 V and *FF* = 0.57 (Figure 5.4a) were obtained for this tandem cell. This J_{sc} is consonant with the calculated current density generating capacities of the front and back cells (both 4.6 mA/cm^2) and the *FF* of the tandem is virtually equal to those of the single junctions (0.59 and 0.60). The power conversion efficiency (η) of this cell is 3.8% (Table 5.1).

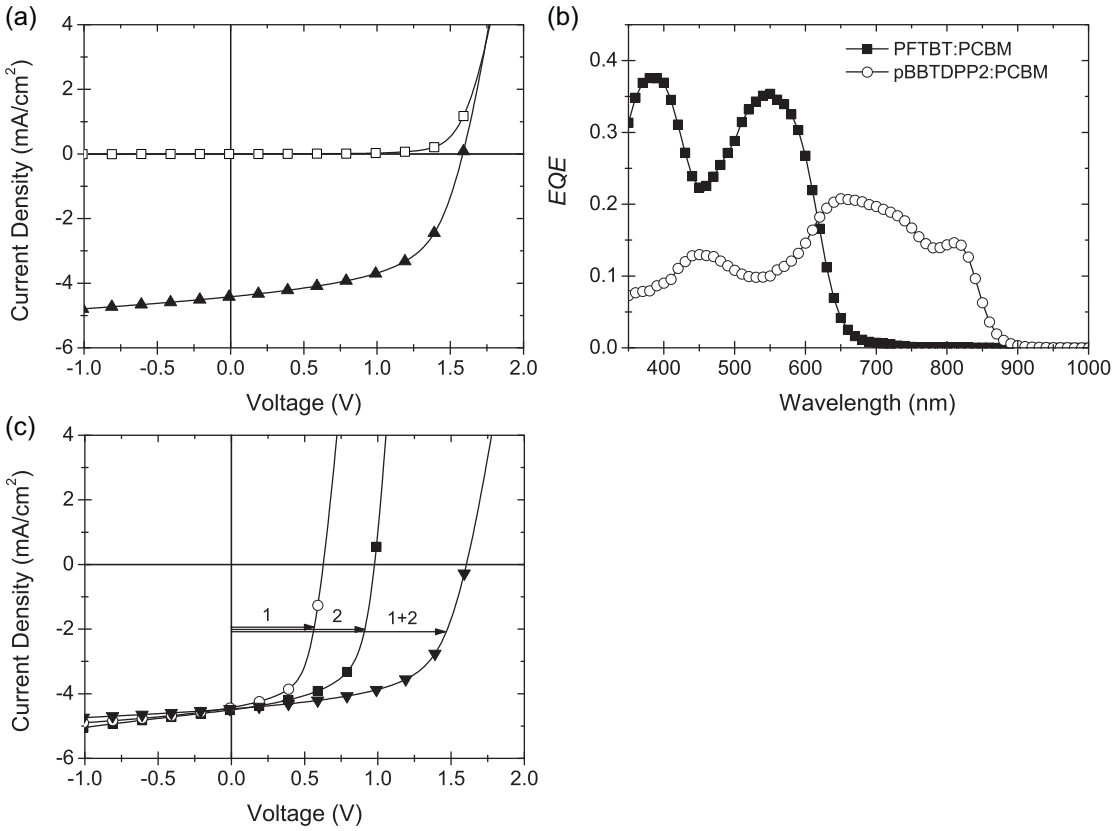

Figure 5.4 (a) *J–V* characteristics in dark (□) and under illumination (▲) and (b) the spectral response of a tandem cell with a 120 nm thick front cell and an 85 nm thick back cell. (c) *J–V* curves of single junction "dummy" cells (■: PFTBT:PCBM and ○: pBBTDPP2:PCBM) measured at representative light intensity and of the constructed tandem cell (▼). The arrows indicate the construction of the tandem *J–V* curve in a series configuration from the two subcells.

Assuming that the intermediate contact does not introduce any electrical losses, the *J–V* curve of the tandem cell can be calculated. In a series configuration the voltage of the tandem cell equals the sum of the voltages of the subcells for each value of current density.[21] Because it is impossible to measure the individual *J–V* curves of the subcells in a two-terminal configuration, two single junction "dummy" cells, identical to the tandem subcells, were made and their *J–V* curves measured under a light intensity that provides the J_{sc} equal to the J_{sc} generating capacity calculated for the subcell inside the tandem under AM1.5G illumination. Combining these two *J–V* curves, the constructed *J–V* curve of the tandem (Figure 5.4c, ▼) is in excellent agreement with the measured curve (Figure 5.4a, ▲), demonstrating that the behavior of a tandem solar cell can be predicted using the single junction "dummy" cells. Moreover, the excellent correspondence indicates that the ZnO/pH neutral PEDOT intermediate contact does not introduce significant losses.

Table 5.1 Performance parameters of a tandem cell with a 120 nm thick front cell and an 85 nm thick back cell. Front cell and back cell describe the characteristics of the single junction "dummy" cells measured under representative light intensity.

Device	Front Cell Thickness (nm)	Back Cell Thickness (nm)	J_{sc} (mA/cm^2)	V_{oc} (V)	*FF*	Efficiency (%)
Front cell	120	—	4.6	0.98	0.60	—
Back cell	—	85	4.6	0.62	0.59	—
Constructed tandem cell	120	85	4.6	1.60	0.59	4.1
Measured tandem cell	120	85	4.3	1.59	0.57	3.8

The current generation in each subcell in the tandem cell can be experimentally assessed by spectral response measurements. Data were obtained under representative illumination intensity to generate an AM1.5G equivalent current density or corrected for the intensity difference. Additionally, an electrical bias was applied to ensure short-circuit conditions for the subcell under investigation. The actual bias was determined from the *J–V* curve of the non-current-limiting "dummy" cell at the J_{sc} of the tandem cell under the light conditions of that subcell in the spectral response measurement.[25] The J_{sc}s of 4.5 and 4.4 mA/cm^2 obtained by convolution of the spectral response (Figure 5.4b) with the AM1.5G solar spectrum for front and back cells, respectively, are in good correspondence with the predicted value of 4.6 mA/cm^2 and the measured value of the *J–V* curve (4.3 mA/cm^2).

5.5 Predicting the performance of polymer tandem solar cells

With a loss-free intermediate contact, the methodology of predicting the *J–V* curve of a tandem cell can be universally applied, also for subcells with non-matching J_{sc} generating capacities and *FF*s. By mathematically constructing the *J–V* curves of the tandem cells from representative single junction cell characteristics and taking into account the electronic and optical interactions between the subcells, we identified that maximum efficiencies of about 4.8% can be reached for configurations with a 150–200 nm front cell and a 120–150 nm back cell (Figure 5.6d).

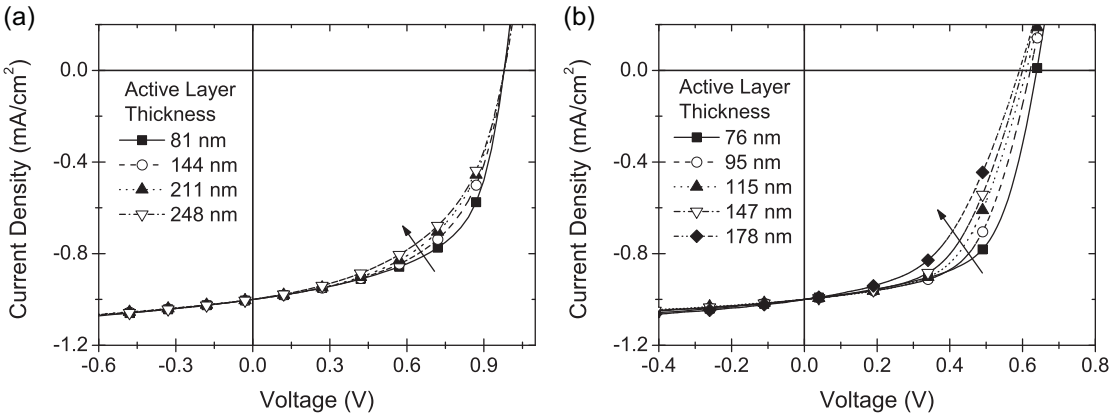

Figure 5.5 Normalized *J*–*V* curves of (a) PFTBT:PCBM and (b) pBBTDPP2:PCBM single junction solar cells with varying layer thickness.

For the analysis of the electrical interactions of the subcells in the tandem cell, we used *J*–*V* curves of representative single junction cells with thicknesses covering the whole range of interest. After normalization, these curves were interpolated to have a complete picture of the evolution of the *J*–*V* characteristics (V_{oc} and *FF*) for varying layer thickness of the active layer (Figure 5.5). After multiplication with the calculated J_{sc} generating capacity, the resulting *J*–*V* curves of front and back cell are added up according to Kirchhoff's law for series connection. This resulting addition represents the *J*–*V* curve of a tandem cell with the concerned subcell layer thicknesses and the corresponding parameters (J_{sc}, V_{oc}, *FF* and η) were extracted (Figure 5.6).

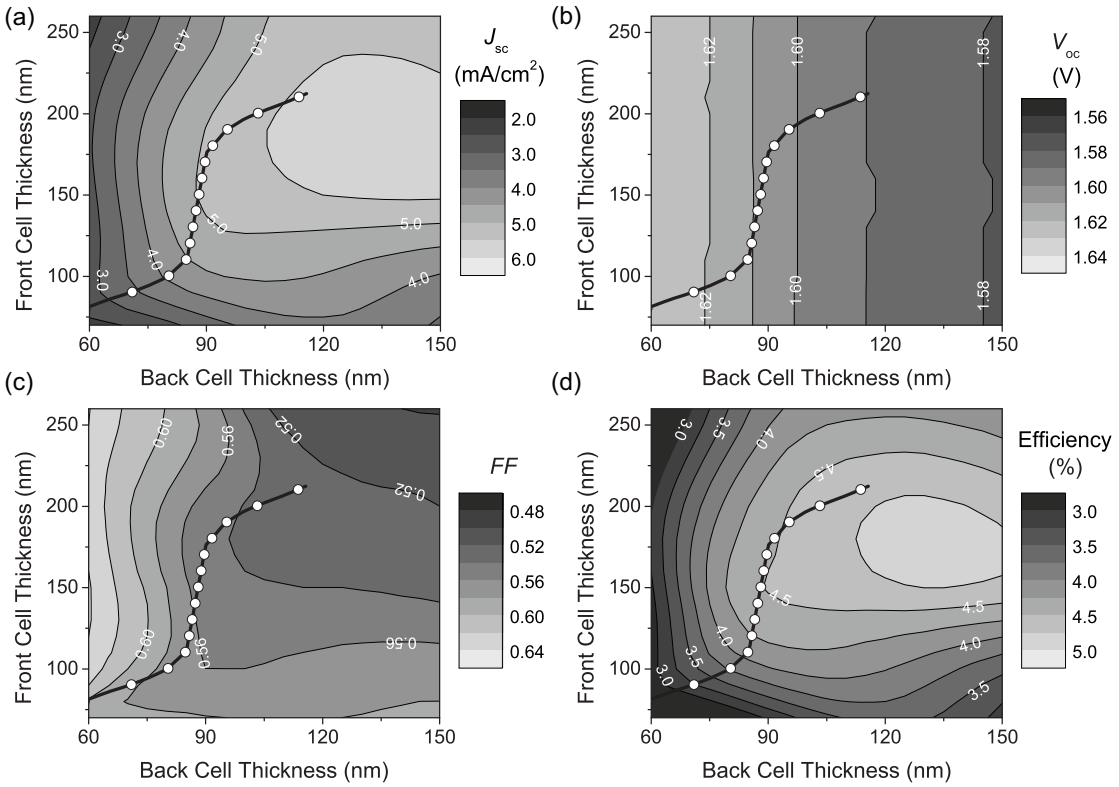

Figure 5.6 Contour plot of predicted J_{sc}s, V_{oc}s, *FF*s, and efficiencies of tandem cells calculated by mathematically constructing *J*–*V* curves from representative single junction characteristics. The isoline of matching J_{sc} generating capacities of the subcells is represented by the bold line.

5.6 Polymer tandem solar cell with optimized active layer thicknesses

The predictions of tandem cells presented in Figure 5.6 were tested by constructing a tandem cell with active layer thickness combination resulting in the highest predicted efficiency: a front cell thickness of 180 nm and a back cell thickness of 125 nm. The calculated J_{sc} generating capacities (5.5 vs. 6.2 mA/cm^2) and the expected *FF*s (0.52 vs. 0.57) of the front and back cell differ substantially. Constructing the *J*–*V* curve from the *J*–*V* characteristics of the corresponding single junction cells under appropriate illumination provides the following expected values: J_{sc} = 5.8 mA/cm^2, V_{oc} = 1.59 V and *FF* = 0.53. As mentioned previously, the *FF* of the tandem cell is primarily dictated by the *FF* of the current-limiting subcell.[1,6] Notably, the J_{sc} of the tandem cell surpasses the lowest J_{sc} generating capacity of the two subcells. The increased photocurrent generation in the front cell originates from an increased electric field over this subcell.[21] Holes extracted from the back cell are not completely compensated for as fewer electrons from the front cell reach the intermediate

contact. At steady-state, this reduces the electric field across the back cell and enhances the effective field across the front cell. Hence, at short-circuit conditions for the tandem cell, the back cell operates in forward bias, whereas the front cell experiences an equally large but opposite reverse bias, which assists carrier collection in this subcell (Figure 5.7d). Especially for organic solar cells, which generally exhibit a field-assisted collection, this can be a large effect. The significance of the bias often depends on the *FF* of the current-limiting subcell and more specifically on the shunt resistance. Here, the *FF* of 0.52 of the PFTBT:PCBM subcell enables a higher current density in the tandem cell than the current density generating capacity of the PFTBT:PCBM subcell.

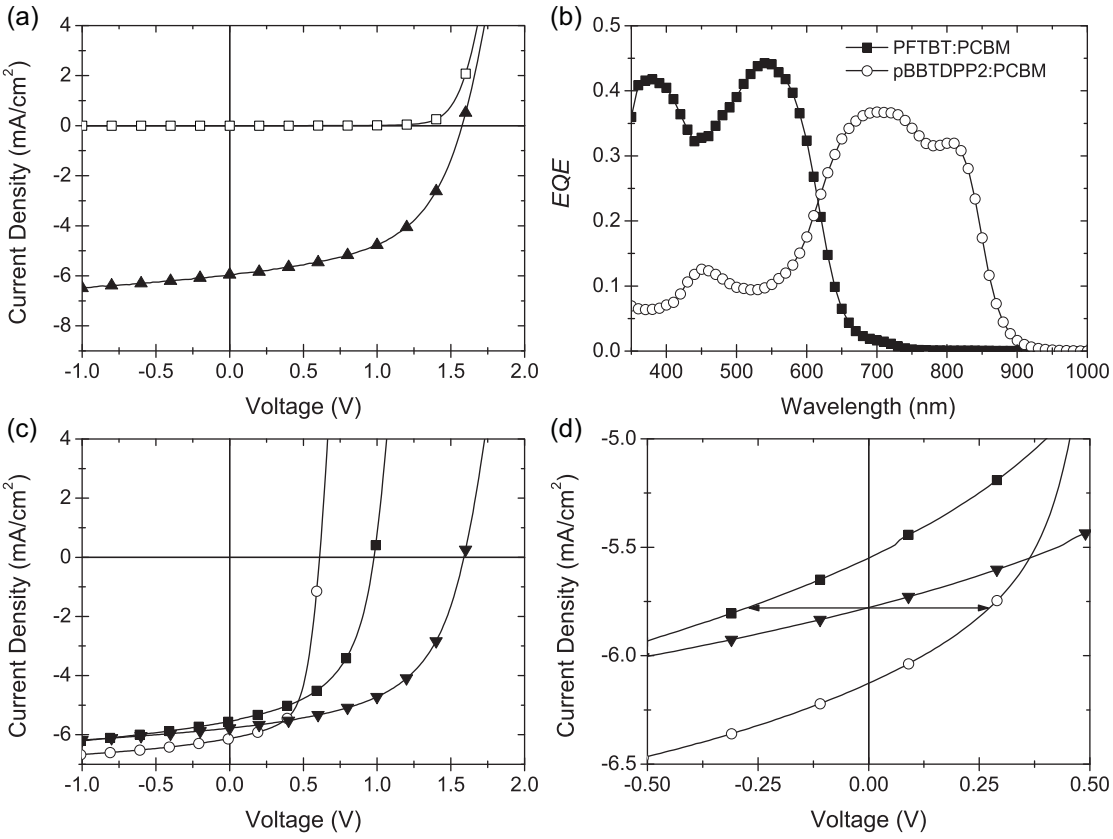

Figure 5.7 (a) *J–V* characteristics in dark (□) and under illumination (▲) and (b) the spectral response of a tandem cell with a 180 nm thick front cell and a 125 nm thick back cell. (c) *J–V* curves of single junction "dummy" cells (■: PFTBT:PCBM and ○: pBBTDPP2:PCBM) measured at representative light intensity and of the constructed tandem (▼). (d) An enlarged area of the *J–V* curves in Figure 5.7c with arrows indicating the forward and reverse electrical bias over the two subcells for short-circuit conditions of the tandem cell.

The measured device performance (J_{sc} = 6.0 mA/cm^2, V_{oc} = 1.58 V, FF = 0.52, η = 4.9%, Figure 5.7a and Table 5.2) is in good agreement with the predicted behavior (Figure 5.7c and Table 5.2). These values were determined using a class-A solar simulator at the Energy research Centre of the Netherlands (ECN), using the mismatch factor of the current-limiting subcell. The J_{sc}s of the subcells inferred from convoluting the external quantum efficiency (Figure 5.7b) are 5.8 and 7.0 mA/cm^2 for front and back cell, respectively, and are clearly non-matched. These results evidence that in the actual tandem cell, the J_{sc} surpasses the J_{sc} generating capacity of the current-limiting subcell.

Table 5.2 Performance parameters of a tandem cell with a 180 nm thick front cell and a 125 nm thick back cell. Front cell and back cell describe the characteristics of the single junction "dummy" cells measured under reduced illumination.

Device	Area (cm^2)	Front Cell Thickness (nm)	Back Cell Thickness (nm)	J_{sc} (mA/cm^2)	V_{oc} (V)	FF	Efficiency (%)
Front cell		180	—	5.5	0.98	0.52	—
Back cell		—	125	6.2	0.61	0.57	—
Constructed tandem cell		180	125	5.8	1.59	0.53	4.8
Measured tandem cell	0.16	180	125	6.0	1.58	0.52	4.9
	1.0			6.0	1.53	0.52	4.8

5.7 Conclusions

We have shown that in a polymer tandem solar cell the current-limiting subcell can be assisted by the other subcell. Using the optical constants and electrical characteristics of the subcells, the performance of tandem cells can be accurately predicted by combining the J–V curves of representative single junction cells under the lighting conditions experienced in the tandem cell. This strategy provides a universal method to establish the optimal device layout and to further enhance the efficiency of future polymer tandem solar cells.

5.8 Experimental

Devices

For preparing organic solar cells, precleaned ITO coated substrates (Naranjo Substrates) were covered with a 50 nm thick PEDOT:PSS film (Clevios® P VP AI 4083, H.C. Starck, passed a 5.0 µm Whatman Puradisc FP30 syringe filter). The active layer was then deposited on top in air. For tandem solar cells, subsequent to the first active layer a 30 nm ZnO layer spin cast from a 10 mg/ml ZnO nanoparticles solution in acetone is deposited in a nitrogen filled glovebox, followed by a 15 nm pH neutral PEDOT layer (Orgacon, batch 5541073, *p*H = 7, 1.2 wt %, Agfa NV) deposited in air.[11] All devices were transferred into a nitrogen filled glovebox after the solution processing, where 1 nm of LiF and 100 nm of Al were thermally evaporated at a pressure of 10^{-7} mbar.

PFTBT:PCBM: Poly[2,7-(9,9-didecylfluorene)-*alt*-5,5-(4′,7′-di-2-thienyl-2′,1′,3′-benzothia-diazole)] (PFTBT)[9] (TNO) was mixed with PCBM (Solenne BV) in chlorobenzene in a 1:4 ratio at 5 mg/ml polymer concentration. A spin speed of 2100 and 1300 RPM resulted in a 120 and 180 nm thick layer respectively.

pBBTDPP2:PCBM: poly[3,6-bis(4'-dodecyl-[2,2']bithiophenyl-5-yl)-2,5-bis(2-ethylhexyl)-2,5-dihydro-pyrrolo[3,4-]pyrrole-1,4-dione] (pBBTDPP2)[10] (CIBA SC) was mixed with PCBM in a 80/20 chloroform/*o*-dichlorobenzene mixture in a 1:2 ratio at 7.5 mg/ml polymer concentration. A spin speed of 5000 and 2000 RPM resulted in an 85 and 125 nm thick layer respectively.

Device characterization

Tandem cells were UV illuminated for 20 min. with a Spectroline EN-160L/F 365 nm hand lamp from Spectronics Corporation. The thickness of the devices was verified with a Dektak 150 profilometer from Veeco.

J–V measurements were performed under simulated solar light (1000 W/m^2) from a tungsten-halogen lamp filtered by a Schott GG385 UV filter and a Hoya LB120 daylight filter or with a WXS-300S-50 solar simulator (WACOM ELECTRIC Co.), using a Keithley 2400 source measurement unit. In the latter case, the light intensity was adjusted to compensate for the spectral mismatch factor (0.95), which was calculated using a recent spectrum of the simulator lamp, the spectral responses of the Si reference cell (calibrated at PTB, Braunschweig) and the tandem cell. For the tandem cell, the spectral response is based on the external quantum efficiency of the current-limiting subcell as this subcell mainly appoints the spectral response of the tandem cell. To prevent parasitic charge collection by utilizing highly conductive intermediate layers, a thin black mask was used with apertures identical in size to the overlap of the ITO and aluminum electrode.[26-27] The devices were fixed on top of the mask during measurement to minimize dislocation errors.

Spectral response measurements were done in a home-built set-up. Continuous bias light from a solid state laser (B&W Tek Inc., λ = 532 nm of 30 mW and λ = 780 nm of 21 mW) was added to the mechanically modulated (SR 540, Stanford Research) monochromatic (Oriel Cornerstone 130 1/8 m, Newport) light (Halotone halogen lamp, Philips) to address one of the two subcells.[2,28] The intensity of the bias laser light was adjusted, using a variable neutral density filter. The sample is connected to a lock-in-amplifier (SR 830, Stanford Research) over a load of 50 Ω. For the pBBTDPP2 subcell the measurement was carried out under representative illumination intensity (AM1.5G equivalent, provided by the 532 nm laser flood light). For the PFTBT subcell, the data was mathematically corrected for the intensity difference between the monochromatic light and AM1.5G according to the procedure outlined in Chapter 6. Because both subcells are electrically connected in a series configuration, extra electrical bias is applied by the lock-in-amplifier to ensure short-circuit conditions in the subcell during the spectral response measurements.

Optical modeling

Calculations of the optical electric field were performed with the Essential Macleod software package (Thin Film Center, Inc., Tucson, USA). The optical constants of glass and ITO were provided by Thin Film Center. The other optical constants were obtained from variable angle ellipsometry measurements or literature.[29-30]

5.9 References

[1] Ameri T., Dennler G., Lungenschmied C. and Brabec C.J. *Energy Environ. Sci.* **2009**, *2*, 347.

[2] Dennler G., Prall H.-J., Koeppe R., Egginger M., Autengruber R. and Sariciftci N.S. *Appl. Phys. Lett.* **2006**, *89*, 073502.

[3] Dennler G., Scharber M., Ameri T., Denk P., Forberich K., Waldauf C. and Brabec C.J. *Adv. Mater.* **2008**, *20*, 579.

[4] Drechsel J., Männig B., Kozlowski F., Gebeyehu D., Werner A., Koch M., Leo K. and Pfeiffer M. *Thin Solid Films* **2004**, *451-452*, 515.

[5] Hadipour A., de Boer B. and Blom P.W.M. *Adv. Funct. Mater.* **2008**, *18*, 169.

[6] Kim J.Y., Lee K., Coates N.E., Moses D., Nguyen T.-Q., Dante M. and Heeger A.J. *Science* **2007**, *317*, 222.

[7] Tvingstedt K., Andersson V., Zhang F. and Inganäs O. *Appl. Phys. Lett.* **2007**, *91*, 123514.

[8] Xue J., Uchida S., Rand B.P. and Forrest S.R. *Appl. Phys. Lett.* **2004**, *85*, 5757.

[9] Moet D.J.D., Slooff L.H., Kroon J.M., Chevtchenko S.S., Loos J., Koetse M.M., Sweelssen J. and Veenstra S.C. *Mater. Res. Soc. Symp. Proc.* **2006**, *974E*, CC03.

[10] Wienk M.M., Turbiez M., Gilot J. and Janssen R.A.J. *Adv. Mater.* **2008**, *20*, 2556.

[11] See Chapter 3.

[12] Andersson B.V., Persson N.-K. and Inganäs O. *J. Appl. Phys.* **2008**, *104*, 124508.

[13] Andersson V., Tvingstedt K. and Inganäs O. *J. Appl. Phys.* **2008**, *103*, 094520.

[14] Dennler G., Forberich K., Ameri T., Waldauf C., Denk P., Brabec C.J., Hingerl K. and Heeger A.J. *J. Appl. Phys.* **2007**, *102*, 123109.

[15] Eerenstein W., Slooff L.H., Veenstra S.C. and Kroon J.M. *Thin Solid Films* **2008**, *516*, 7188.

[16] Männig B., Drechsel J., Gebeyehu D., Simon P., Kozlowski F., Werner A., Li F., Grundmann S., Sonntag S., Koch M., Leo K., Pfeiffer M., Hoppe H., Meissner D., Sariciftci N.S., Riedel I., Dyakonov V. and Parisi J. *Appl. Phys. A-Mater. Sci. Process.* **2004**, *79*, 1.

[17] Persson N.-K. and Inganäs O. *Sol. Energy Mater. Sol. Cells* **2006**, *90*, 3491.

[18] Dennler G., Forberich K., Scharber M.C., Brabec C.J., Tomis I., Hingerl K. and Fromherz T. *J. Appl. Phys.* **2007**, *102*, 054516.

[19] Gilot J., Barbu I., Wienk M.M. and Janssen R.A.J. *Appl. Phys. Lett.* **2007**, *91*, 113520.

[20] Hoppe H., Arnold N., Sariciftci N.S. and Meissner D. *Sol. Energy Mater. Sol. Cells* **2003**, *80*, 105.

[21] Hadipour A., de Boer B. and Blom P.W.M. *Org. Electron.* **2008**, *9*, 617.

[22] Yang H.B., Song Q.L., Li C.M. and Lu Z.S. *Energy Environ. Sci.* **2008**, *1*, 389.

[23] Slooff L.H., Veenstra S.C., Kroon J.M., Moet D.J.D., Sweelssen J. and Koetse M.M. *Appl. Phys. Lett.* **2007**, *90*, 143506.

[24] Kotlarski J.D., Blom P.W.M., Koster L.J.A., Lenes M. and Slooff L.H. *J. Appl. Phys.* **2008**, *103*, 084502.

[25] See Chapter 6.

[26] Cravino A., Schilinsky P. and Brabec C.J. *Adv. Funct. Mater.* **2007**, *17*, 3906.

[27] Kim M.-S., Kang M.-G., Guo L.J. and Kim J. *Appl. Phys. Lett.* **2008**, *92*, 133301.

[28] Burdick J. and Glatfelter T. *Sol. Cells* **1986**, *18*, 301.

[29] Gilot J., Wienk M.M. and Janssen R.A.J. *Appl. Phys. Lett.* **2007**, *90*, 143512.

[30] Lakhwani G. *PhD Thesis* Eindhoven University of Technology **2009**.

Chapter 6

Spectral response measurement of two-terminal polymer tandem solar cells

Abstract

Accurate spectral response (SR) measurements of the subcells of two-terminal organic or polymer tandem solar cells pose specific challenges that are caused by two characteristics of these cells, *i.e.* sub-linear light intensity dependence of the current and field-assisted charge collection. These properties necessitate that SR experiments are carried out under representative illumination conditions and electrical bias to maintain short-circuit conditions for the addressed subcell. We describe a method to determine the magnitudes of the bias illumination and bias voltage, based on the behavior of single junction "dummy" cells and optical modeling. The resulting short-circuit current densities of the subcells, obtained after convolution of the SR with the AM1.5G solar spectrum, were shown to be accurate by optical calculations and current density to voltage curves of the tandem cell.

6.1 Introduction

In single junction solar cells a fundamental tradeoff between current and voltage limits the ultimately obtainable power conversion efficiency. Photons with energies exceeding the band gap energy will lose the surplus energy via non-radiative relaxation and photons with energies smaller than the band gap cannot be absorbed. Tandem solar cells offer the opportunity to reduce these transmission and thermalization losses by combining complementary absorption spectra of a wide (>1.8 *e*V) and small (<1.7 *e*V) band gap subcell. As such, tandem cells can retain more of the absorbed photon energy. Also the efficiency of polymer solar cells can be improved by adopting this approach.[1] Ideally, polymer tandem solar cells, including the intermediate contact layers, should be processable from solution, which would allow for commercial applications based on printing techniques.[2-4] Efficiencies up to 6.5% have been reported.[3]

Accurate characterization of polymer tandem solar cells requires correct measurement of the spectral response (SR) of the individual subcells. The SR is a measure for the external quantum efficiency (*EQE*) of a solar cell that indicates the incident photon to current conversion efficiency. However, the commercially most attractive two-terminal configuration of the tandem cell complicates SR measurements, because the intermediate contact is inaccessible. SR measurements for two-terminal inorganic tandem and triple junction solar cells have been described in detail.[5-10] However, recent literature on polymer tandem solar cells shows that there is a strong need for a customized protocol to correctly measure the SR of these organic counterparts.[3-4,11-12]

SR measurements of single junction solar cells are carried out with monochromatic light. However, in tandem solar cells, the response to monochromatic light represents the response of the current-limiting subcell as the two subcells are connected in series.[13] To determine the SR of individual subcells, bias illumination is required. The spectrum and intensity of bias illumination is chosen such that the bias light is predominantly absorbed by one of the two subcells, resulting in a charge generation in that subcell that largely exceeds the charge generation in the other subcell. As a consequence, this other subcell becomes current-limiting for the tandem cell over the entire wavelength range and the SR of the tandem cell represents the SR of the current-limiting subcell.

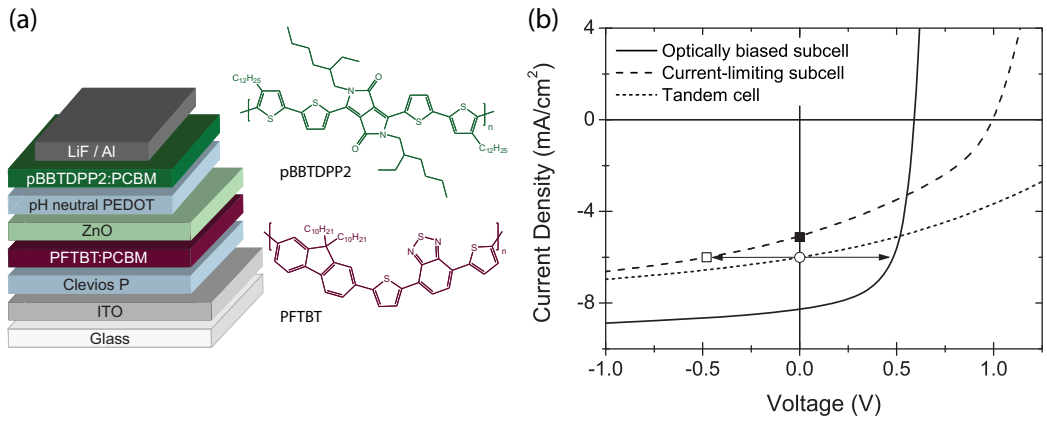

Figure 6.1 (a) Device layout of the studied polymer tandem solar cell and the molecular structure of the applied polymers. (b) Influence of the bias voltage of the optically biased subcell on the current-limiting subcell. ■ is the target value while □ is the obtained value when measuring the tandem cell under short-circuit conditions.

Yet, by optically biasing the tandem cell, the much more strongly absorbing subcell (denoted as "optically biased subcell") will be operating close to its open-circuit voltage (V_{oc}). Therefore, at short-circuit conditions for the tandem cell, the current-limiting subcell must be operating under reverse bias (Figure 6.1b) which causes the photocurrent to increase compared to short-circuit conditions (*cf.* ■ and □ in Figure 6.1b). To measure the SR of the subcell under short-circuit conditions, the reverse bias created has to be compensated by applying a forward electrical bias on the tandem cell.

Here, we present a method to accurately regulate the magnitude of the optical and electrical bias in order to determine the SR of the subcells in a two-terminal polymer tandem solar cell. We verify the obtained short-circuit current densities (J_{sc}s) after convolution of the *EQE* with the solar spectrum.[14]

In this method, representative single junction "dummy" cells, identical to the tandem subcell, are used to mimic the behavior of the tandem subcell. We have previously shown that in the current device structure the properties of the tandem cell can be represented correctly by the properties of single junction "dummy" cells.[15] The J_{sc} depends on the absorption in the active layer and hence the optical field distribution. The V_{oc}, fill factor (*FF*) and shape of the current density to voltage (*J*–*V*) curve of the active layer on the other hand are comparable in a single junction and tandem cell. This property will be exploited here.

6.2 Experimental set-up for the SR measurement

A schematic picture of the SR set-up is given in Figure 6.2a. It consists of a monochromator which disperses modulated white light to obtain the monochromatic probe light, two lasers for bias illumination, the sample, and a lock-in-amplifier as measuring unit. Optical components like lenses and mirrors to focus the incident light on the sample are omitted for clarity.

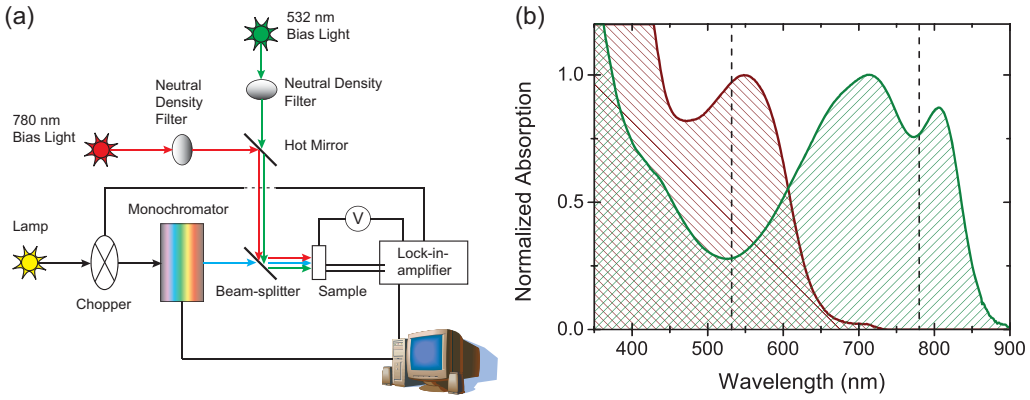

Figure 6.2 (a) Set-up for the SR measurement of tandem solar cells. (b) Normalized absorption spectra of both individual active layers (PFTBT:PCBM in wine and pBBTDPP2:PCBM in green). The dotted lines represent the wavelengths of the bias illumination.

The device whose SR measurement is presented here, has been described previously and was based on poly[2,7-(9,9-didecylfluorene)-alt-5,5-(4',7'-di-2-thienyl-2',1',3'-benzo-thiadiazole)] (PFTBT) as wide band gap polymer and poly[3,6-bis(4'-dodecyl-[2,2']bithio-phenyl-5-yl)-2,5-bis(2-ethylhexyl)-2,5-dihydropyrrolo[3,4-]pyrrole-1,4-dione] (pBBTDPP2) as small band gap polymer, both in combination with [6,6]-phenyl-C_{61}-butyric acid methyl ester ([60]PCBM or PCBM in short) (Figure 6.1a).[15] The tandem structure with a 180 nm thick PFTBT:PCBM front cell and a 125 nm thick pBBTDPP2:PCBM back cell resulted in an overall efficiency of 4.9%.

The normalized absorption spectra of individual films of the active layers of the subcells are displayed in Figure 6.2b and show the wavelengths used for the bias illumination. The PFTBT:PCBM layer is insensitive to light above 750 nm while pBBTDPP2:PCBM still absorbs up to 900 nm. As a result, bias illumination with a 780 nm laser is well suited to generate excess charges in the small band gap back cell and measure the current-limiting wide

band gap front cell in the tandem configuration. On the other hand, the low absorption of pBBTDPP2:PCBM in the 500 to 550 nm region enables selective addressing of the small band gap back cell in the SR measurement of the tandem cell with bias illumination from a 532 nm laser. The intensity of the bias illumination was adjusted by a variable neutral density filter.

6.3 Challenges in polymer tandem solar cells

In contrast to inorganic solar cells, the SR of polymer solar cells under reduced light intensity is often overestimated compared to the response under standard operating conditions due to the sub-linear light intensity dependence of polymer solar cells.[16] For example, the number of absorbed photons by the wide band gap front cell or small band gap back cell in the tandem cell is orders of magnitude lower under monochromatized white light than under one-sun intensity (1000 W/m^2) (Figure 6.3a). Representative illumination conditions can be obtained by sufficient additional continuous flood light. Ideally this flood light would be AM1.5G simulated solar light to proportionally illuminate both subcells, but this is in our set-up not practically feasible.

The approach to solve this problem differs for the two subcells. For the small band gap back cell, sufficient flood light can be provided by the 532 nm bias illumination. Because the small band gap back cell absorbs a substantial amount at this wavelength, the intensity can be tuned to generate one-sun operating conditions in the small band gap back cell.

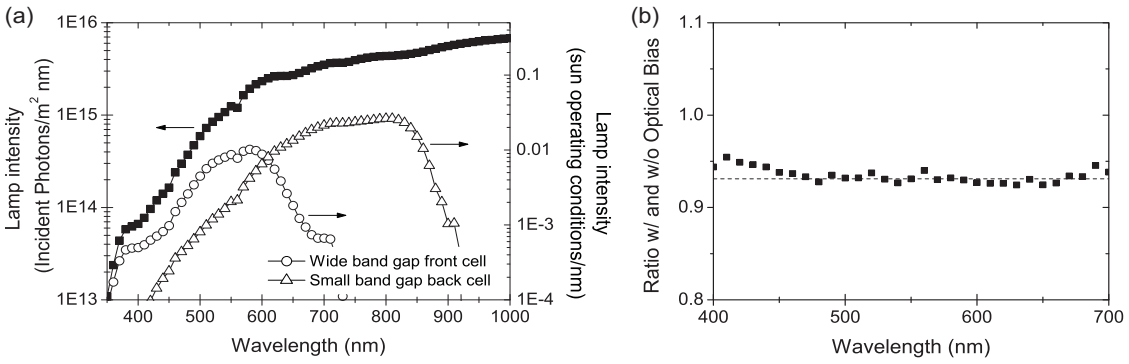

Figure 6.3 (a) Intensity of the modulated monochromatic light expressed in incident photons/m^2 (■) and relative to one-sun operating conditions for the wide band gap front cell and small band gap back cell (open symbols). (b) Ratio between the *EQE* determined with and without optical bias on a wide band gap single junction "dummy" cell.

On the other hand, the wide band gap front cell is insensitive to the 780 nm light, used to bias the small band gap back cell. Therefore, a mathematical correction of the *EQE* values is applied to correct for the sub-linear light intensity dependence of the current. This correction factor is determined as the average ratio between the *EQE* measurements with and without one-sun intensity flood light of a wide band gap single junction "dummy" cell.

A second problem to address is the negative electrical bias on the current-limiting subcell caused by the bias light on the other subcell under short-circuit conditions of the *tandem* cell. This phenomenon is more relevant in polymer tandem solar cells than in inorganic devices, where the influence is stated to be marginal.[7-8] Polymer solar cells generally have a lower shunt resistance eventuating in sloped *J–V* curves under reverse bias and can display field-assisted charge collection. This results in a higher current density in the current-limiting subcell and to an overestimation of the *EQE* in SR measurements, when the *tandem* cell is operating at short-circuit conditions.[15] Therefore, a forward electrical bias is required to compensate for this overestimation.

Applying a forward bias voltage on a solar cell moves the *J–V* curve of the entire cell towards more negative voltage (Figure 6.4a). In a tandem cell, the optically biased subcell is continuously operating close to V_{oc} regardless the voltage over the tandem cell. Therefore, applying a forward bias voltage on the tandem cell moves the *J–V* curve of the tandem and the current-limiting subcell to more negative voltages enabling the measurement of the current-limiting subcell operating at short-circuit conditions (Figure 6.4b). This is illustrated by an energy band diagram of the tandem cell under 780 nm bias illumination in Figure 6.4c,d.

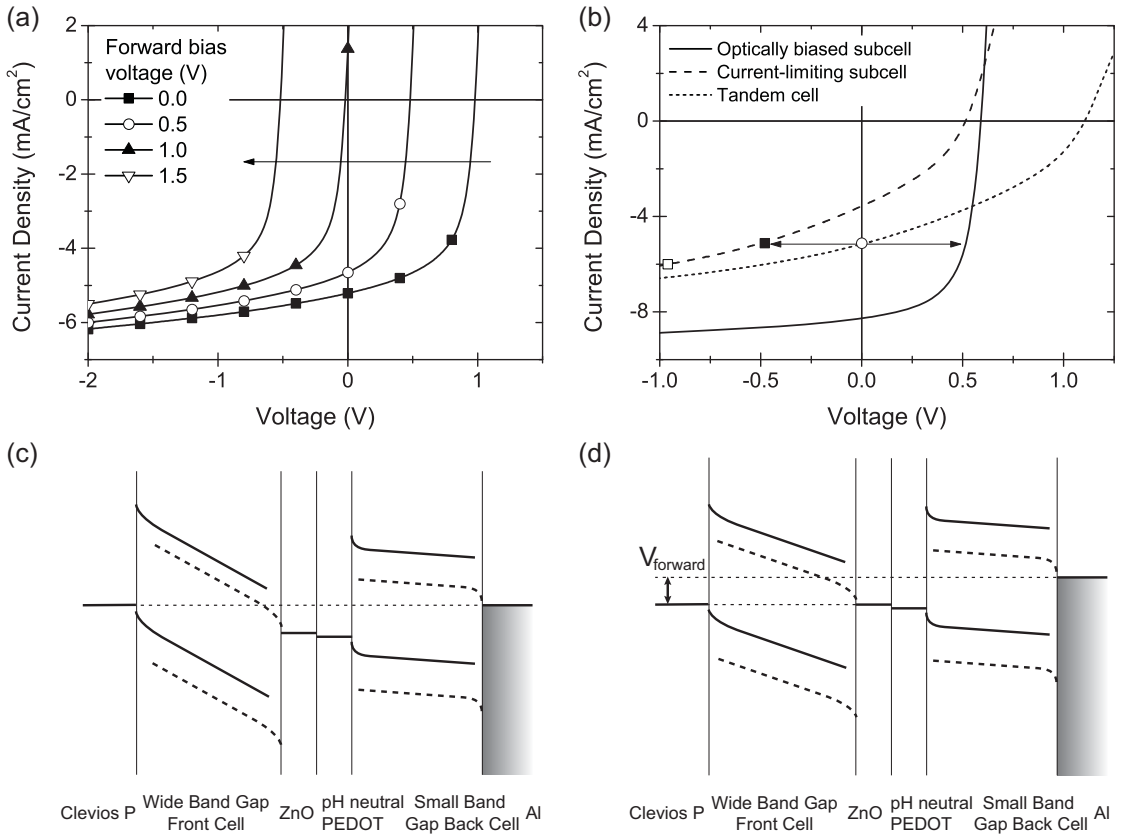

Figure 6.4 (a) The effect of a forward bias voltage on a single junction solar cell and (b) on the subcells of a tandem solar cell. This enables the measurement of the current-limiting subcell at short-circuit conditions in contrast to Figure 6.1b. (c) Energy band diagram of the tandem cell under illumination of 780 nm light at short-circuit condition of the tandem cell and (d) with an applied forward bias voltage to keep the current-limiting wide band gap front cell at short-circuit.

6.4 Determination of the magnitude of the light bias

For *EQE* measurements on the small band gap back cell, the appropriate, one-sun equivalent intensity for 532 nm laser flood light can be determined from the absorption profile of the tandem subcells obtained by optical modeling. At this intensity, the wide band gap front cell absorbs ca. three times more light, which ensures that the small band gap back cell remains current-limiting.

On the other hand, for the SR measurement of the wide band gap front cell, the 780 nm laser light can only be used as bias light for the small band gap back cell, but cannot act as flood light to have the wide band gap front cell operating under one-sun conditions. Hence, the intensity of this 780 nm bias illumination is arbitrary as long as the charge generation in the small band gap back cell exceeds the charge generation in the wide band gap front cell at any wavelength of the modulated probe light to make it not current-limiting. The intensity of

the 780 nm bias light is standardly tuned to one-sun intensity for the small band gap "dummy" cell comparable to the 532 nm bias light.

6.5 Determination of the magnitude of the electrical bias

It has been explained that under bias illumination, the current-limiting subcell is operating under reverse bias as a result of the optically biased subcell operating close to V_{oc}. A forward bias voltage on the tandem cell is required to compensate for this, avoiding overestimation of the SR induced especially in polymer solar cells by leakage current and field-assisted charge collection.

In a first-order approximation, the optically biased subcell is operating close to V_{oc}. However, as shown in Figure 6.5b this voltage can deviate substantially from V_{oc}. The precise magnitude of the electrical bias is hard to define in a two-terminal solar cell where the intermediate contact is inaccessible. However, the correct electrical bias can be determined by making use of *J–V* characteristics of single junction "dummy" cells under illumination conditions that are representative for the subcells in the tandem obtained by optical modeling.

During the SR measurement, the tandem cell also experiences the modulated probe light on top of the bias illumination generating additional current in the subcells. The intensity of the probe light, however, varies for different wavelengths, causing a variable electrical bias for different wavelengths. For the ease of the experiment we opted for an average value of the electrical bias at wavelengths of minimal and maximal additional current generation of the modulated probe light. These wavelengths are 350 nm and 550 nm, respectively for the wide band gap front cell and 350 nm and 800 nm for the small band gap back cell.

The *J–V* curves of the "dummy" cells under bias illumination plus probe light are plotted in Figure 6.5. The *J–V* curve of the optically biased subcell hardly changes with variation of the probe light wavelength and therefore only one curve is shown. The forward bias voltage, to be applied on the tandem cell to ensure short-circuit conditions for the measured subcell, is the absolute value of the voltage of the data points of the *J–V* curves with equal current densities and voltages opposite in sign (Figure 6.5). The average electrical bias was 0.60 V and 0.90 V for the SR measurement of respectively the wide band gap front cell and the small band gap back cell. Notice that the electrical bias to be applied on the small band gap back cell deviates substantially from the V_{oc} of the PFTBT:PCBM "dummy" cell (0.98 V).

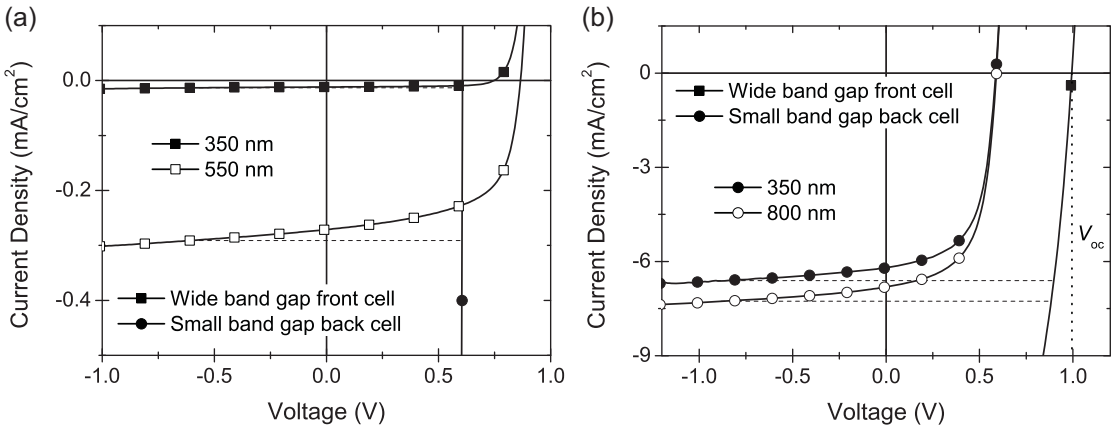

Figure 6.5 *J–V* curves of wide and small band gap "dummy" cells under illumination conditions representative for the subcells during the SR measurements: (a) represents the situation during the SR measurement of the wide band gap front cell, (b) reflects the situation during the SR measurement of the small band gap back cell. The required electrical bias is indicated by the dotted lines.

6.6 Combination of light and electrical bias

The SR of the subcells of the polymer tandem solar cell changes significantly under influence of applied optical and electrical bias (Figure 6.6). Consequently, also the estimated J_{sc}s, obtained from convolution of the SR with the AM1.5G solar spectrum,[17] differ considerably (Table 6.1). Without optical and electrical bias, the J_{sc} of the wide band gap front cell is overestimated by almost 15%. The small band gap back cell has been measured and the deviation is only related to the electrical bias, but this alone accounts for an error of 13%. This clearly demonstrates that accurate determination of the magnitude of the optical and electrical bias is essential for accurate SR measurements. The convoluted J_{sc} of the wide band gap front cell is 5.8 mA/cm^2 with a maximum *EQE* of 0.44 at 540 nm and of the small band gap back cell 7.0 mA/cm^2 with a maximum *EQE* of 0.37 at 700 nm.

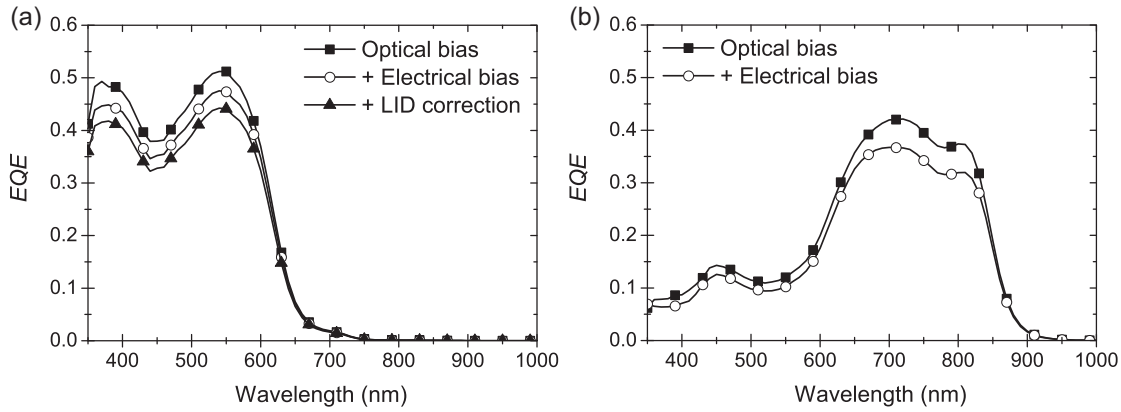

Figure 6.6 The *EQE* of the (a) wide band gap front cell and (b) small band gap back cell after applying relevant optical and electrical biases. For the wide band gap front cell an extra light intensity dependence (LID) correction is required.

Table 6.1 The short-circuit current densities of the subcells in the tandem cell obtained from SR measurements after convolution with the AM1.5G solar spectrum.

Subcell	Corrections	J_{sc} (mA/cm^2)
Wide band gap front cell	Optical bias	6.7
	+ electrical bias	6.2
	+ LID correction	5.8
Small band gap back cell	Optical bias	8.1
	+ electrical bias	7.0

6.7 Verification of the method

If we assume that the internal quantum efficiency (*IQE*) of the subcells is identical to the (known) *IQE* of the representative single junction "dummy" cells,[15] the *EQE* of the tandem subcells can also be calculated by using optical modeling. The calculated absorption spectra of both subcells in the tandem cell multiplied by the *IQE* of the subcells for these active layer thicknesses (0.69 and 0.60 for the wide band gap front cell and small band gap back cell respectively) are compared to the *EQE* values (Figure 6.7).

$$EQE(\lambda) = \text{absorption}(\lambda,\%) \cdot IQE \qquad \textbf{(6.1)}$$

The magnitude of the measured *EQE* is similar to the calculated values for both subcells. This demonstrates the validity of the assumption that the *IQE* of the subcells and single junction "dummy" cells are comparable. Moreover, the good match between measured and calculated *EQE* is a strong indication that the *EQE* measuring protocol provides accurate measurements. The shape of the two curves is comparable demonstrating that the optical modeling closely approximates the optical processes in the tandem stack.

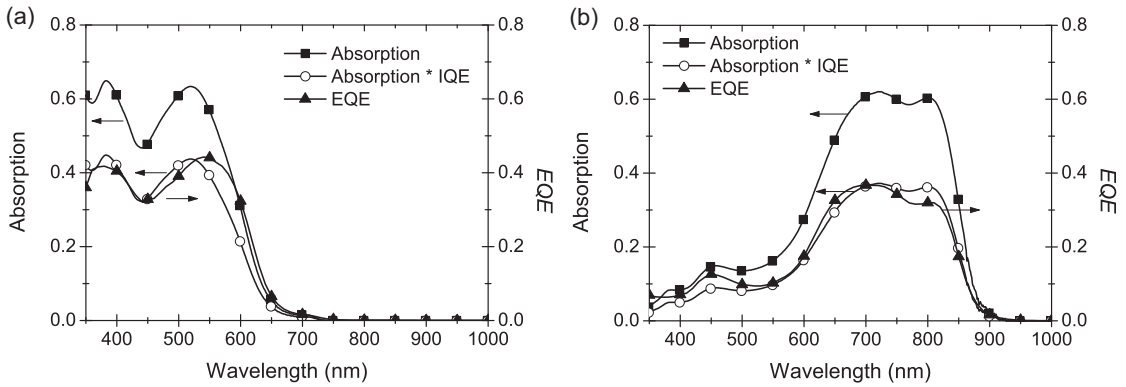

Figure 6.7 Comparison between the calculated and measured *EQE* for the (a) wide band gap front cell and (b) small band gap back cell of the tandem cell.

The *EQE*, convoluted with the AM1.5G solar spectrum is a measure for the current density generating capacity of the two subcells under solar irradiation. Using the method that was introduced in Chapter 5, these J_{sc} generating capacities can be combined with the V_{oc}, *FF* and the shape of an equally thick single junction cell, to obtain the *J–V* curves of both subcells (Figure 6.8). Kirchhoff's law then allows construction of the *J–V* curve of the complete tandem cell. This constructed tandem *J–V* curve coincides with the actual *J–V* curve, measured under a class A solar simulator, and corrected for the spectral mismatch. This proves that the magnitude of the current generation capacity and thus the *EQE* has accurately been determined with the presented SR measurement protocol.

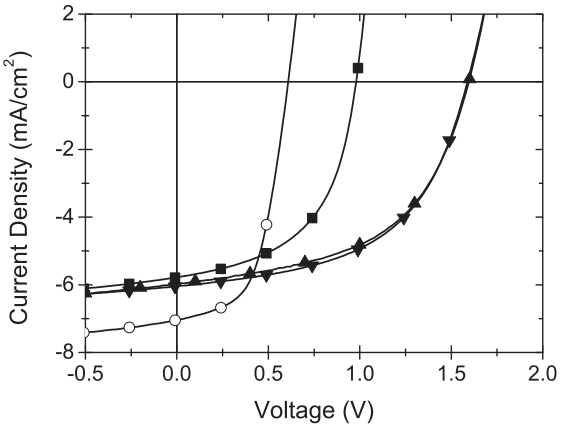

Figure 6.8 Constructed *J–V* curves of the wide band gap front cell (■) and small band gap back cell (○) in the tandem cell with J_{sc} based on the SR measurements. The constructed *J–V* curve of the tandem cell (▼) by addition of the *J–V* curves of the two subcells is compared to the *J–V* curve measured under simulated solar light (▲).

6.8 Conclusions

We described a method to measure the spectral response of two-terminal polymer tandem solar cells using an optical and electrical bias. The sub-linear light intensity dependence and field-assisted current generation complicate the measurements in organic tandem solar cells compared to inorganic tandem solar cells and require flood light to operate the subcell at one-sun conditions and a forward bias voltage to create short-circuit conditions for the addressed subcell. The method presented here relies on the behavior of single junction "dummy" cells, identical to the subcells. One-sun operating conditions in the subcell are generated for the SR measurement of the small band gap back cell by tuning the intensity of the bias light, while the SR measurement of the wide band gap front cell requires a mathematical correction. The magnitude of the electrical bias was determined by comparing *J–V* curves of the "dummy" cells under representative illumination conditions of the subcells in the tandem cell. For the specific materials used, the SR changed almost 15% under influence of applied optical and electrical bias demonstrating the importance of accurate determination of the magnitude of the optical and electrical bias. This resulted in short-circuit current density generating capacities of 5.8 mA/cm^2 and 7.0 mA/cm^2 for the wide band gap front cell and small band gap back cell respectively from convolution of the SR with the AM1.5G solar spectrum. For verification of the method, the measured and calculated *EQE* and the measured and constructed *J–V* curves of the tandem cell were compared and a good agreement was found proving the accuracy of the SR measurement protocol.

6.9 Experimental

Devices

The fabrication of the device has been described before.[15]

Device characterization

The SR measurements were done in a home-built set-up. The modulated monochromatic (Oriel Cornerstone 130 1/8 m, Newport) probe light (Halotone halogen lamp, Philips) was mechanically chopped at a frequency of 165 Hz with an optical chopper (SR 540, Stanford Research). The bias illumination was provided by a 532 nm (B&W, Tek Inc., 30 mW) and 780 nm (B&W, Tek Inc., 21 mW) solid state laser. The sample was stored in a nitrogen filled container during the measurements and illuminated through an aperture of 2 mm which is smaller than the device area to avoid errors. The measurements were executed with a lock-in-amplifier (SR 830, Stanford Research) over a load of 50 Ω. All data were recorded by a Labview program on a computer. The electrical bias over the tandem cell was provided by the lock-in-amplifier.

Optical modeling

Calculations of the optical electric field were performed with the Essential Macleod software package (Thin Film Center, Inc., Tucson, USA). The optical constants of glass and ITO were provided by Thin Film Center. The other optical constants were obtained from variable angle ellipsometry measurements or literature.[18-19]

6.10 References

[1] Dennler G., Scharber M., Ameri T., Denk P., Forberich K., Waldauf C. and Brabec C.J. *Adv. Mater.* **2008**, *20*, 579.

[2] See Chapter 3.

[3] Kim J.Y., Lee K., Coates N.E., Moses D., Nguyen T.-Q., Dante M. and Heeger A.J. *Science* **2007**, *317*, 222.

[4] Sista S., Park M.-H., Hong Z., Wu Y., Hou J., Kwan W.L., Li G. and Yang Y. *Adv. Mater.* **2009**, *22*, 380.

[5] Bücher K. and Schönecker A. *Eur. Photovoltaic Sol. Energy Conf.* **1991**, 107.

[6] Burdick J. and Glatfelter T. *Sol. Cells* **1986**, *18*, 301.

[7] Meusel M., Baur C., Letay G., Bett A.W., Warta W. and Fernandez E. *Prog. Photovoltaics* **2003**, *11*, 499.

[8] Mueller R.L. *Sol. Energy Mater. Sol. Cells* **1993**, *30*, 37.

[9] Nakata Y. and Inoguchi T. *Optoelectron.-Dev. Technol.* **1989**, *4*, 75.

[10] Ran D., Zhang S., Zhang J., Zhang X. and Wan F. *SPIE-Int. Soc. Opt. Eng. Proc.* **2007** *6723*, 672316.

[11] Slooff L.H., Böhme S., Eerenstein W., Veenstra S.C., Verhees W., Kroon J.M. and Söderström T. *SPIE-Int. Soc. Opt. Phot. Proc.* **2008**, *7052*, 705217.

[12] Yang H.B., Song Q.L., Li C.M. and Lu Z.S. *Energy Environ. Sci.* **2008**, *1*, 389.

[13] Dennler G., Prall H.-J., Koeppe R., Egginger M., Autengruber R. and Sariciftci N.S. *Appl. Phys. Lett.* **2006**, *89*, 073502.

[14] American Society for Testing and Materials (ASTM) Standard G173-03. Source: http://rredc.nrel.gov/solar/spectra/am1.5/.

[15] See Chapter 5.

[16] See Chapter 1.

[17] Kroon J.M., Wienk M.M., Verhees W.J.H. and Hummelen J.C. *Thin Solid Films* **2002**, *403-404*, 223.

[18] Gilot J., Barbu I., Wienk M.M. and Janssen R.A.J. *Appl. Phys. Lett.* **2007**, *91*, 113520.

[19] Lakhwani G. *PhD Thesis* Eindhoven University of Technology **2009**.

Chapter 7

Measuring current density to voltage characteristics of subcells in two-terminal polymer tandem solar cells

Abstract

The measurement of the current density to voltage (*J–V*) characteristics of the subcells in solution processed two-terminal polymer tandem solar cells can improve the understanding of the working of the tandem cell. *E.g.* it allows assessing the individual contributions of the two subcells to the total efficiency. Two techniques, which both do not interfere with the light incoupling in the optical stack, enable the determination of the performance of the subcells in the tandem cell. In the first method a three-terminal configuration with one extra accessible metal electrode in between the two subcells and situated just outside of the active area of the solution processed polymer tandem solar cell makes electrical characterization of the subcells possible. The second method exploits the spectral response measurements of two-terminal tandem solar cells to determine the *J–V* curves of the subcells. The resulting curves obtained by both techniques show an excellent agreement and match with the previously predicted behavior of the subcells.

7.1 Introduction

The tandem configuration in solar cells enables the reduction of energy losses inherent to single junction cells, making use of a wide and small band gap subcell. The wide band gap subcell reduces the energy loss of thermal equilibration of high energy photons in the small band gap subcell and on the other hand the small band gap subcell absorbs the low energy photons for which the wide band gap subcell is insensitive. Recently semiconducting organic molecules and polymers are being considered for tandem solar cells, resulting in power conversion efficiencies over 5%.[1-4]

The performance of the total tandem cell is determined from the current density to voltage (*J–V*) characteristics; however, a deeper insight in the working of the tandem cell is missing. Measuring the *J–V* characteristics of the subcells can result in a better understanding of the interplay between the two subcells. These measurements have been demonstrated before with a metal intermediate contact accessible in a three-terminal device.[5-8] Also, polymer tandem solar cells connected in a parallel configuration enable the determination of the *J–V* characteristics of the subcells.[9-10]

A solution processed intermediate contact is, however, commercially the most interesting because printing techniques are less time and energy consuming and eventually allow roll-to-roll processing. Recently polymer tandem solar cells with electron transporting (ET) and hole transporting (HT) layers processed from solution in a two-terminal device have been reported.[3-4,11-12] The conductivity of the solution processed intermediate contact parallel to the surface is, however, too low for external *J–V* measurements.

Here, we present two techniques to measure the *J–V* characteristics of the subcells of a polymer tandem solar cell with an electrically inaccessible intermediate contact. Both methods preserve the exact layout of the tandem cell, so also the optical electric field inside the device remains identical. In the first method an extra metal proximity electrode located just outside of the active area is evaporated between the ET and HT layer and enables a three-terminal device for the measurement of the voltage difference between the intermediate contact and one of the two electrodes. The second technique exploits the spectral response measurement of the polymer tandem solar cell in a two-terminal device as described before.[13] Varying the bias voltage over the tandem cell enables the determination of a *J–V* curve of the subcell under appropriate bias illumination.

7.2 Experimental device

The device studied with both techniques was based on poly[2,7-(9,9-didecylfluorene)-alt-5,5-(4',7'-di-2-thienyl-2',1',3'-benzothiadiazole)] (PFTBT) as wide band gap polymer and poly[3,6-bis(4'-dodecyl-[2,2']bithiophenyl-5-yl)-2,5-bis(2-ethylhexyl)-2,5-di-hydropyrrolo [3,4-]pyrrole-1,4-dione] (pBBTDPP2) as small band gap polymer, both in combination with [6,6]-phenyl-C_{61}-butyric acid methyl ester ([60]PCBM or PCBM in short) (Figure 7.1a).[12] The tandem structure with a 180 nm thick PFTBT:PCBM front cell and a 115 nm thick pBBTDPP2:PCBM back cell resulted in an overall efficiency of 4.7% under simulated solar light.

7.3 Accessible intermediate contact situated outside the active area

In the first method a Ag proximity electrode is evaporated after the deposition of the ET layer and prior to deposition of the HT layer just outside of the active area of the solar cell, *i.e.* the overlap between the indium tin oxide and Al electrode (Figure 7.1) to create a three-terminal device. In this way the light incoupling in the device is not disturbed and does not change the performance of a device with optimal active layer thicknesses as predicted before.[12] This is interesting for optimization and understanding of a specific configuration of polymer tandem solar cells.

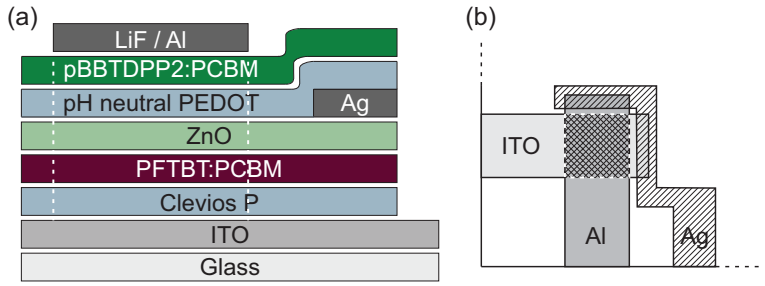

Figure 7.1 Schematic side (a) and top (b) view of the device layout for a polymer tandem solar cell with an accessible intermediate contact situated just outside of the active area. The active area is indicated by white dashed lines.

Measuring a *J–V* curve directly with this intermediate contact is not possible due to the low conductivity parallel to the surface of the ET and HT layers that makes it impossible to measure a current through the intermediate contact without significant resistance losses.

However, this set-up allows for the measurement of the voltage difference between the intermediate contact and one of the two electrodes. The internal impedance of the measuring unit is preferentially large to minimize current and voltage losses in the tandem cell. By sweeping the voltage over the entire tandem cell and recording the current density of the tandem cell and the voltage difference between the intermediate contact and one of the two electrodes, one can determine the *J–V* characteristics of the subcells in a tandem cell (Figure 7.2).

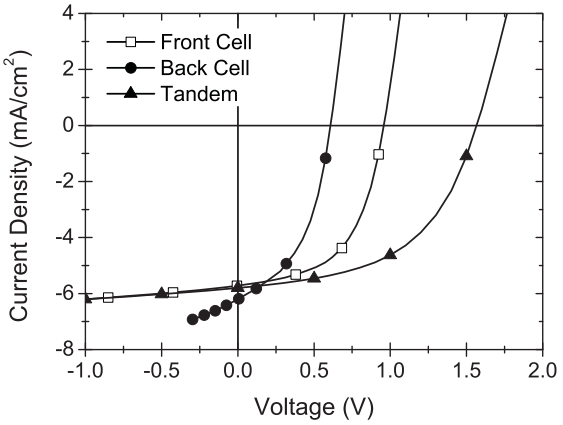

Figure 7.2 *J–V* characteristics of the front, back, and tandem cell measured with an intermediate contact situated just outside of the active area under simulated solar light.

From these measurements the contribution of both subcells to the performance of the tandem cell can easily be deducted. The power density of the tandem cell in the maximum power point (*MPP*) is 4.7 mW/cm^2. For the current density corresponding to the *MPP* of the tandem cell, the power density of the subcells (2.9 and 1.8 mW/cm^2 respectively for the front and back cell) is in this particular case very similar to the *MPP* of the individual subcells (3.0 and 1.7 mW/cm^2), but this is not a generality.

7.4 Electrical bias sweep in the *EQE* measurement of the subcells

The previous technique requires an additional evaporation step during the processing of the device. The second method exploits the spectral response measurement of the polymer tandem solar cell as described before without the need for additional processing steps and is performed on the same device as the first method.[13] The exact determination of the external quantum efficiency (*EQE*) of the subcell requires, besides specific illumination, an electric forward voltage to measure the subcell under short-circuit conditions. Convolution of the spectral response (SR) at this bias voltage with the AM1.5G solar spectrum results in the J_{sc} of the subcell in the tandem cell. Measuring the *EQE* of the subcell at variable bias voltages and convolution of the SR with the AM1.5G solar spectrum corresponds to measuring the *J–V* characteristics of the subcells. This is demonstrated by measuring the *J–V* characteristics of a single junction PFTBT:PCBM solar cell. The *J–V* curve measured under simulated solar light and the *J–V* curve obtained from the SR with varying electrical bias showed a good correspondence for the single junction cell (Figure 7.3). In an *EQE* measurement only the photocurrent is determined as the response of the cell to modulated light is measured. Therefore, the photo *J–V* curve obtained from

$$J_{\text{photo}} = J_{\text{light}} - J_{\text{dark}} \qquad \textbf{(7.1)}$$

measured under simulated solar light is plotted.

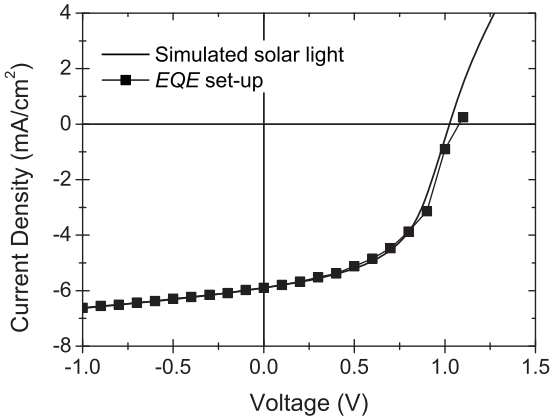

Figure 7.3 Comparison of photo *J–V* characteristics of a single junction PFTBT:PCBM solar cell measured under simulated solar light and measured in the *EQE* set-up with varying electrical bias after convolution of the SR with the AM1.5G solar spectrum.

This experiment was performed identically for the tandem cell used for the first technique. For the PFTBT:PCBM front cell, all *EQE* curves at the different electrical biases were measured under a 780 nm bias illumination and subsequently mathematically corrected for the sub-linear light intensity dependence of the current. For the pBBTDPP2:PCBM back cell, the sample was illuminated by 532 nm light serving as flood light and bias illumination during the measurements. Under these conditions, the short-circuit condition in the subcells was obtained at an applied electrical bias of 0.59 V and 0.88 V for the front and back cell, respectively. This resulted in a J_{sc} of 5.8 mA/cm^2 for the front cell and 6.3 mA/cm^2 for the back cell.

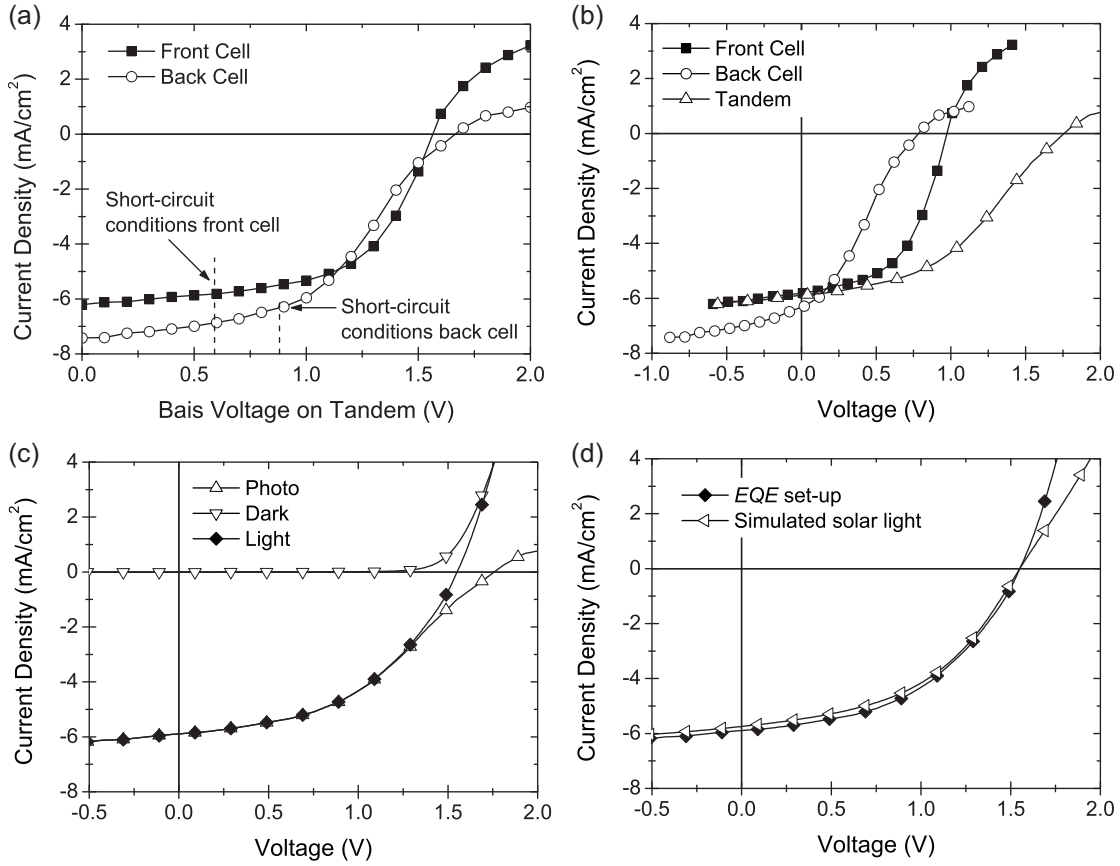

Figure 7.4 (a) Current density vs. bias voltage on the polymer tandem solar cell of the front and back cell obtained from the *EQE* measurement after convolution of the SR with the AM1.5G solar spectrum. The dotted line represents the electrical bias required for measuring under short-circuit conditions. (b) Photo *J–V* characteristics of the front and back cell. The photo *J–V* curve of the tandem cell is the addition of photo *J–V* curves of the subcells. (c) The photo, dark, and light *J–V* curve of the tandem cell. (d) Comparison between the constructed *J–V* curve obtained from *EQE* measurements and the measured *J–V* curve under simulated solar light recorded after completing the series of SR measurements.

After convolution of the SR with the AM1.5G solar spectrum for variable electrical bias, the current densities of front and back cell were plotted vs. the bias voltage on the tandem cell (Figure 7.4a). These curves were rectified with the appropriate forward bias voltage on the tandem cell, shifting the curves, so that the short-circuit current densities end up at 0 V (Figure 7.4b). The *J–V* curves of the subcells were summed using Kirchhoff's law to result in the *J–V* curve of the tandem cell (Figure 7.4b). Addition of this photocurrent curve of the tandem cell to the measured dark curve led to the *J–V* curve of the tandem cell under illumination (Figure 7.4c). This *J–V* curve obtained from the SR of the subcells in the tandem shows an excellent agreement with the *J–V* curve measured under simulated solar light, recorded after completing the series of SR measurements (Figure 7.4d).

7.5 Comparison of the *J–V* curves of the subcells from both methods

The two techniques described determine the *J–V* characteristics of the subcells in a polymer tandem solar cell with a solution processed intermediate contact. Figure 7.5 plots the *J–V* curves of the front and back cell obtained using the proximity electrode (method 1) and via the SR measurement (method 2). The performance parameters of the subcells are summarized in Table 7.1. For the determination of the V_{oc} of the subcells in method 2, the photocurrent curve of the subcell is summed with a measured dark curve of a single junction "dummy" cell, identical to the subcell.

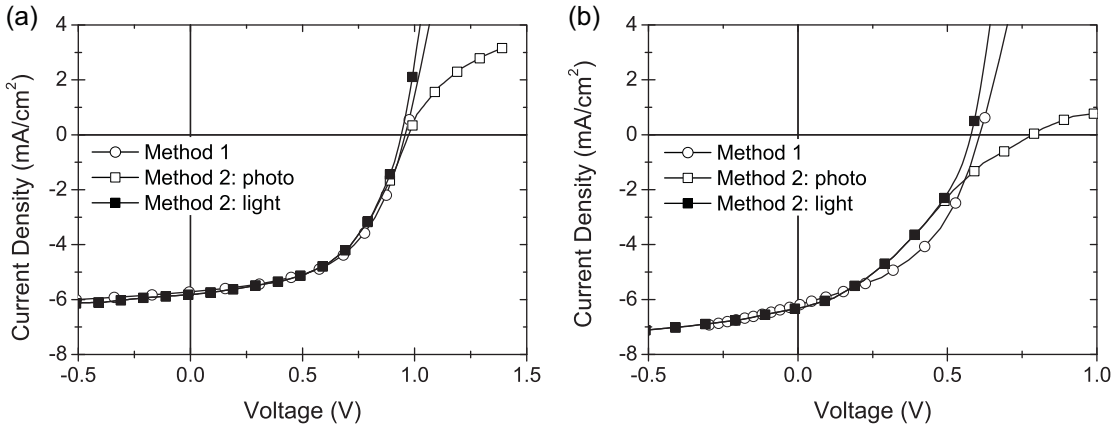

Figure 7.5 Comparison between both methods of the *J–V* characteristics of the front (a) and back (b) cell in the polymer tandem solar cell.

Table 7.1 Performance parameters of the front, back, and tandem cell measured with a proximity electrode (method 1), measured via the SR measurement of the subcells (method 2), and predicted similarly to the procedure described in Chapter 5.

Cell	J_{sc} (mA/cm^2)	V_{oc} (V)	*FF*	*MPP* (mW/cm^2)
Method 1				
Front cell	5.7	0.96	0.54	3.0
Back cell	6.3	0.61	0.46	1.7
Tandem cell	5.8	1.57	0.52	4.7
Method 2				
Front cell	5.8	0.94	0.53	2.9
Back cell	6.3	0.58	0.39	1.4
Constructed tandem cell	5.9	1.55	0.47	4.3
Measured tandem cell	5.7	1.55	0.47	4.2
Predicted				
Front cell	5.6	0.98	0.53	2.9
Back cell	6.2	0.61	0.55	2.1
Tandem cell	5.7	1.59	0.53	4.8

For the PFTBT:PCBM front cell, the *J–V* curves of the two methods match well (Figure 7.5a). On the other hand, the *J–V* curves of the pBBTDPP2:PCBM back cell diverge slightly in the region of 0.2 to 0.5 V (Figure 7.5b). Moreover, these performance parameters of the subcells and the tandem cell correspond well with the predicted values obtained via the procedure described in Chapter 5, except for the fill factor (*FF*) of the back cell.

One of the reasons for this discrepancy might be the stability of the tandem cell during the spectral response measurements. Long and intense illumination induces some degradation and hence a difference in device performance before and after the *EQE* measurements (Figure 7.6 and Table 7.1). Also inhomogeneous illumination in the SR set-up may influence the results.

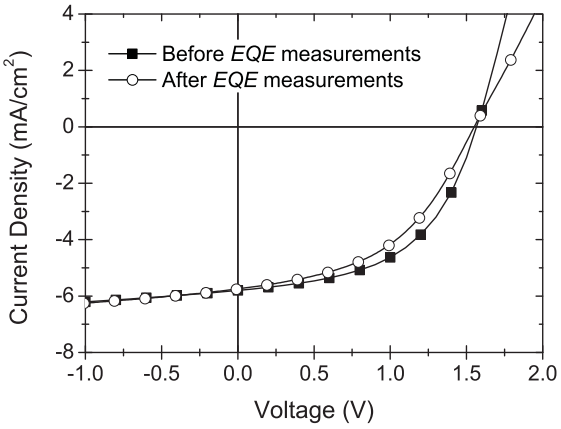

Figure 7.6 The *J–V* characteristics of the tandem cell before and after the *EQE* measurements.

7.6 Conclusions

J–V characteristics of the subcells of polymer tandem solar cells permit a better understanding of the working of a tandem cell. The conductivity parallel to the surface in a solution processed intermediate contact is too limited to enable a three-terminal device. Therefore, we developed two techniques to measure the *J–V* curves of the subcells in the tandem cell. In the first method, an auxiliary Ag electrode was evaporated between the ET and HT layer located just outside of the active area to prevent disturbance of the optical electric field in the stack. This extra proximity contact allows the determination of the voltage difference between the intermediate contact and one of the two electrodes. The second method employs the SR measurement of a tandem cell by varying the electrical bias over the tandem cell. After convolution with the AM1.5G solar spectrum, the current density as a function of the voltage over the tandem cell is determined for both subcells and can be transformed in the *J–V* curves of the subcells of the tandem cell. The results of both techniques are similar, but deviate slightly due to degradation of the tandem cell during the measurements.

7.7 Experimental

Devices

The fabrication of the devices has been described before.[12] For the accessible intermediate contact, 30 nm Ag was evaporated through a shadow mask on top of the ZnO layer prior to the deposition of the pH neutral PEDOT.

Device characterization

J–V measurements were performed under simulated solar light (1000 W/m^2) from a tungsten-halogen lamp filtered by a Schott GG385 UV filter and a Hoya LB120 daylight filter using a Keithley 2400 source measurement unit.

The voltage difference between the accessible intermediate contact and one of the two electrodes was determined with a Keithley 6512 programmable electrometer.

The spectral response measurement of the tandem cell has been described before.[13]

7.8 References

[1] Ameri T., Dennler G., Lungenschmied C. and Brabec C.J. *Energy Environ. Sci.* **2009**, *2*, 347.

[2] Hadipour A., de Boer B. and Blom P.W.M. *Adv. Funct. Mater.* **2008**, *18*, 169.

[3] Kim J.Y., Lee K., Coates N.E., Moses D., Nguyen T.-Q., Dante M. and Heeger A.J. *Science* **2007**, *317*, 222.

[4] Sista S., Park M.-H., Hong Z., Wu Y., Hou J., Kwan W.L., Li G. and Yang Y. *Adv. Mater.* **2009**, *22*, 380.

[5] Hadipour A., de Boer B. and Blom P.W.M. *J. Appl. Phys.* **2007**, *102*, 074506.

[6] Hadipour A., de Boer B., Wildeman J., Kooistra F.B., Hummelen J.C., Turbiez M.G.R., Wienk M.M., Janssen R.A.J. and Blom P.W.M. *Adv. Funct. Mater.* **2006**, *16*, 1897.

[7] Shrotriya V., Wu E.H.-E., Li G., Yao Y. and Yang Y. *Appl. Phys. Lett.* **2006**, *88*, 064104.

[8] Yang H.B., Song Q.L., Li C.M. and Lu Z.S. *Energy Environ. Sci.* **2008**, *1*, 389.

[9] Guo X., Liu F., Yue W., Xie Z., Geng Y. and Wang L. *Org. Electron.* **2009**, *10*, 1174.

[10] Sista S., Hong Z., Park M.-H., Xu Z. and Yang Y. *Adv. Mater.* **2010**, *22*, E77.

[11] See Chapter 3.

[12] See Chapter 5.

[13] See Chapter 6.

Summary

Polymer tandem solar cells

Solar cells convert solar energy directly into electricity and are attractive to contribute to the increasing energy demand of modern society. Commercial mono-crystalline silicon based devices are infiltrating the energy market but their expensive, time and energy consuming production process necessitates alternative semiconductor materials. Recently, advances in the field of polymer based solar cells have resulted in devices that feature power conversion efficiencies over 7% which approaches the threshold for successful commercialization.

A fundamental tradeoff between current and voltage limits the ultimate power conversion efficiency in single junction solar cells because photons with energies larger than the band gap will lose their excess energy via thermal equilibration and photons with energies smaller than the band gap cannot be absorbed. In a tandem solar cell, a wide band gap subcell will reduce the thermalization losses of high energy photons and a small band gap subcell will lower the transmission losses of low energy photons. For efficient operation of the tandem cell, these subcells must be combined via a transparent intermediate contact consisting of an electron transporting and hole transporting layer that enables a good physical separation of the two photoactive layers and a good electrical connection without voltage loss.

This thesis aims to fabricate, optimize, and characterize polymer tandem solar cells with all layers processed from solution. Solution based techniques (*e.g.* printing) are commercially more interesting than evaporation or sputter steps in vacuum because these techniques are less time and energy consuming and eventually allow for high speed roll-to-roll production. The main challenge is to find materials that possess optimized optical and electronic properties for efficient operation and that can be processed into thin multilayer stacks from solution in such a way that each successive layer is deposited without disrupting the integrity of underlying layers.

As a first step towards polymer tandem solar cells a transparent electron transporting layer has been developed that can be processed from solution (Chapter 2). It was found that a ZnO layer, deposited in the form of nanoparticles from acetone, can be employed. ZnO fulfills

all requirements for an electron transporting layer and acetone is one of the few solvents that is innocuous to the underlying active layer and provides sufficient wetting to enable the formation of thin, closed, and transparent layers. Incorporating a ZnO layer in solar cells between the active layer and the reflective electrode led to working devices for active layers consisting of various polymers mixed with a fullerene derivative. In fact, insertion of the thin ZnO layer even led to an improved current density. Optical modeling showed that this beneficial effect can be attributed to a redistribution of the optical electric field inside the device that shifts the position of the maximum optical field into the active layer and increases the absorption of light. ZnO works as an optical spacer. This is especially interesting for polymer solar cells where the optimal layer thickness is limited by a low charge carrier mobility.

For the completion of the recombination layer, a hole transporting layer is needed. Because of its acidic nature, the commonly used PEDOT:PSS dispersion is detrimental for the ZnO layer. In Chapter 3, it is shown, however, that a pH neutral PEDOT can be used successfully as a hole transporting layer to fabricate solution processed polymer multiple junction solar cells. Contact problems at the ZnO/pH neutral PEDOT interface were resolved by photodoping of the ZnO layer. This increases the concentration of mobile electrons in the ZnO and creates an Ohmic contact between ZnO and pH neutral PEDOT. The open-circuit voltage of multiple junction solar cells increased from 1.57 to 2.19 and 3.58 V for two, three and six active layers.

To make an efficient tandem cell, efficient wide and small band gap subcells must be combined. Chapter 4 describes the optimization of a small band gap cell based on a novel alternating copolymer of diketopyrrolopyrrole and quarterthiophene units. The morphology of the active layer and the performance of the solar cell were optimized by varying the processing conditions. Power conversion efficiencies of 3.6% and 4.0% were obtained in combination with C_{60} and C_{70} derivatives as acceptors by processing from a mixed chloroform/*o*-dichlorobenzene solution to ensure the correct balance between solubility and aggregation of polymer chains.

In Chapter 5, it is demonstrated how a combined analysis of the optical absorption and electrical characteristics of the individual wide and small band gap single junction subcells can be used to identify the optimum device layout of the corresponding tandem cell. In contrast to existing views, matching the photocurrents of the subcells is not the best criterion for optimum performance, because the short-circuit current of a polymer tandem cell can

exceed that of the current-limiting subcell. Using the new methodology, a solution processed polymer tandem cell with a power conversion efficiency of 4.9% was made, higher than the efficiency of the optimized single layer devices. This experimental result agrees well with the predicted value, indicating that this technique represents a universal method to improve the efficiency of future tandem solar cells. The current density generating capacities of the subcells were unmatched proving that the current-limiting subcell can be assisted by the other subcell in a polymer tandem solar cell.

The strong optical and electrical interplay of the two subcells has important consequences for the accurate characterization of the tandem cell, especially with respect to measuring the external quantum efficiency. Chapter 6 describes a new procedure to accurately characterize two-terminal polymer tandem solar cells. The spectral response measurement of polymer tandem solar cells is complicated by sub-linear light intensity dependence and field-assisted current generation, requiring the use of an optical and electrical bias. The required magnitude of the optical and electrical biases was determined using single junction “dummy” cells, identical to the tandem subcell, and by determining the absorption spectra of the active layers in the stack obtained via optical modeling.

Finally, the current density to voltage characteristics of the subcells of polymer tandem solar cells—permitting a better understanding of the functioning of the tandem cell—has been explored via two techniques (Chapter 7). First, an auxiliary electrode in between the electron and hole transporting layer but situated just outside of the photoactive area enabled making a three-terminal device structure without disturbing the optical electric field in the stack. This auxiliary electrode can be used for determining the bias offset between the recombination layer and either terminal electrode to provide the subcell characteristics. As an alternative method, an electrical bias sweep in the spectral response measurement of the subcells results in the current density to voltage curves of the subcells after convolution of the spectral response with the AM1.5G solar spectrum. The results of the different methods were verified and validated by cross-checking.

In conclusion, the research described in the thesis has established new methods for fabricating, optimizing, and characterizing polymer tandem solar cells that can be processed from solution. The methods that have been developed are general and can be used to manufacture efficient tandem structures based on a detailed knowledge of the characteristics of single junction cells. Combined with the recent advances in the efficiency of solar cells based on new materials, the prospects for efficient polymer tandem solar cells are excellent.

Samenvatting

Polymere tandemzonnecellen

Zonnecellen zetten zonne-energie direct om in elektriciteit en zijn daarmee aantrekkelijk om bij te dragen aan de steeds toenemende energiebehoefte van de moderne samenleving. Commerciële cellen gebaseerd op monokristallijn silicium infiltreren in de energiemarkt, maar hun kostbaar en tijd- en energierovend productieproces noodzaakt tot alternatieve halfgeleidende materialen. Recente ontwikkelingen op het gebied van polymere zonnecellen hebben geleid tot cellen met een energierendement van meer dan 7% waarmee een succesvolle commercialisering in zicht komt.

Een fundamentele wisselwerking tussen stroom en spanning limiteert het hoogsthaalbare energierendement in enkellaagszonnecellen doordat fotonen met een energie groter dan de bandafstand hun extra energie verliezen door thermische relaxatie en fotonen met een energie kleiner dan de bandafstand niet geabsorbeerd kunnen worden. In een tandemcel zal een subcel met een grote bandafstand het thermalisatieverlies van de hoogenergetische fotonen verminderen en de subcel met een kleine bandafstand zal de transmissieverliezen van de laagenergetische fotonen reduceren. Voor een efficiënte werking van de tandemcel moeten deze subcellen worden gecombineerd met een transparant tussencontact dat bestaat uit een elektronen- en een gatentransporterende laag die de twee fotoactieve lagen fysieke scheidt en zorgt voor een goed elektrisch contact zonder spanningsverlies.

Dit proefschrift heeft als doel polymere tandemzonnecellen te fabriceren, optimaliseren en karakteriseren waarbij alle lagen vanuit oplossing zijn aangebracht. Oplossingsgebaseerde productietechnieken, zoals drukken, zijn commercieel interessanter dan opdamp- of sputterstappen in vacuüm omdat deze technieken minder tijd- en energierovend zijn en uiteindelijk ‘roll-to-roll’ productie met hoge snelheid mogelijk maken. De belangrijkste uitdaging daarbij is materialen te vinden met optimale optische en elektrische eigenschappen voor een efficiënte werking en die vanuit oplossing aangebracht kunnen worden in dunne multilaagstructuren zodanig dat de depositie van een nieuwe laag de onderliggende lagen niet nadelig beïnvloedt.

Als eerste stap naar polymere tandemzonnecellen is een transparante elektronentransporterende laag ontwikkeld die uit oplossing kan worden aangebracht (Hoofdstuk 2). Het bleek dat voor dit doel een ZnO laag gebruikt kan worden die gedeponeerd wordt in de vorm van nanodeeltjes vanuit aceton. ZnO voldoet aan alle eisen voor een elektronentransporterende laag en aceton is een van de weinige oplosmiddelen die niet schadelijk is voor de onderliggende actieve laag en tegelijkertijd leidt tot een goede bevochtiging en daarmee tot een dunne, gesloten en transparante laag. Het gebruik van een ZnO-laag tussen de actieve laag en de reflecterende elektrode leidde tot werkende zonnecellen voor actieve lagen die bestonden uit diverse polymeren gemengd met een fullereenderivaat. Het gebruik van een dunne ZnO-laag leidde zelfs tot een verbetering in stroomdichtheid. Optische modellering toonde aan dat dit toegeschreven kan worden aan een herverdeling van optisch elektrisch veld in de cel waarbij de positie van het maximale optische veld verschuift tot in de actieve laag en de absorptie van licht toeneemt. ZnO verhoogt de optische weglengte van het bruikbare licht in de cel. Dit is in het bijzonder interessant voor polymere zonnecellen waarbij de optimale laagdikte beperkt wordt door een lage mobiliteit van de ladingsdrager.

Om de recombinatielaag te completeren is een gatentransporterende laag noodzakelijk. Vanwege het zure karakter is de veelgebruikte PEDOT:PSS dispersie ongeschikt in combinatie met ZnO. In Hoofdstuk 3 is aangetoond dat een pH-neutrale PEDOT succesvol gebruikt kan worden als gatentransporterende laag voor het maken van polymere multilaagszonnecellen. Contactproblemen aan het ZnO/pH-neutrale PEDOT-grensvlak werden opgelost door fotodopen van de ZnO-laag. Dit verhoogt de concentratie aan mobiele elektronen en creëert een Ohms contact tussen de ZnO en de pH neutrale PEDOT. De openklemspanning van multilaagszonnecellen nam toe van 1.57 tot 2.19 en 3.58 V voor twee, drie en zes actieve lagen.

Om een efficiënte tandemcel te maken moeten subcellen met grote en kleine bandafstand gecombineerd worden. Hoofdstuk 4 beschrijft de optimalisatie van een cel met een kleine bandafstand, gebaseerd op een alternerend copolymeer van diketopyrrolopyrrool en quaterthiofeen eenheden. Door de depositiecondities te variëren is de morfologie van de actieve laag en het rendement van de zonnecel geoptimaliseerd. Efficiënties van 3.6% en 4.0% zijn verkregen voor dit polymeer in combinatie met C_{60} en C_{70} derivaten als acceptor door de actieve laag aan te brengen vanuit een gemengde chloroform/*o*-dichloorbenzeen oplossing die de juiste balans geeft tussen oplosbaarheid en aggregatie van polymeerketens.

In Hoofdstuk 5 wordt aangetoond hoe een gecombineerde analyse van de optische absorptie en elektrische karakteristieken van de individuele grote en kleine bandafstand enkellaagscellen gebruikt kan worden om de optimale celarchitectuur van de tandemcel te bepalen. In tegenstelling tot de heersende gedachte, is het balanceren van de fotostroom in de twee subcellen niet het beste ontwerpcriterium voor de optimale werking van de cel omdat de kortsluitstroom van een polymere tandemzonnecel die van de stroomlimiterende cel kan overstijgen. Gebruikmakend van de nieuwe methodologie is een polymere tandemzonnecel met een efficiëntie van 4.9% gemaakt, hoger dan die van geoptimaliseerde enkellaagscellen. Dit experimentele resultaat kwam goed overeen met de voorspelde waarde en toont aan dat dit een universele methode is om de efficiëntie van toekomstige tandemzonnecellen te verbeteren. Het vermogen van beide subcellen om stroomdichtheid te genereren is niet gelijk en toont aan dat de stroomlimiterende subcel geholpen kan worden door de andere subcel in een polymere tandemzonnecel.

De sterke optische en elektrische wisselwerking van de twee subcellen heeft belangrijke gevolgen voor de nauwkeurige karakterisering van de tandemzonnecel, in het bijzonder voor het meten van de externe kwantumefficiëntie. Hoofdstuk 6 beschrijft een nieuwe methode om polymere tandemzonnecellen met twee contacten nauwkeurig te karakteriseren. De meting van de spectrale afhankelijkheid van de stroomdichtheid van polymere tandemzonnecellen wordt gecompliceerd door een sublineaire lichtintensiteitsafhankelijkheid en een veldafhankelijke stroomgeneratie. Deze effecten maken het noodzakelijk om een optische bevoordeling van één van de subcellen en een elektrische spanning over de tandemcel toe te passen. De mate van correctie kon worden bepaald aan de hand van enkellaags “namaak” zonnecellen die identiek zijn aan de subcel van de tandemcel en de absorptiespectra van de actieve lagen in de cel die gesimuleerd werden door optische modellering.

Tenslotte zijn de stroomdichtheid vs. spanning karakteristieken van de subcellen in de polymere tandemzonnecellen bestudeerd met twee technieken om een beter begrip van de werking van de tandemcel mogelijk te maken (Hoofdstuk 7). Door een additionele elektrode te gebruiken die aangebracht is tussen de elektronen- en gatentransporterende laag, maar zich net buiten het fotoactieve oppervlak bevindt, kan een tandemzonnecel gemaakt worden met drie contacten zonder het optische elektrische veld in de cel te verstoren. De extra elektrode kan gebruikt worden om het spanningsverschil te meten tussen de recombinatielaag en elk van de beide uitwendige elektroden waarmee de karakteristiek van de subcel bepaald kan worden. Als alternatieve methode is een variabele elektrische spanning in de meting van de spectrale

afhankelijkheid van de stroomdichtheid gebruikt om de stroomdichtheid vs. spanning curven van de subcellen te bepalen na convolutie van de spectrale data met het zonnespectrum. De uitkomsten van deze methoden zijn geverifieerd en gevalideerd door onderlinge controle van de resultaten.

Samenvattend heeft het onderzoek dat beschreven is in dit proefschrift geleid tot nieuwe methoden voor het maken, optimaliseren en karakteriseren van polymere tandemzonnecellen die vervaardigd worden vanuit oplossingen van halfgeleiders. De methoden die ontwikkeld zijn, zijn algemeen toepasbaar en kunnen gebruikt worden om efficiënte tandemcellen te maken gebaseerd op een gedetailleerde kennis van de karakteristieken van enkellaagszonnecellen. In combinatie met de recente toename van het rendement van organische zonnecellen op basis van nieuwe materialen, zijn de vooruitzichten voor efficiënte polymere tandemzonnecellen uitstekend.

Curriculum vitae

Jan Gilot werd geboren op 5 april 1982 te Turnhout (België). Na het voltooien van het secundair onderwijs aan het Sint-Jozefcollege te Turnhout, werd in 2000 begonnen met een studie Industrieel Ingenieur Chemie aan Groep T Hogeschool te Leuven (België). Deze opleiding werd afgerond met een bedrijfsstage bij Janssen Pharmaceutica waar gezocht werd naar methoden voor de concentratiebepaling van plant- en materiaalbeschermingsproducten onder leiding van dr. J.H.K.K. Hirschberg. Vervolgens begon hij in 2004 aan de master 'Molecular Engineering' aan de Technische Universiteit Eindhoven welke voltooid werd in 2006 met een afstudeeronderzoek in de groep van prof. R.A.J. Janssen gericht op polymere tandem zonncellen onder begeleiding van dr. M.M. Wienk. In augustus 2006 startte hij zijn promotieonderzoek aan hetzelfde onderwerp waarvan de belangrijkste behaalde resultaten staan beschreven in dit proefschrift.

Jan Gilot was born on April 5th 1982 in Turnhout (Belgium). After finishing secondary school at the 'Sint-Jozefcollege' in Turnhout, he studied Master of Engineering in Chemistry at Group T university college at Leuven (Belgium). This education was finalized with an internship at Janssen Pharmaceutics where methods were investigated for concentration determination of plant and material protection products under supervision of dr. J.H.K.K. Hirschberg. Subsequently he started in 2004 the master track 'Molecular Engineering' at the Eindhoven University of Technology which was completed in 2006 with a graduation project in the group of prof. R.A.J. Janssen focusing on polymer tandem solar cells under supervision of dr. M.M. Wienk. In August 2006 he became a PhD student on the same topic of which the most important results are described in this thesis.

List of publications

Published and accepted papers

Polymer Photovoltaic Cells Sensitive to the Circular Polarization of Light
Gilot J., Abbel R., Lakhwani G., Meijer E.W., Schenning A.P.H.J., Meskers S.C.J.
Advanced Materials **2010**, Accepted for publication.

Optimizing Polymer Tandem Solar Cells
Gilot J., Wienk M.M., Janssen R.A.J.
Advanced Materials **2010**, *22*, E67-71.

Design and Synthesis of Side-chain Functionalized Regioregular Roly(3-hexylthiophene)-based Copolymers and Application in Polymer:Fullerene Bulk Heterojunction Solar Cells
Campo B., Oosterbaan W.D., Gilot J., Cleij T.J., Lutsen L., Janssen R.A.J., Vanderzande D.
Proceedings of SPIE - Organic Photovoltaics X **2009**, *7416*, 74161G.

The Effect of Three-Dimensional Morphology on the Effciency of Hybrid Polymer Solar Cells
Oosterhout S.D., Wienk M.M., van Bavel S.S., Thiedmann R., Koster L.J.A., Gilot J., Loos J., Schmidt V., Janssen R.A.J.
Nature Materials **2009**, *8*, 818-824.

Copolymers of Cyclopentadithiophene and Electron-Deficient Aromatic Units Designed for Photovoltaic Applications
Bijleveld J.C., Shahid M., Gilot J., Wienk M.M., Janssen R.A.J.
Advanced Functional Materials **2009**, *19*, 3262-3270.

*Effect of Extended Thiophene Oligomers in Small Band Gap Polymers with Thienopyrazin*e
Zoombelt A.P., Gilot J., Wienk M.M., Janssen R.A.J.
Chemistry of Materials **2009**, *21*, 1663-1669.

Narrow-Bandgap Diketo-Pyrrolo-Pyrrole Polymer Solar Cells: The Effect of Processing on the Performance
Wienk M.M., Turbiez M., Gilot J., Janssen R.A.J.
Advanced Materials **2008**, *20*, 2556-2560.

On the Efficiency of Polymer Solar Cells
Gilot J., Wienk M.M., Janssen R.A.J.
Nature Materials **2007**, *6*, 704.

The Use of ZnO as Optical Spacer in Polymer Solar Cells: Theoretical and Experimental Study
Gilot J., Barbu I., Wienk M.M., Janssen R.A.J.
Applied Physics Letters **2007**, *91*, 113520.

Double and Triple Junction Polymer Solar Cells Processed From Solution
Gilot J., Wienk M.M., Janssen R.A.J.
Applied Physics Letters **2007**, *90*, 143512.

Submitted papers

Probing Charge Carrier Density in a Layer of Photodoped ZnO Nanoparticles by Spectroscopic Ellipsometry
Lakhwani G., Roijmans R., Kronemeijer A.J., Gilot J., Janssen R.A.J., Meskers S.C.J.
Submitted to *Journal of Applied Physics*

Fused Ring Thiophene-based Poly(heteroarylene ethynylene)s for Organic Solar Cells
Ashraf R.S., Gilot J., Janssen R.A.J.
Submitted to *Solar Energy Materials and Solar Cells*

Effect of Ester-Functionalized Side Chains in Poly(3-hexylthiophene) on Performance in Polymer:Fullerene Bulk Heterojunction Solar Cells
Campo B.J., Gilot J., Bolink H.J., Zhao J., Bolse J.-C., Oosterbaan W.D., Bertho S., Ruttens B., D'Haen J., Cleij T.J., Manca J., Lutsen L., Van Assche G., Janssen R.A.J., Vanderzande D.
Submitted to *Chemistry of Materials*

Papers in preparation

Broadening the Absorption of Conjugated Polymers by "Click" Functionalization with Phtalocyanines
Campo B.J., Duchateau J., Ruiz-Ganivet C., Ballesteros B., Gilot J., Oosterbaan W.D., Lutsen L., De la Torre G., Janssen R.A.J., Vanderzande D., Torres T.
In preparation for *Chemistry of Materials*

Spectral Response Measurement of Two-Terminal Polymer Tandem Solar Cells
Gilot J., Wienk M.M., Janssen R.A.J.
In preparation for *Advanced Functional Materials*

Measuring Current Density to Voltage Characteristics of Subcells in Two-Terminal Polymer Tandem Solar Cells
Gilot J., Wienk M.M., Janssen R.A.J.
In preparation for *Organic Electronics*

Dankwoord

Ook voor mij is het bijna voorbij. Al die jaren zie je toekomstige doctors stressen en vervolgens promoveren en denk je bij jezelf ‘dat is nog ver weg voor mij’. Maar nu ben ik aan de beurt en kan wel stellen dat ik er van genoten heb. Zoals alles in het leven was het met vallen en opstaan, maar het zijn toch onvergetelijke jaren geweest. Je doet al het werk dat beschreven staat in zo’n proefschrift niet alleen. Daarom wil ik een aantal personen extra vermelden buiten al diegenen die er geweest zijn voor de hulp en steun in het lab en de lach, kwinkslag of gezellige babbel buiten het lab en de werktijd. Zij die niet met naam en toenaam vermeld worden, ben ik toch echt wel erkentelijk voor hun steun en aandacht voor mij persoonlijk en mijn onderzoek.

Maar een aantal mensen verdienen toch een extra woordje uitleg, te beginnen met René en Martijn. Jullie hebben me ongelofelijk gesteund en vooral begeleid de afgelopen 1+4 jaar in de wording van een volwassen onderzoeker die zich klaar voelt de stap naar het bedrijfsleven te zetten. René, ik vind het merkwaardig dat ondanks je overvolle agenda je deur steeds openstaat. Je creativiteit en kennis om een nieuwe draai te geven aan een project, maar ook aan een artikel is echt bewonderenswaardig. Martijn, ‘advocaat van de duivel’, je bent een beetje het manusje-van-alles in de groep. Maar naast je praktisch inzicht etaleerde je ook steeds weer je wetenschappelijke kwaliteiten als ik er weer eens niets van snapte. Ik heb bijzonder veel van je geleerd en apprecieer je manier van aanpak heel erg. De komende AIO’s en studenten die door jou begeleid worden, mogen zich zeer gelukkig prijzen.

I would like to acknowledge Paul Blom, Richard van de Sanden, Christoph Brabec, Dick Broer, and Jan Kroon for taking part in the reading and defense committee.

Stefan Meskers ben ik ook zeer dankbaar voor zijn bijdrage aan hoofdstuk 3 en al het werk en tijd die we in onze gezamenlijke, mooie paper over chirale fotodiodes hebben gestoken, maar jammer genoeg niet in de structuur van het proefschrift paste. Voor mij ben jij toch de enige echte Maestro.

Ik wil ook Wijnand Dijkstra bedanken, een voor scheikundigen waarschijnlijk onbekend iemand binnen de groep, maar zonder zijn geautomatiseerde Labview programma’s om

spectrale afhankelijkheid van de stroomdichtheid te meten, was ik waarschijnlijk nu nog bezig met het praktische werk van hoofdstuk 6 en 7.

Ik heb de eer en het genoegen gehad om een vijftal studenten te begeleiden tijdens mijn promotie die aan zeer gevarieerde onderwerpen hebben gewerkt, maar wel telkens zeer nauw aansluitend bij hun interessegebied. De juiste persoon op de jusite plaats op het juiste moment zeg maar. Ionuț, in spite of the covering the inside of the evaporation bell jar with aluminum, you really surprised me with your enthusiasm, writing and presenting skills. One half of chapter 2 is entirely your contribution. I'm convinced that the Holst Centre has gained a very capable employee. Sandra, je was zeer verdienstelijk in je pogingen om een inverted tandemzonnecel te maken, iets wat twee jaar later nog steeds niet triviaal is. Veel succes met je promotie bij MST. Koen, jouw programma heeft me enorm veel tijd bespaard. Waar het eerst handmatig ging, is het nu tot wel honderd keer sneller. In this respect I also would like to thank Dominique for the further completion and perfection of the program that resulted in the very nice Figure 5.6. Melvin, je had de pech dat we vele dingen geprobeerd hebben die niet zo succesvol waren, maar toch bleef je er telkens weer voor gaan met die gedoopte ZnO synthese. Veel succes met je promotie in Delft/Eindhoven en hopelijk werken deze fosforen beter. Harm, ik ben nog steeds onder de indruk van al het werk dat je op 6 maanden verzet hebt naast je informatica studie. We zijn net niet tot het eindresultaat geraakt, maar ik hoop dat er iemand dit mooie project van triple junction cellen zal voortzetten. Nog veel succes met het afronden van je twee masters en het vinden van een geschikte baan nadien.

Als je je focust op de fabricatie van zonnecellen, ben je afhankelijk van anderen voor het ter beschikking stellen van materialen. Daarom ben ik steeds zeer verheugd geweest met de goede samenwerking met bedrijven zoals TNO (Marc Koetse en Jörgen Sweelssen voor MDMO-PPV, PFTBT), Agfa N.V. (Frank Louwet voor pH neutral PEDOT) en Ciba SC (Mathieu Turbiez voor pBBTDPP2). Ook de vlotte contacten en informatieuitwisseling met ECN (Jan, Sjoerd, Lenneke en Wiljan) en RuG (Date, Jan en Paul) in het kader van ZOMER hebben het project een duw in de rug gegeven.

Wetenschappers worden afgerekend op hun publicaties en ik mag me gelukkig prijzen dat ik door zonnecellen te maken vaak als coauteur mee bovenaan een publicatie terecht kwam. Ik wil daarvoor Johan, Arjan, Martijn, Shahid, Stefan O., Girish, Bert C. (Universiteit Hasselt) en Jan D. (Universiteit Hasselt) bedanken voor de vruchtbare coöperaties.

Door de jaren heen is het een komen en gaan geweest van labgenoten. Ik ben iedereen zeer erkentelijk voor het prettige werken in het device lab waar het niet altijd vanzelfsprekend is om jouw experimenten te plannen en uit te voeren door de drukke bezetting en de niet altijd even ordelijke omgeving. Some of them I would like to thank in particular for performing measurements for me or teaching me how to do it myself: Marta (AFM) (it has been a while since our daily coffee break, but I haven't forgotten them), Frank (ZnO synthesis, Labview programs), Patrick (TEM), Alex (conductivity measurements), Klara (SKPM), Girish (ellipsometry, UV illumination of ZnO/pH neutral PEDOT), Jan Anton (discussions on the physical aspect of solar cells), and Erik (Matlab figure).

Na eerst een jaar de kamer gedeeld te hebben met Maarten, Michel en Cameron in STO 4.47, kwam ik bij Patrick, Martijn V. en Thomas terecht in STO 4.31 voor een betere groepering van de verschillende onderzoeksgroepen. Maar de cohesie in onderzoeksonderwerpen op die kamer was moeilijk te vinden. Dit werd enkel nog maar versterkt toen Maartje Patrick verving. Maar het ontbreken van raakvlakken op onderzoeksgebied gaf wel de aanleiding tot conversaties over persoonlijke interesses en belevenissen. Dit heb ik de afgelopen jaren heel sterk gewaardeerd en maakte een maandagochtend toch iets om een beetje naar uit te kijken. Hartelijk dank daarvoor en ik denk dat ik dit in de toekomst toch zal missen. Maartje, ik vind het ongelofelijk hoe jij al je activiteiten gecombineerd krijgt en steeds zo'n hoog niveau haalt. Veel geluk nog met het promoveren, triathlonnen, musiceren en... Ik ben ook zeer blij dat je samen met Johan mijn paranimf wilt zijn. Martijn, jouw computerkennis steekt zo hard af tegen die van Michel dat van kamer veranderen op dat vlak echt wel een verbetering was. Veel succes met het zoeken van een nieuwe baan en het samenwonen in Nijmegen. Thomas, jouw vastberadenheid en ondernemerschap hebben je een zeer succesvolle promotie opgeleverd, maar Play-Doh in zonnecellen zal het toch nooit gaan maken. Veel plezier en wetenschappelijk succes gewenst in Chicago.

Verder wil ik ook iedereen van SMO/MST/M2N bedanken voor de spontane en gezellige sfeer in de gangen, op de labs, op conferenties, op skireis,... Hierbij mag ook vooral de hulp van de secretaresses (het verloop ervan de laatste jaren is bijna gelijk aan het verloop van AIO's), Henk en Hans niet vergeten worden.

Zonder de aansporing van één persoon om eens kennis te maken met de TU/e om daar te gaan studeren, was ik waarschijnlijk nooit zo ver geraakt. Ky, ik ben je bijzonder dankbaar dat je me er op gewezen hebt dat je ook buiten de landsgrenzen kan gaan verder studeren.

Naast het werk heb ik me veel bezig gehouden met sporten. Ik moet oprecht bedankt zeggen aan de mannen van de tweede ploeg voor al de afgelopen jaren en aan die van de eerste ploeg voor het afgelopen anderhalf jaar voor de geweldige ontspannende momenten op en vooral naast het veld. Volgend jaar een sabbatjaar, maar daarna er weer vollen bak tegen aan. Ook kijk ik telkens weer uit naar de gezellige etentjes met de oriënteurs. Dat moeten we vooral in stand houden.

In de laatste lijnen van het dankwoord is er natuurlijk plaats voor de familie. Moeder, vader, broer en schoonfamilie, dank jullie wel voor de steun de laatste jaren, dat jullie interesse hadden in wat ik aan het doen was en ons uit de nood wilden helpen als de planning eens wat moeilijk was of misliep.

De laatste woorden van dit proefschrift wil ik wijden aan mijn twee dierbaarsten, An en Lene. Wat heb ik ongelofelijk veel aan jullie. We hebben het de laatste maanden tijdens het schrijven best lastig gehad, maar ik ben er zeker van dat we binnenkort met ons vieren in ons nieuwe huis een geweldig mooie tijd samen tegemoet gaan. Ik zie jullie heel graag!

Jan